Chapter 9
Knocking and Combustion Noise Analysis

Abbreviations and Symbols

AEFD	Average energy in frequency domain
AEHR	Average energy of the heat release
AEHRO	Average energy of heat release oscillations
ATDC	After top dead center
BDC	Bottom dead center
BTDC	Before top dead center
CA	Crank angle
CAD	Crank angle degree
CDC	Convention diesel combustion
CDF	Cumulative distribution function
CI	Compression ignition
CNL	Combustion noise level
COV	Coefficient of variation
CPL	Cylinder pressure level
dB	Decibel
DI	Direct injection
DISI	Direct injection spark ignition
DKI	Dimensionless knock indicator
DMP	Derivative at maximum pressure position
EGR	Exhaust gas recirculation
EMD	Empirical mode decomposition
EOC	End of combustion
FFT	Fast Fourier transform
GCI	Gasoline compression ignition
GIMEP	Gross indicated mean effective pressure
HCCI	Homogeneous charge compression ignition
HRR	Heat release rate

R. K. Maurya, *Reciprocating Engine Combustion Diagnostics*, Mechanical Engineering Series, https://doi.org/10.1007/978-3-030-11954-6_9

ID	Ignition delay
IMEP	Indicated mean effective pressure
IMPG	Integral of modulus of pressure gradient
IMPO	Integral of the modulus of pressure oscillations
IVC	Intake valve closing
KDI	Knocking damage index
KI	Knock intensity
KI1	Knocking index
KLSA	Knock-limited spark advance
KO	Knock onset
LSPI	Low-speed preignition
MAHRO	Maximum amplitude of heat release oscillations
MAPO	Maximum amplitude of pressure oscillations
MIAA	Main injection advanced angle
MNL	Mechanical noise level
MON	Motor octane number
MPRR	Maximum pressure rise rate
NCS	Noise-canceling spike
NVH	Noise vibration and harshness
OH	Hydroxyl radical
OI	Octane index
ON	Octane number
ON	Overall noise
PCCI	Premixed charge compression ignition
PDF	Probability density function
PFI	Port fuel injection
PIC	Pilot injection combustion
PPC	Partially premixed combustion
PPRR	Peak pressure rise rate
PRF	Primary reference fuel
PRR	Pressure rise rate
PTP	Peak to peak
RCCI	Reactivity controlled compression ignition
RI	Ringing intensity
RMS	Root mean square
$ROHR_u$	Rate of heat release in unburnt charge
RON	Research octane number
RSD	Relative standard deviation
S	Sensitivity
SA	Structure attenuation
SACI	Spark-assisted compression ignition
SEHRO	Signal energy of heat release oscillations
SEPO	Signal energy of pressure oscillations
SER	Signal energy ratio

SI	Spark ignition
SNR	Signal-to-noise ratio
SPL	Sound pressure level
ST	Spark timing
STFT	Short-time Fourier transform
TDC	Top dead center
TN	Toluene number
TRF	Toluene reference fuels
TVE	Threshold value exceeded
WD	Wigner distribution
A	Area of the reaction front
a	Speed of sound
$B_{i,j}$	Bessel constant
D	Cylinder diameter
E_{res}	Signal energy of the resonance pressure oscillations
$f_{i,j}$	Resonance frequency
f_{Nyq}	Nyquist frequency
f_{s}	Sampling frequency
I_1	Combustion indicator
I_2	Resonance indicator
n_{idle}	Idle engine speed
P	Pressure
p_{bp}	Band-pass filtered pressure
P_{in}	Intake pressure
P_{max}	Maximum pressure
P_{RMS}	Root mean square (RMS) value of the filtered pressure
p_{ub}	Unburned gas pressure
R^2	Correlation coefficient
T	Temperature
T_{comp15}	Compression pressure of 15 bar
t_{IVC}	Time of intake valve closing
t_{KNOCK}	Time of knock onset
T_{max}	Maximum temperature
T_{ub}	Unburned temperature
u_{a}	Velocity relative to the unburned gas
V	Volume
τ	Autoignition delay time
θ	Crank angle position
ε	Dimensionless reactivity parameter of hot spot
ξ	Dimensionless resonance parameter
μ	Mean
γ	Specific heat ratio
σ	Standard deviation

9.1 Introduction

Knock is one of the key phenomena which requires close observation during the engine development and calibration process. During the engine development process, combustion chamber design needs to ensure some resilience to knocking combustion particularly for engine operation over a wide range of fuels. During engine production stage, the tuning of the engine control system needs to ensure the non-knocking combustion over a wide range of operating conditions. In spark ignition (SI) engines, knock represents one of the major constraints on performance and efficiency because it limits the maximum value of the engine compression ratio. Additional reasons for investigating engine knock are that when it's very severe, it can also quickly lead to engine damage [1–3]. Furthermore, being a source of noise, engine knock is typically considered a drivability issue. The occurrence of engine knock over a long period of time leads to adverse effects such as breakage of piston rings, piston crown and top land erosion, engine cylinder head erosion, melting of piston, increasing emissions, significant increase in fuel consumption, piston ring sticking, cylinder head gasket leakage, cylinder bore scuffing, reduction in engine efficiency, limiting the vehicle acceleration performance, and possibility of structural harms to engine [1, 3].

Combustion in SI engine can proceed as a normal or abnormal combustion process depending on engine operating conditions and engine design. Figure 9.1 illustrates the normal and abnormal combustion phenomena occurring in the SI engines. In normal combustion, the combustion of the fuel-air mixture begins at the correct time, and solely via the ignition system, that produces a controlled and

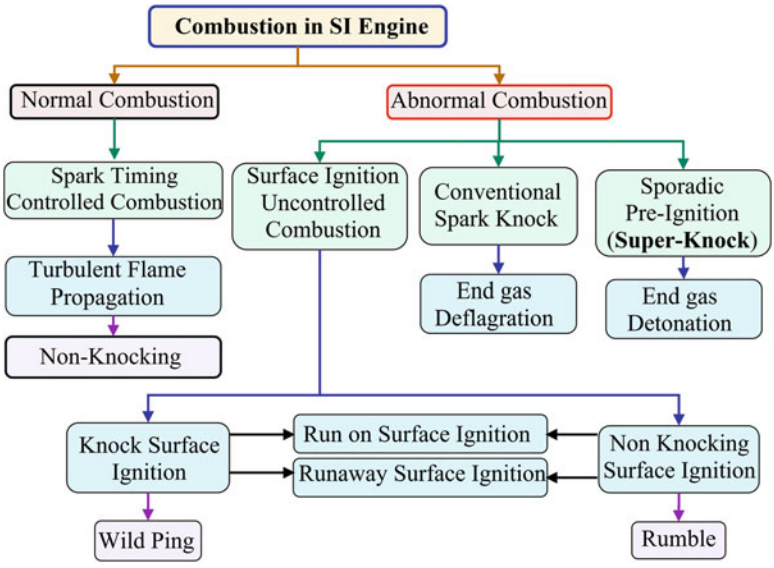

Fig. 9.1 Normal and abnormal combustion in SI engines (adapted from [2, 4])

predictable burning (energy release) of the in-cylinder charge. In the normal combustion of SI engine, the entire charge is consumed by turbulent flame propagation, and combustion is controlled by the spark timing, and via charge state (turbulence).

Abnormal combustion in SI engine can refer to a variety of conditions where normal combustion does not take place in the combustion chamber. The abnormal combustion includes modes wherein the turbulent flame fails to consume all of the charge—known as partial burns or misfires—as well as conditions such that the flame front is initiated before or after the timed spark ignition by other means (i.e., pre- or post-ignition) or wherein some or all of the charge is combusted spontaneously (Fig. 9.1) [2, 5]. The autoignition of the fuel-air mixture ahead of the propagating flame front leads to uncontrolled burning and high instantaneous energy release which results into local over-pressurization in the gas. This produces damaging, high-amplitude pressure waves that impart the acoustic resonance, which is typically referred as knock. Knocking is generally referred to the noise transmitted to the engine structure due to the autoignition of unburned end gas charge [2].

There are different types of the engine knock distinguished by the source of the ignition. Preignition is autoignition of the fuel mixture well before the spark ignition. Surface ignition is occurred when the engine surface is hot enough to ignite the fuel mixture. Preignition can occur due to several reasons including too hot spark plug, carbon deposits that remain incandescent, sharp edges in the combustion chamber, overheating, and valves operating at higher than normal temperature because of excessive guide clearance or improper seal with valve seats. Surface ignition is typically initiation of the flame front by a hot surface other than the spark, and it may occur before the spark (preignition) or after the spark (post ignition) [2]. Knocking due to surface ignition is initiated by preignition caused by glowing combustion chamber deposits or other sources, and the severity of knock depends on the timing of preignition. Run-on surface ignition occurs when engine continues to fire after the spark is switched off. Run-away surface ignition condition appears when surface ignition occurs earlier and earlier in the cycle which leads to overheating and damage to the engine. Wild ping is defined as irregular sharp combustion knock caused by early surface ignition from deposits. Non-knocking surface ignition is typically associated with the surface ignition that occurs late in the combustion cycle. Rumble is a relatively stable low profile noise (600–1200 Hz) caused by deposit surface ignition generating high rates of pressure rise in the cylinder [2]. The surface ignition problems can be addressed by adequate attention to engine design as well as fuel and lubricant quality.

Spark knock is recurrent and repeatable (occurring more than occasionally) in terms of audibility, and it is controlled by spark timing. The knock varies significantly cycle to cycle and cylinder to cylinder (in multicylinder engine). The knocking occurs due to end-gas autoignition of unburned charge in the front of the turbulent propagating flame. Figure 9.2 illustrates the knocking engine cycle and depicts the different combustion parameters. In the knocking engine cycle, the combustion process occurs in two stages, i.e., turbulent flame propagation initiated by a spark and end-gas autoignition causing pressure oscillations in the combustion

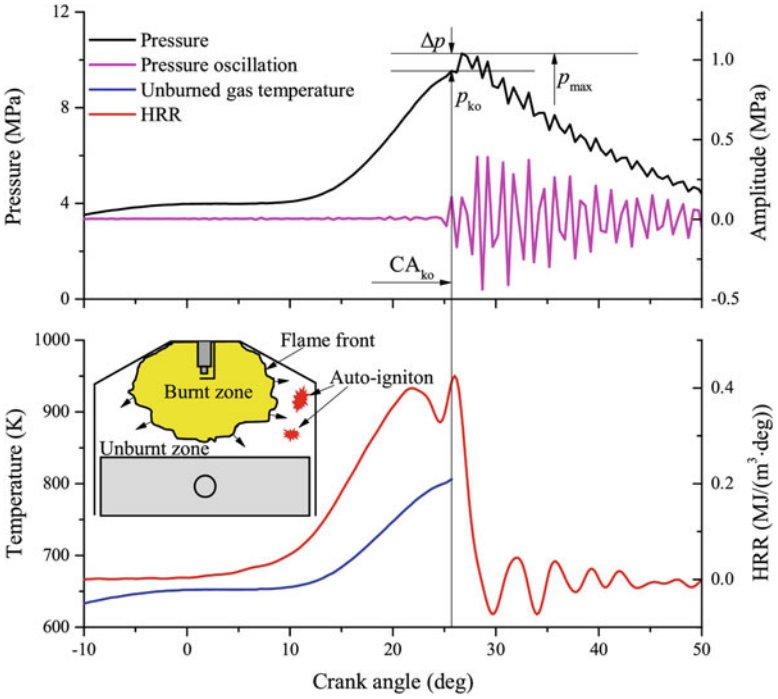

Fig. 9.2 Conventional engine knock illustration in SI engine [1]

chamber. The flame propagation stage is considered between spark timing to crank angle position of the onset of pressure oscillation (CA_{ko}) (Fig. 9.2). The heat release rate (HRR) increases during flame propagation stage with a possible short-term drop due to the movement of the piston toward BDC and heat transfer [1]. The unburned gas temperature stably increases due to the compression heating effect of the burned gas and propagating flame, as well as the compression induced by piston motion. Knocking is the abnormal combustion occurring in SI engine by the autoignition of the unburned fuel and air mixture before the flame front consumes it. This occurs after spark plug ignition and causes the high-frequency pressure oscillation that can be audibly detected. In the autoignition stage of the combustion process, the pressure signal in the cylinder at first increases dramatically reaching a peak value, and then it oscillates with decaying amplitude. The amplitude of this oscillation after a high-pass filter is used as an indicator to characterize the severity of the knock event. Thus, engine knocking is usually defined as the "clanging" or "pinging" sound that vibrations of the engine's block (and head) produce when these structures are excited by pressure waves generated inside the cylinder. Knock limitation is severe in case of low engine speeds due to lower turbulence levels in the cylinder and hence low flame speeds. This gives the end gas longer residence time at higher temperature to overcome the chemical delay. It can be noted that knocking occurs at the end of combustion in SI engine.

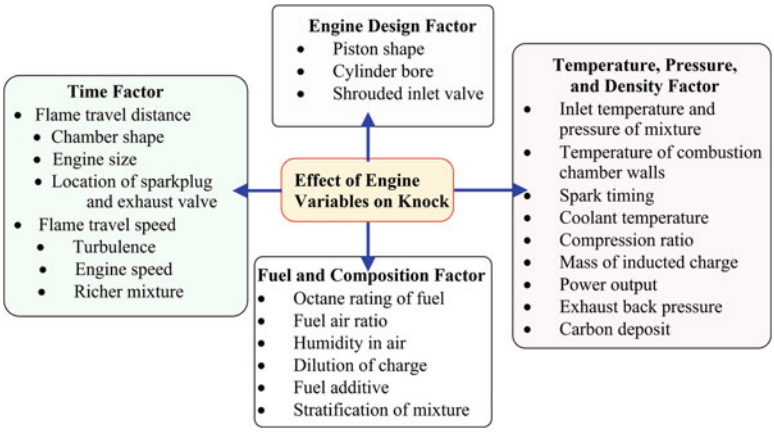

Fig. 9.3 Summary of factors affecting SI engine knock

There are certain engine operating conditions under which knock is most likely: generally high-load conditions, particularly at low engine speed. There are several variables which affect the engine knocking in SI engine, are summarized in Fig. 9.3. The parameters are categorized in four factors, namely, (1) engine design factor; (2) temperature, pressure, and density factor; (3) time factor; and (4) fuel and its composition factor.

In general, any action which tends to lower the temperature of unburned charge will tend to prevent the knocking by reducing the possibility of unburned charge to reach to the autoignition temperature. Factors reducing the density of charge tend to lower the possibility of knocking by providing lower energy release (lower rates of pre-combustion reactions in the end charge). Factors listed in temperature, pressure and density factor (Fig. 9.3) affects the knocking. Time spent by turbulent flame to consume entire charge affects the tendency of knocking, and the factors involved are presented as a time factor. Flame travel distance and flame travel speed are responsible for time required for consuming the charge by turbulent flame. The factors increase the time for entire charge consumption by turbulent flame, increases the tendency of knocking combustion. In shorter combustion duration, less time is available for which the unburned charge is exposed to high temperature and pressure. The factors such as small engine bore, compact combustion chamber, and central spark plug location decrease the flame travel distance. A high flame speed provides faster combustion leading to shorter flame propagation time. The flame speed increases with higher turbulence, which increases with the engine speed. Additionally, the engine design factors such as piston shape or shrouded valves can also be used to increase the turbulence in the combustion chamber which affects the engine knocking.

Fuel chemical composition and air-fuel ratio are the two main factors which affect the chemical characteristics of charge. Dilution of charge (by EGR or residual gases) affects the charge composition and knocking behavior. Isoparaffins, aromatics, and

olefinic hydrocarbons have higher octane number (ON), while longer chain n-paraffins have poor knock resistance [2]. The octane number is typically used to define autoignition or knock-resistant quality of fuel. Alcohols such as methanol or ethanol are high-octane fuels and thus, they have lower tendency of knock in SI engine. Dilution by residual gases lowers the tendency of knocking as residuals are inert gases and acts as sink absorbing some energy released which reduces the chemical reaction rate and retards the combustion. Humidity affects the engine knock similar to charge dilution. In full-load operation, cooled EGR is shown to reduce knock tendency. The main mechanism for this improvement is by an increase of the specific heat capacity of the charge air and reduced combustion temperatures, thereby enabling a more favorable combustion phasing [6]. The benefit of EGR is that stoichiometric operation is maintained and a three-way catalyst can be used while diluting the mixture.

Substantial cycle-to-cycle variability also exists in the knock phenomenon. Cyclic variability is largely caused by cycle-to-cycle variations in the burn rate. The burn rate is affected by several engine operating parameters, which are susceptible to cycle-to-cycle variations. Flame geometry also varies cycle-to-cycle basis, and thus, end-gas location and shape will vary. With four-valve cylinder heads with a central spark plug location, the circumferential location of the end-gas region is unclear and may vary significantly cycle by cycle. Additionally, end-gas composition and temperature nonuniformities can be significant which results in variability of the autoignition process and subsequent rate of chemical energy release. All of these factors result in the cycle-to-cycle variability in the knocking phenomenon being substantially larger than the cycle-to-cycle combustion variability [7].

9.2 Knock Fundamentals

9.2.1 Knock Onset

Knocking combustion in SI engine is caused by autoignition of the end gas ahead of the advancing flame front, and it depends on the pressure and temperature history of the end gas. Knock onset is determined by chemical kinetics as the pressure and temperature in the end gas increase with crank angle (as combustion proceeds). The autoignition of end-gas charge during knocking operation is validated using optical experimental measurements. Figure 9.4 depicts the series of images (corresponding to light emission from the high-temperature burned gases) of combustion during knocking and non-knocking operating conditions. The figure shows the normal flame front propagation in non-knocking operating conditions. During knocking operating conditions, image A shows the normal flame front propagation, and the position of the combustion flame with the dark crescent-shaped end-gas region ahead of it, before any autoignition. In image B, the hot spots occur at the upper left of the frame, which creates the autoignition region in the end gas, the autoignition region moves upward, and it is brighter and hotter. The autoignition

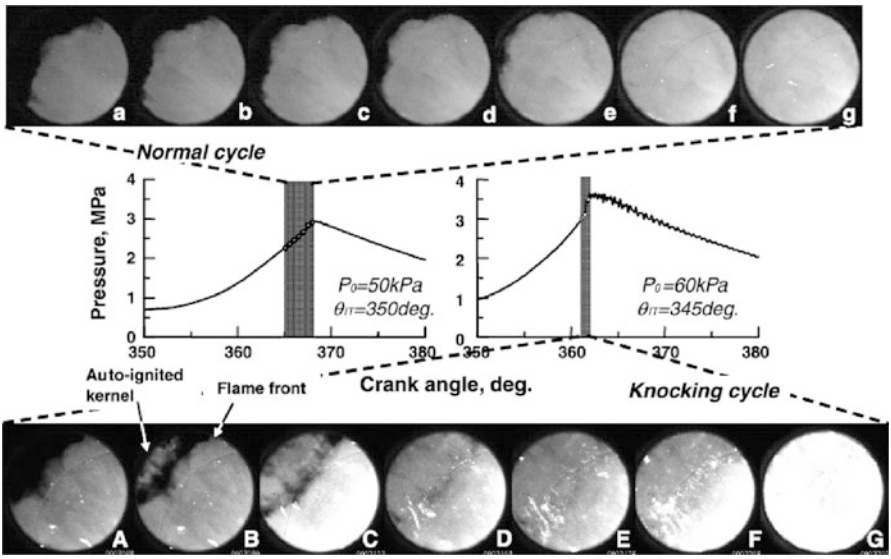

Fig. 9.4 Series of high-speed direct images for both non-knocking and knocking engine cycles in SI engine [8]

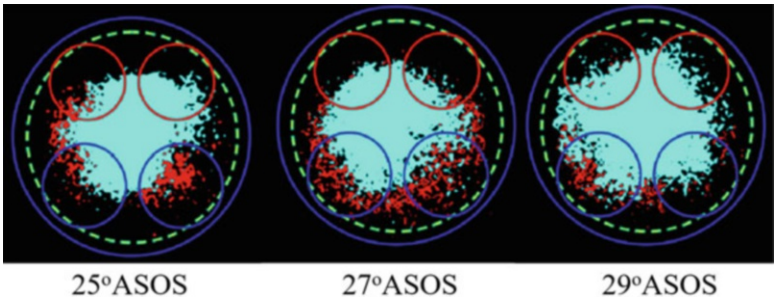

Fig. 9.5 HCO (red) and OH (cyan) spatial distributions during the knocking combustion cycle [9]

region has shifted to the right with propagation of the autoignition region, and, finally, the end gas is burned completely [3, 8]. Knocking combustion is further investigated in optical engines using spectroscopic measurements by visualizing flame structures, intermediate species, and pressure evolution during combustion in SI engine [9]. Figure 9.5 shows the spatial distributions of radicals HCO and OH during the knocking combustion cycle. Green dashed line (Fig. 9.5) indicates optical window, and blue solid line indicates the cylinder liner. Radical species such as OH and HCO are correlated to the onset and duration of knock and the occurrence of hot spots in the end-gas region [9]. The occurrence of the HCO radical in the end gas indicates the start of autoignition (knocking) combustion, and OH radical characterizes the burned zone during combustion (Fig. 9.5).

Engine knock analysis can be divided into two parts: (1) the phenomena leading to knock or knock onset and (2) what happens after the knock onset or modes of knocking (Sect. 9.2.2). Investigation for knock analysis after the knock onset (how it progress) includes the visualization of the knocking phenomenon and the numerical simulation of knock in a particular fuel-air mixture. Knock onset analysis include (1) studying ignition delay (ID) through measurements in shock tubes and rapid compression machines, (2) modeling by basic chemical kinetics, (3) developing empirical correlations using engine data, and (4) assessing the fuel effects [10].

The chemical kinetics of autoignition leading up to autoignition and knock onset has been reviewed [11]. With the progress of combustion process after spark, the pressure and temperature of the end gas (charge) increase which generates the radicals from stable fuel species by initiation reactions. Knock onset occurs once chain reactions in the charge lead an exponential growth in temperature resulting into the eventual consumption of the fuel to release its chemical energy as sensible energy [11, 12]. Different reactions become significant at different pressures and temperatures in the combustion chamber. Chemical kinetic models can be used to analyze the chemistry of autoignition at different thermodynamic conditions. These models are useful in characterizing autoignition in terms of an autoignition delay time (τ). The autoignition delay time is the induction time required for a fuel and air mixture to react and autoignite.

Phenomenological models typically use a one-step reaction instead of detailed chemical kinetics, and the autoignition delays are expressed as the Arrhenius equation as presented by Eq. (9.1) [13]:

$$\tau = C_1 \cdot p^{-C_2} \cdot \mathrm{e}^{\frac{C_3}{T}} \tag{9.1}$$

where p and T are the pressure and temperature of the end gas and C_1 to C_3 are the fitting coefficients. The phenomenological models are extensively used in simulations because of their simplicity and low computing cost. A number of correlations have been developed to predict autoignition of end gas. The typical correlation for autoignition delay time can be presented by Eq. (9.2) [14]:

$$\tau = C_1 \cdot \left(\frac{\mathrm{ON}}{100}\right)^{C_2} \cdot p^{-C_3} \cdot \mathrm{e}^{\frac{C_4}{T}} \tag{9.2}$$

where ON is fuel octane number and the model constants C_1, C_2, C_3, and C_4 are 17.69, 3.402, 1.7, and 3800, respectively. This model does not include the variables of EGR and excess air ratio (λ), and thus, the prediction of knock onset at engine operating with EGR or fuel enrichment contains error. Thus, the parameters including these variables are added to improve Eq. (9.2) in reference [13, 15].

The Livengood and Wu integral [16] is the simplest method for predicting the onset of knock in an engine. The knock integral can be presented as Eq. (9.3), which relies on an expression for the ignition delay for the current (and changing) thermodynamic state of the end-gas mixture:

$$I = \int_{t_{\mathrm{IVC}}}^{t_{\mathrm{knock}}} \left(\frac{1}{\tau}\right)_{P,T} dt \tag{9.3}$$

where t_{IVC} and t_{knock} refer to the time of intake valve closing (IVC) and knock onset, respectively. Knock occurs at the time t_{knock} when the integral I equals to 1.

A more comprehensive method of calculating the onset of knock in the end gas is to directly integrate a kinetic mechanism under the end-gas thermodynamic conditions. This method will allow for the evolving composition of the end gas to affect the ignition calculation, whereas the knock integral method ignores this effect [17].

Fuel's tendency to autoignite and cause knock is quantified in terms of an octane index (OI). The idea behind the OI development is that fuel's complex autoignition chemistry can be compared to a binary fuel blend which would have a predictable autoignition behavior. The binary blend used in these comparisons is a primary reference fuel (PRF), a blend of isooctane and n-heptane. As the percentage of isooctane increases in the blend, the fuel-air mixture is less prone to autoignition. The OI of a fuel is defined as the volumetric percentage of isooctane in the PRF that knocks at the same intensity at the same conditions [2, 18]. The OI depends on the engine operating conditions, and thus, it is measured at two standardized test conditions for fuel rating purposes. These two conditions are the Research and Motor Octane Number (RON and MON) tests. The octane scale is based on two paraffins, n-heptane and isooctane. The two main differences between the RON and MON tests are the intake air temperature and the engine operating speed. Modern engines have intake air temperatures that are well below the RON and MON tests [18].

The difference between the RON and MON is termed the sensitivity (S). The sensitivity of a PRF is 0. However, most commercial fuels have a sensitivity of about 8 [2].

$$S = \mathrm{RON} - \mathrm{MON} \tag{9.4}$$

The autoignition chemistry of non-paraffinic components in gasoline is different from that of PRF, and RON or MON describes the anti-knock behavior of the gasoline only at the RON or MON test condition [19]. Aromatics and olefins, however, tend to have S values that far surpass those of paraffins [20]. Figure 9.6 illustrates the variations of sensitivity with a different paraffinic fraction of different fuels.

Since the RON and MON are the OI of fuel at two set conditions, the OI can be interpolated from these values using a weighing factor (K). The true anti-knock quality of gasoline is best described by an octane index (OI) defined by Eq. (9.5) [21–24]:

$$\mathrm{OI} = (1 - K) \cdot \mathrm{RON} + K \cdot \mathrm{MON} = \mathrm{RON} - K \cdot S \tag{9.5}$$

The value of K is assumed to be independent of the fuel, and depending only on the engine's operating condition [21]. The value of K is zero for the RON test, and K is one for MON test. The value of K tends to become negative for the most knock-

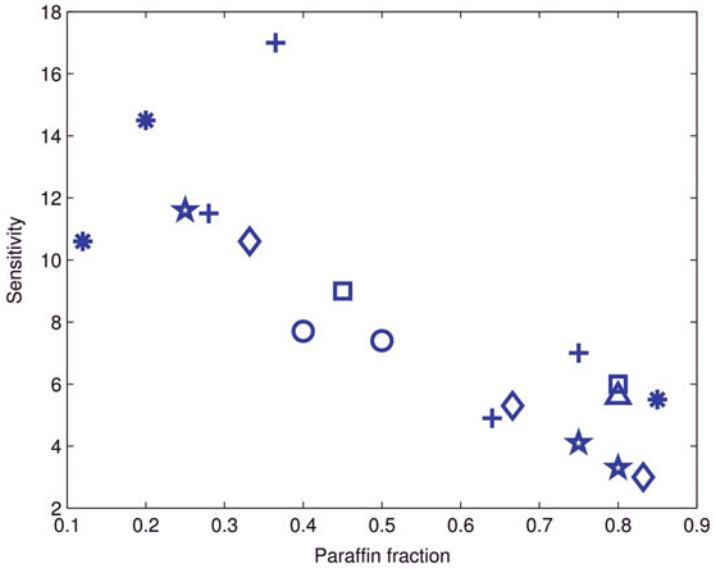

Fig. 9.6 Sensitivity variation with different paraffinic fractions of fuel [20]

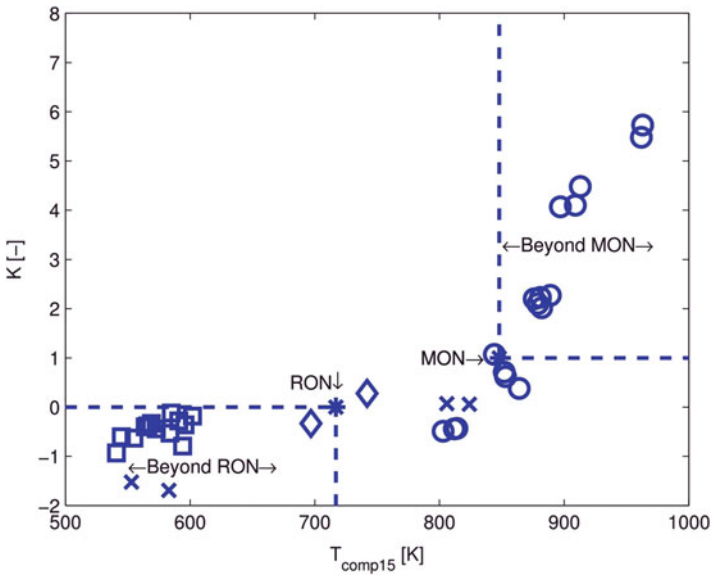

Fig. 9.7 Variation of K vs. T_{comp15} for different studies [20]

limited regions in modern SI engines [1]. There is a good correlation for K with the unburnt gas temperature (e.g., at a compression pressure of 15 bar (T_{comp15})). Figure 9.7 illustrates the variation of K with T_{comp15} from various studies [21–24]. At 15 bar, the K values are found to decrease from around 6 at 1000 K to 0 at

700–800 K, down to at 500 K [25]. For modern engines, much of the autoignition chemistry occurs in the transition region between high- and low-temperature combustion regimes, corresponding to end-gas temperatures between 775 and 900 K. The MON test captures the chemical kinetics of fuel autoignition in the high-temperature regime (above 900 K). Modern engines operate with end-gas temperatures well below the high-temperature regime, and hence the MON test temperatures should be lowered to better capture fuel autoignition chemistry in modern engines [18].

A study proposed that the octane scale based on primary reference fuels, mixtures of isooctane and n-heptane, can be replaced by a scale based on toluene/n-heptane mixtures (TRF, toluene reference fuels) for ranking practical fuels [19]. A calibration curve relating the toluene number (TN), the volume percent of toluene in TRF, to the head position at knock in the RON test is established. Another study developed a simple model which can be used to find the composition of a TPRF surrogate (a mixture of toluene, isooctane, and n-heptane) to match a given RON and sensitivity [26]. The RON and MON of the fuel describe knock behavior only at RON and MON test conditions. Fuels of different chemistry are ranked differently depending on temperature and pressure development in the end gas. In real engines, anti-knock quality of practical fuels depends both on fuel chemistry and on engine design and operating conditions.

Knock onset (KO) detection using in-cylinder pressure measurement is only possible in the time domain because the Fourier transform (frequency domain) does not preserve a signal's timing information [27]. There are a variety of methods for the determination of KO mostly based on the threshold value exceeded (TVE) method. The TVE method for knock onset detection uses the first crank angle where the high- or band-pass filtered pressure signal or the first or third derivatives exceeds a predetermined threshold as knock onset [13, 27]. This method is intuitive and simple; however, it typically detects the KO late by up to a few hundred microseconds (up to 3° CA for typical speeds) for weak to intermediate knock cycles because the threshold value needs to be set high enough to avoid false detection [27]. Additionally, these methods are either sensitive to the sampling rate or predict the crank angle late for the knock onset dependent on the predetermined threshold value [13]. For strong knock cycles, the TVE method detects knocking combustion within ±0.5° CA.

Knock onset detection methods have been proposed based on the first and third derivatives of the pressure signal [28, 29]. The first occurrence at which the first derivative of the pressure signal exceeds a threshold is denoted as KO, and the third derivative of low-pass filtered pressure signal is scanned for the highest negative value, and the corresponding crank angle is defined as KO. Another method is proposed to compute the knock onset based on the signal energy ratio (SER), which is presented as Eq. (9.6) [30]:

$$\mathrm{SER} \equiv \frac{\mathrm{SEPO}_{\mathrm{fwd}}^{2}}{\mathrm{SEPO}_{\mathrm{bwd}}^{1/2}} = \frac{\left(\int_{\theta_o}^{\theta_o+\Delta\theta} P_{\mathrm{filt}}^{2} d\theta\right)^{2}}{\left(\int_{\theta_o-\Delta\theta}^{\theta_o} P_{\mathrm{filt}}^{2} d\theta\right)^{1/2}} \tag{9.6}$$

This method is based on the signal energy of pressure oscillations (SEPO) and embodies a modified signal-to-noise ratio by looking both forward and backward in time. The $\Delta\theta$ was optimized to be 5°CA, $SEPO_{fwd}$ is the SEPO for the next 5°CA, and $SEPO_{bwd}$ is the SEPO for the previous 5°CA. The SER is calculated for a wide range of crank angles around TDC, and the knock onset is defined as the crank angle at which the SER function is a maximum. This method is inadequate for real-time knock detection, but for a posteriori diagnostic purposes, it is considered more accurate [27, 30].

9.2.2 Modes of Knock

Knock occurs when the autoignition of the unburned mixture takes place in the combustion chamber. There are a number of qualitatively different ways in which a nonuniform fuel-air mixture can autoignite [31, 32]. For fully homogeneous air-fuel mixture, the chemical reactions occur at the same rates in the entire mixture. The pressure rises rapidly and uniformly throughout the whole mixture when the reactions and the associated heat release rate become very fast. There are no propagating pressure pulses, and the combustion occurs essentially at constant volume. This mode of autoignition with no spatial gradients comprises a thermal explosion [31]. In real engine operating conditions, perfect homogeneity (of temperaure and fuel concentration spatially) is not possible to achieve. In real engine conditions, the gradients of temperature, mixture strength, and active radicals exist, which produce gradient in ignition delay of the charge. Large temperature gradients can occur through charge stratification, or near the walls. Temperature stratification may be required to ensure that the autoignition (even in the thermal explosion mode) does not happen instantaneously but over a few degrees of crank angle. Additionally, local hot spots or regions of enhanced chemical activity can develop because of the locally high-temperature or active species concentrations. Reaction develops more rapidly at a hot spot, and an autoignition front propagates outward from it. Localized ignitions occur at different instants at different positions [31]. Three modes (deflagration, thermal explosion, and developing detonation) of post-knock combustion have been identified due to the temperature and composition nonuniformity in the end gas (unburned charge) [33].

The local pressure buildup mechanism and modes of propagation are discussed in reference [10] using the first of law of thermodynamics in autoignition region. The local pressure that builds up in the autoignition region is the result of the competition between the heat release rate and the pressure relief due to the volumetric expansion of the burned mixture. Figure 9.8 illustrates the pressure buildup in the autoignition region of radius (R). Assuming burned gas as ideal gas, the pressure rise rate can be written by Eq. (9.7) by rearranging Eq. (7.56):

$$\frac{dP}{dt} = (\gamma - 1)\dot{q} - \gamma P \frac{\dot{V}}{V} \tag{9.7}$$

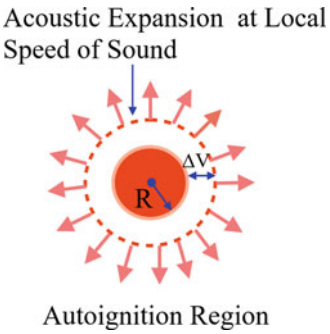

Fig. 9.8 Illustration of pressure buildup in autoignition region

where Q is heat release rate per unit volume and P and V are pressure and volume of autoignition region, respectively.

The local pressure will build up ($dP/dt > 0$) if the heat release term is large compared to the volumetric expansion term as shown in Eq. (9.8) [10]:

$$\dot{q} \gg \frac{\gamma}{\gamma - 1} P \frac{\dot{V}}{V} \tag{9.8}$$

For acoustic expansion with speed of sound "a," the volumetric change can also be written as Eq. (9.9):

$$\frac{\Delta V}{\Delta t} = 4\pi R^2 a \tag{9.9}$$

For a spherical autoignition region (Fig. 9.8), the criteria in Eq. (9.8) can be written as Eq. (9.10):

$$\dot{q} \gg \frac{\gamma}{\gamma - 1} P \frac{3a}{R} \tag{9.10}$$

It can be noted that the criterion on the size R of the autoignition region in relation to the volumetric heat release rate and the local speed of sound (a) is dependent on temperature.

For very small autoignition radius (R), very little pressure builds up, and thus, there will be no or very weak acoustic wave developed. The small R is associated with steep gradients (temperature and/or composition) in the nonuniform end gas, which appears as the regions of ignition are small islands. The radicals and high local temperature of the ignited region initiate a flame (a deflagration or subsonic propagation of the heat release front) in the unburned mixture. Figure 9.9 illustrates the combustion process during a super-knock initiated by preignition. The figure depicts the three stages of the combustion process including deflagration, detonation, and the resulting pressure oscillations. In the deflagration region, the chemical heat released leads to thermal expansion of the burned zone, which compresses the

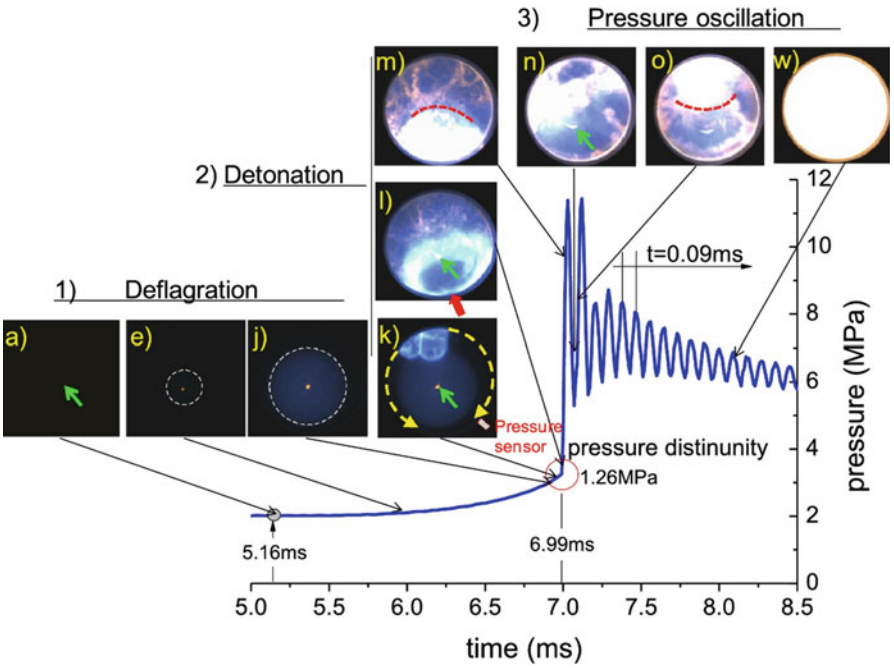

Fig. 9.9 Pressure trace with synchronous images showing three stages of the super-knock process [34]

surrounding unburned mixture to high pressure and high temperature [1]. The flame velocity is subsonic during deflagration, and transport processes involving simultaneous conduction of heat and diffusion of radicals govern the speed of combustion wave or flame.

For moderately large autoignition region (R) which satisfies the criteria in Eq. (9.10), significant local pressure builds up, and pressure waves (acoustic waves) or even weak shock waves are excited. This mode of combustion is termed "thermal explosion" in reference [33] due to the fast heat release from a sizable region. The pressure wave generated in this mode can be noisy or quite intense that can lead to damage of engine components by repeated pounding on the chamber surfaces by the local high pressure and high temperature [10]. The major manifestation of the pressure wave is the excitation of the engine structural vibration; hence, the phenomenon is term acoustic knock. However, these pressure waves are not strong enough to initiate Chapman-Jouguet type of denotation [35]. Depending on the temperature/composition nonuniformity in the end gas, there could be sequential autoignition of isolated regions or successive ignition of connected regions [31, 33]. Figure 9.10 illustrates the non-autoignition and sequential autoignition combustion modes in the end-gas region. In sequential autoignition mode, a flame is initiated at the outer boundary of the autoignited region. The flame speed is much

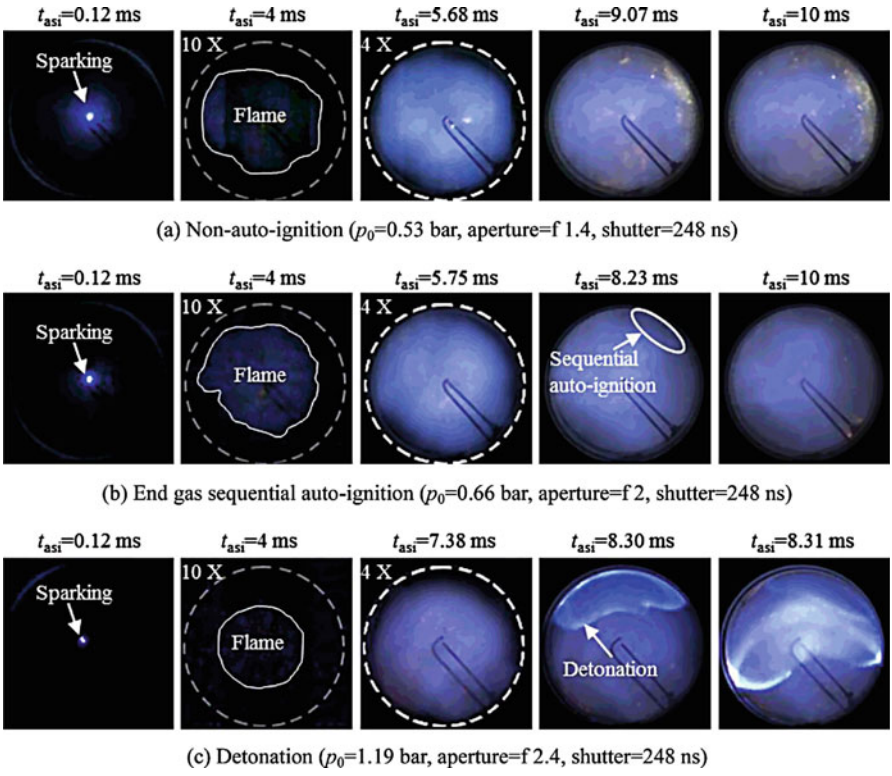

Fig. 9.10 Images of different end-gas combustion modes [36]

slower than that of the pressure wave, and there is no interaction between the heat release and the pressure wave.

For sufficiently large autoignition region (R), a significant pressure ratio between the local pressure and the end gas pressure is developed, and resulting shock wave could induce fast heat-releasing chemical reactions in the end gas at the wave front [10]. Alternatively, the successive ignition along a gradient may be rapid enough to create a combustion wave with speed comparable to the local pressure wave propagation (sonic) speed. Then there is a significant interaction between the heat release reaction and the pressure wave. The latter phenomenon has been termed developing detonation [31, 33]. In both cases, the local post-combustion pressure is higher than the isochoric value at the end-gas condition because of compression by the pressure wave [10].

The name "developing" detonation is little confusing with detonation. When combustion wave undergoes a transition from subsonic to supersonic speed, then it is known as detonation. The speed of detonation is not controlled by heat conduction and radical diffusion like deflagration. Rather, the shock wave causes the temperature and pressure to increase to such extent that it can lead to an explosion and a large

amount of energy is released during this process. McKenzie and Cheng [10] suggested that if definition of detonation is broaden from a combustion wave which is induced by the pressure wave to that which has significant interaction with the pressure wave, then both the normal and the developing detonation can be described by the term "detonation" since, in both cases, the combustion wave and the pressure wave travel together, and there is significant interaction between them. Detonation of end gas in super-knock condition is illustrated in Figs. 9.9 and 9.10.

The mode of combustion is affected by thermodynamic conditions (pressure and temperature) of end gas which is affected by several engine and operating parameters such as intake pressure, temperature, compression ratio, etc. The charge density can be used to represent the coupling effect of the ambient pressure and temperature ($\rho \propto p/T$), and it affects the end-gas combustion mode. Figure 9.11 illustrates the

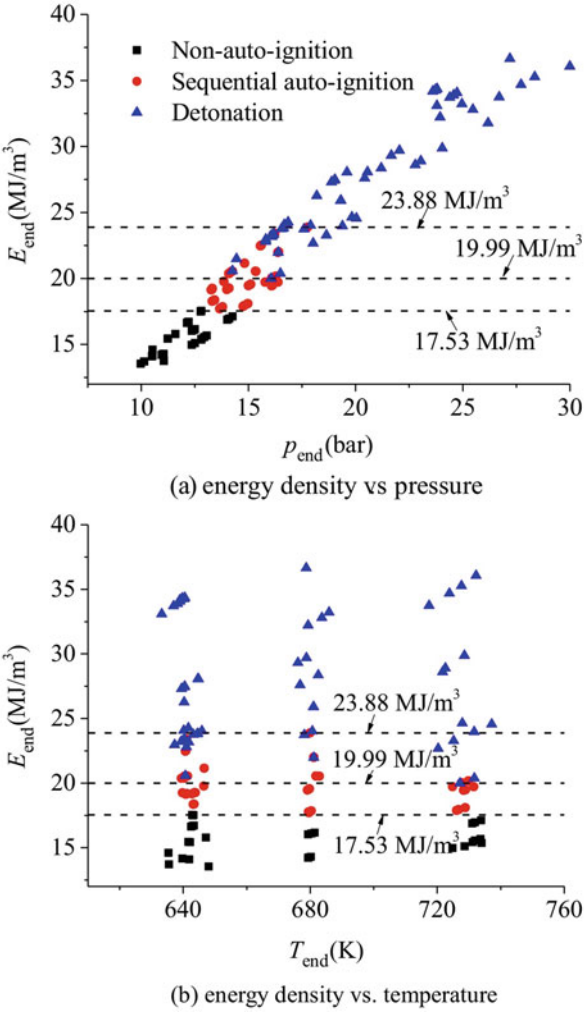

Fig. 9.11 Relationship between energy density at the end of compression and combustion mode [36]

relationship between energy density at the end of compression and combustion mode. The mixture density is shown as energy density (E_{end}) to consider the lower heating value of the mixture. The boundary between non-autoignition and autoignition modes is very clear and shown by the dashed line of 17.53 MJ/m^3 (Fig. 9.11). The figure shows that with an increase in energy density, the end-gas combustion mode gradually transits from sequential autoignition to detonation if the energy density exceeds 17.53 MJ/m^3. Only the sequential autoignition can be induced if the energy density is below 19.99 MJ/m^3, while the detonation always occurs if the energy density is higher than 23.88 MJ/m^3 [36].

A number of strategies may be adopted to avoid entering the into detonation mode of knocking combustion. A study proposed two dimensionless parameters, ε and ξ, for investigating the hot spot-induced combustion mode using the $\varepsilon - \xi$ diagram [31]. The ε is the ratio of the residence time of the acoustic wave in the hot spot to the short excitation time in which most of the chemical energy is released, and ξ is the ratio of the acoustic speed to the localized autoignitive velocity. Super-knock in boosted SI engines is investigated by the relative differences between the spatial distribution of ignition delay and the ignition wave propagation speed [37, 38]. In a particular situation, when an autoignition front is propagating from a hot spot and the autoignition delay time (τ_i), increases with the distance from the hot spot (r), the autoignition front propagates at a velocity relative to the unburned gas (u_a) that is characterized by Eq. (9.11), which can also be related to a temperature gradient:

$$u_a = \left(\frac{\partial \tau_i}{\partial r}\right)^{-1} = \left(\frac{\partial \tau_i}{\partial T}\frac{\partial T}{\partial r}\right)^{-1}. \tag{9.11}$$

When the temperature gradient attains a critical value, $(\partial T/\partial r)_c$, such that the autoignition front moves into the unburned mixture at approximately the acoustic speed (a), the front of the pressure wave generated by the rate of heat release can couple with the autoignition front. The fronts are mutually reinforced to create a damaging pressure spike propagating at high velocity in a developing detonation [31]. The critical temperature gradient for such a chemical resonance between the chemical and acoustic waves, with $u_a = a$, can be presented by Eq. (9.12):

$$\left(\frac{\partial T}{\partial r}\right)_c = \frac{1}{a(\partial \tau_i/\partial T)} \tag{9.12}$$

The actual temperature gradient is normalized by this critical value, and parameter ξ is defined by Eq. (9.13):

$$\xi = \left(\frac{\partial T}{\partial r}\right) \Big/ \left(\frac{\partial T}{\partial r}\right)_c = \frac{a}{u_a} \tag{9.13}$$

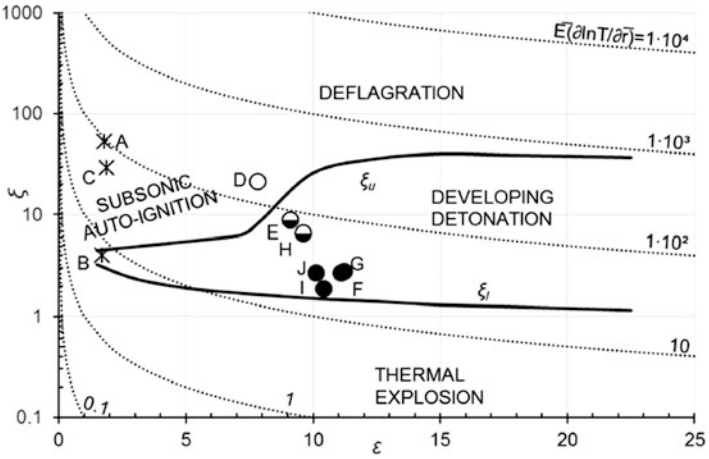

Fig. 9.12 ξ/ε regime diagram, for hotspot autoignition (increasing black fill of the symbols indicates the increasing severity of knock from no knock through mild knock to super-knock) [41]

In the case of $\xi \geq 1$, the pressure pulses run ahead of an autoignitive deflagration ($u_a \leq a$). Values of ξ are only readily known at the initial value, based on the initial boundary condition temperature gradient. In practice, heat conduction, species diffusion, and some reaction modify the initial boundary before autoignition occurs. It is demonstrated numerically that there are lower and upper limits, ξ_l and ξ_u, based on the initial boundary condition, between which a developing detonation can occur (Fig. 9.12) [31].

In severe knocking combustion, large mass fraction of the original charge is burned instantaneously to create a rapid increase of the pressure and rapid rate of change of the volume (dV/dt). The instantaneous sound pressure $p(t)$, at the distance d from the source, can be provided by Eq. (9.14) using acoustic theory [39]. The volumetric expansion rate of the hot spot with the area of the reaction front (A) propagating to the unburned gas at a velocity (u_a) is A^*u_a. The burned and unburned gas density difference should be accounted to calculate the net rate of the volume expansion as given in Eq. (9.15), where σ is the ratio of unburned to burned gas densities. Assuming a small spherical hot spot of radius r and differentiating Eq. (9.15) with respect to t give the volume expansion rate as stated in Eq. (9.16). The nondimensional form of pressure oscillation is given by Eq. (9.17) where $\xi = a/u_a$ [37, 38, 40]:

$$p(t) = \frac{\rho}{4\pi d}\left|\frac{d}{dt}\left(\frac{dV}{dt}\right)\right|_{t-t_a} \tag{9.14}$$

$$\frac{dV}{dt} = Au_a(\sigma - 1) = 4\pi r^2 u_a(\sigma - 1) \tag{9.15}$$

$$\left|\frac{d}{dt}\left(\frac{dV}{dt}\right)\right|_{t-t_a} = 4\pi r(\sigma-1)\left(2\sigma u_a^2 + r\frac{du_a}{dt}\right) \tag{9.16}$$

$$\frac{\Delta p(t)}{p} = \left[\frac{r\gamma}{d}(\sigma-1)\left(2\sigma\xi^{-2} + \frac{r}{a}\frac{d\xi^{-1}}{dt}\right)\right]_{t-t_a} \tag{9.17}$$

An additional parameter affecting the probability of a detonation is likely to be one associated with the rate at which chemical energy is unloaded into the developing acoustic wave. During detonation condition, there are large changes in density at the pressure front, and chemical energy can be fed into the developing strong pressure wave at a hot spot. Under these conditions, the principal energy release occurs during an excitation time (τ_e), which is orders of magnitude less than τ_i [38]. By using an excitation time for energy release energy (τ_e), another dimensionless parameter $\varepsilon = (r_0/a)/\tau_e$ is defined, which is a measure of the hot spot reactivity. Figure 9.12 illustrates the ξ/ε regime diagram, for hot spot autoignition which characterizes the modes of combustion. Conditions of developing detonation are marked with the upper and lower limit. No developing detonation is observed in two regions of the parameter space (Fig. 9.12). The first is when the mixture is close to homogeneity, and ξ is low. A low value of ξ also is aided by a small dependence of ignition delay on temperature $\partial\tau_i/\partial T$, which is a characteristic of paraffinic hydrocarbons. The second region of low detonability occurs at high values of ξ or spatial temperature gradient, but only in less reactive mixtures, with $\varepsilon < 10$ [31]. Reactive hot spots leading to autoignition/ knock can arise by a number of factors such as partial mixing with hot gas or burned products, heat transfer from hot surfaces, and turbulent energy dissipation in flowing reactants. The size of hot spots may be of the order of millimeters [41].

The detonation diagram identifies the knock-limited conditions. Figure 9.13 shows the rate of heat release in unburned charge (RoHR-u) and the detonation peninsula along with the calculated $\xi - \varepsilon$ data for different spark timings at constant initial NO content (287 ppm) in the mixture. The figure shows that advancing of spark timing increases the propensity for autoignition. The value of the first peak in the RoHR-u trace is not significantly affected by spark timings, and only position where the first peak occurs changes with spark timing (ST). The spark timing (ST = −11.5 CAD ATDC) seems to be engine knock limit, and further advancing of ST by 0.5 CAD leads to a transition from the regime of subsonic autoignition to the regime of developing detonation (Fig. 9.13) [42]. Further advancement of spark timing moves the $\xi - \varepsilon$ solution toward the lower limit of the resonance parameter (ξ_l) and slightly higher values of the reactivity parameter (ε). Figure 9.13 also depicts that knock-limited operating conditions typically shows the occurrence of two peaks in the RoHR-u. Hence, the RoHR-u trace can also be used for very first and rough estimation of the end-gas conditions with respect to knocking occurrence [42].

Typically, external EGR is used for the mitigation of knock in the engines. The EGR can also add the initial NO in the air-fuel mixture. The presence of NO in the charge strongly affects the knock onset [42]. Figure 9.14 illustrates the effect of

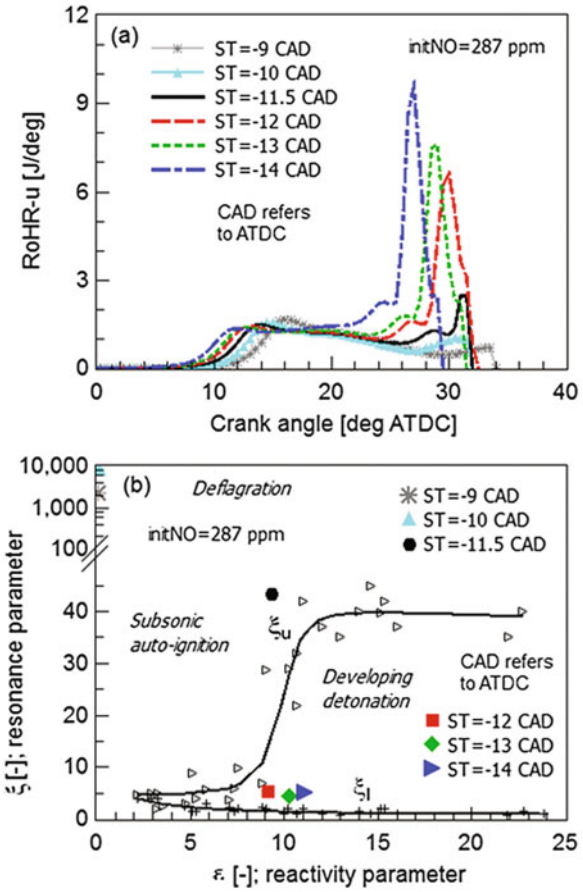

Fig. 9.13 (**a**) Rate of heat release in unburned charge (RoHR-u) and (**b**) the detonation peninsula [31] along with the calculated $\xi - \varepsilon$ data for different spark timings at constant initial NO content (287 ppm) in the mixture [42]

initial NO content in the mixture on knocking combustion mode. Figure 9.14 depicts that the RoHR-u is very sensitive to the changes of NO in the end gas. Generally, the reactivity of the charge is improved by increasing NO which is depicted by significantly higher values of the second peak of RoHR-u curve. Thus, the knock margin can be increased by lowering NO content in the charge.

9.2.3 Super-Knock and Preignition

To increase the fuel conversion efficiency, the SI engine design utilizes the downsized and turbocharged concepts. In turbocharged conditions, extremely high-intensity knock events informally described as "megaknock" or "superknock" are found to occur occasionally even when spark timings have been expressly chosen to avoid knock. Super-knock is a type of autoignition phenomenon

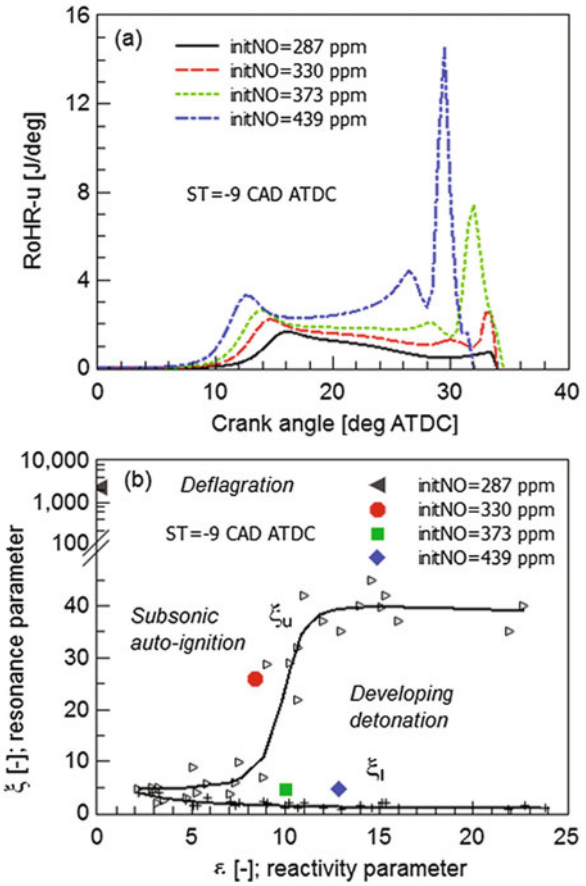

Fig. 9.14 (**a**) Rate of heat release in unburned charge (RoHR-u) and (**b**) the detonation peninsula [31] along with the calculated $\xi - \varepsilon$ data for different initial NO content in the mixture at constant spark timing [42]

that can occur in highly boosted SI engines under the conditions of low speed and high intake pressure. Additionally, super-knock events occur randomly with little direct relation with engine combustion control parameters, such as ignition timing, intake temperature, equivalence ratio, etc. Thus, typical knock mitigation techniques, such as retarding spark timing, cooling the intake charge, and enhancing heat transfer, are not very effective at eliminating super-knock [1]. Super-knock combustion can result into very high peak pressure (~30 MPa) and pressure oscillation (~10 MPa), which can significantly damage the cylinder or piston. Therefore, the super-knock occurrence is a major challenge in improving the fuel conversion efficiency of SI engine [43].

The super-knock combustion process is significantly different from traditional knocking process. Super-knock combustion can originate from the preignition in which a stable flame kernel is set off by a hot spot prior to the spark timing. The hot spot can possibly be induced by one of the following sources including fuel, particles, lubricant oil droplets, and surface ignition [44]. Additionally, the super-

knock combustion mechanism is constituted by hot spot-induced deflagration to detonation followed by high-pressure oscillation [34]. Super-knock with a high-pressure fluctuation is typically produced by the occasional preignition that might depend on the critical conditions of autoignition within the combustion chamber [38].

Figure 9.15 illustrates the super-knock, heavy knock, and normal combustion in an SI engine with the same spark timing of 8° bTDC. The figure shows that under the same operating conditions, normal combustion, conventional knock, and super-knock (spark ignition-induced super-knock and preignition-induced super-knock) appeared in different combustion cycles [43]. The spark timing retarded because of knock limit and the peak cylinder pressure is observed to be 2.98 MPa during normal combustion. In the super-knock caused by preignition (shown by red color), the peak pressure reaches up to 25 MPa along with a strong pressure oscillation with an oscillation amplitude of 13.1 MPa (Fig. 9.15) due to pressure wave propagation in the cylinder. The extremely high knock intensities can be explained in terms of developing detonation (Sect. 9.2.2). Super-knock induced by spark ignition is indicated by the black line in Fig. 9.15. In this mode, combustion follows the pressure profile of normal combustion for several crank angles after the spark timing, and compression of flame propagation leads to high pressure and temperature in the end gas (charge). The high-temperature and high-pressure in the end gas results in autoignition at 10° CA aTDC (Fig. 9.15), and pressure curve deviates from normal combustion. A severe pressure oscillation with an amplitude of 16.8 MPa occurs,

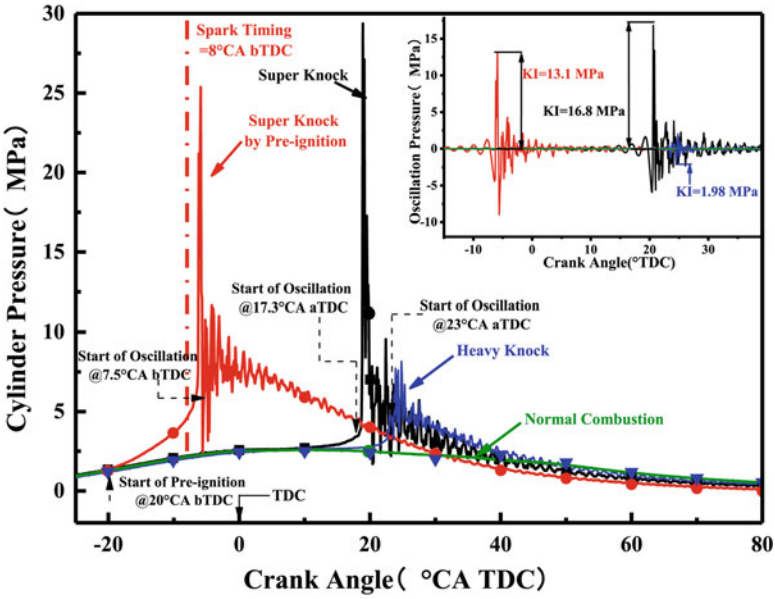

Fig. 9.15 Pressure traces and pressure oscillations for typical knock combustion at spark timing of 8° CA bTDC [43]

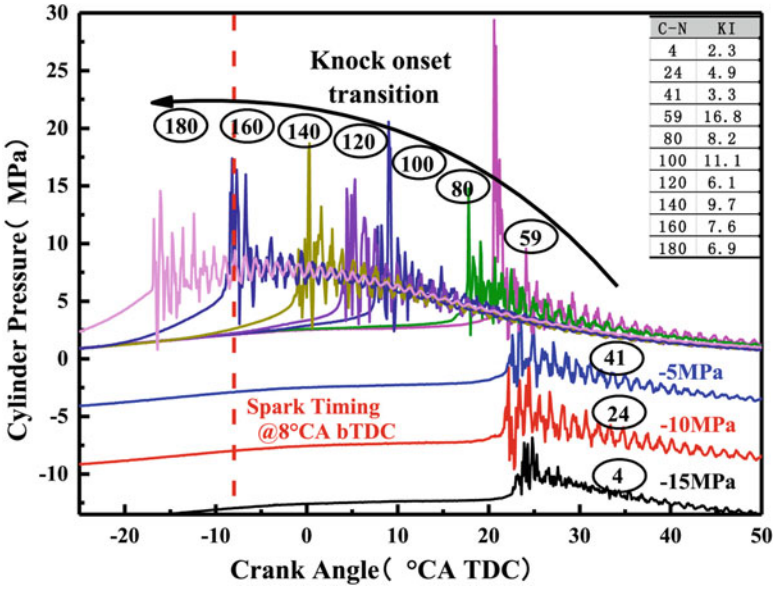

Fig. 9.16 Pressure traces for different cycles at a particular engine operating condition [43]

and knock intensity-based criteria meet the condition of super-knock [43]. Thus, the super-knock can be induced by spark ignition not only by preignition, and the difference between the two is the onset of super-knock.

The various combustion modes are sensitive to the different engine operating conditions, like cooling water temperature, wall temperature, cycle-to-cycle variations, etc. Figure 9.16 depicts the pressure trace and knock intensity (KI) of numerous typical super-knock combustion cycles between 200 consecutive engine cycles. To eliminate the cylinder pressure trace overlap, the pressure traces of super-knock cycle numbers of 4, 24, and 41 were offset by −15, −10, and − 5 MPa, respectively [43]. The figures illustrate that the onset of super-knock progressively advances with an increase in a number of cycles. This occurs possibly due to the enhancement of thermodynamic state of the end gas (charge) leading to shorter ignition delay. The onset of pressure oscillation advances with the number of cycles (80–180). The knock intensity values in different cycles are 8.2, 11.1, 6.1, 9.7, 7.6, and 6.9 MPa for cycle numbers 80, 100, 120, 140, 160, and 180, respectively (Fig. 9.16), which indicates the nonlinear relationship between knock onset and knock intensity. The knock intensity is governed by heat release rate of the unburned charge, and there is no direct relation between knock onset and intensity. The super-knock or knock combustion is dominantly induced by the spark ignition and is later induced by the preignition after several cycles. The results show that the occurrence of super-knock can be caused by spark ignition at particular thermodynamic conditions, not only by preignition [43].

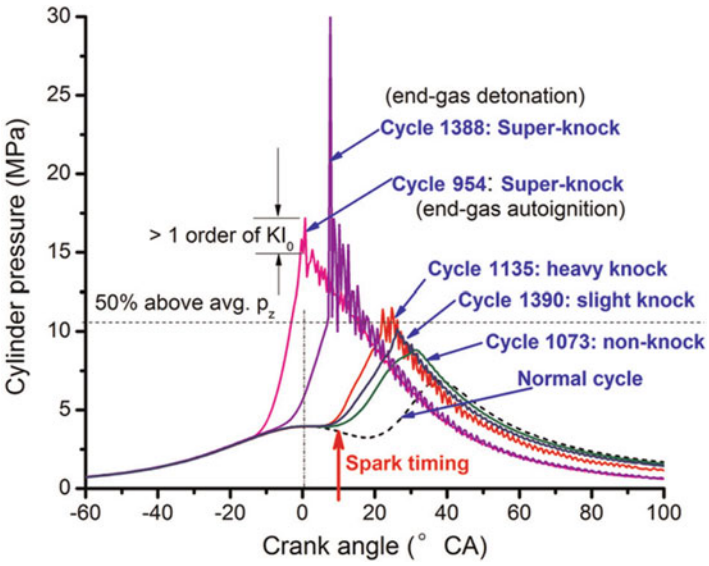

Fig. 9.17 Cylinder pressure profiles of typical preignition cycles and normal combustion cycle [4]

Although preignition can lead to the occurrence of super-knock combustion, it is not always necessary. Preignition can also lead to non-knocking, slight knock, or heavy knock combustion. Figure 9.17 illustrates the normal combustion cycle along with five different preignition lead combustion cycles. The figure shows that no engine knock is found in cycle 1073, which is a preignition cycle. However, it is typically expected that early preignition will lead to more severe engine knock combustion, which is not always true. The earliest preignition timing cycle 954 has lower knock intensity than cycle 1388 which has relatively late preignition timing (almost at the TDC). Furthermore, another study showed that the stationary autoignition events with a very early combustion phasing could take place without knocking [45], which is illustrated in Fig. 9.18. A reliable detection of this type of autoignitions by the knock control system is not guaranteed because the events occurred outside the knock detection window or the maximum permissible knock adjustment had already been used up [45].

For preignition, the temperature in a local area has to be increased sufficiently so that runaway chemical reactions start and an incipient flame is formed. The start of preignition was always associated with hot surfaces such as spark plug electrodes or hot spots on exhaust valves in older engines. However, in modern DISI engines, the flame initiation appears to be mostly away from internal surfaces. In any condition, the initial hot spot cannot be produced from the autoignition of the fuel-air mixture because the ignition delays are too large during the compression stroke when preignition is seen to be initiated [46]. Thus, fuels RON or MON is not expected to influence the onset of preignition. The most reasonable description is that, in modern engines, droplets of mixtures of oil and fuel fly into the combustion chamber

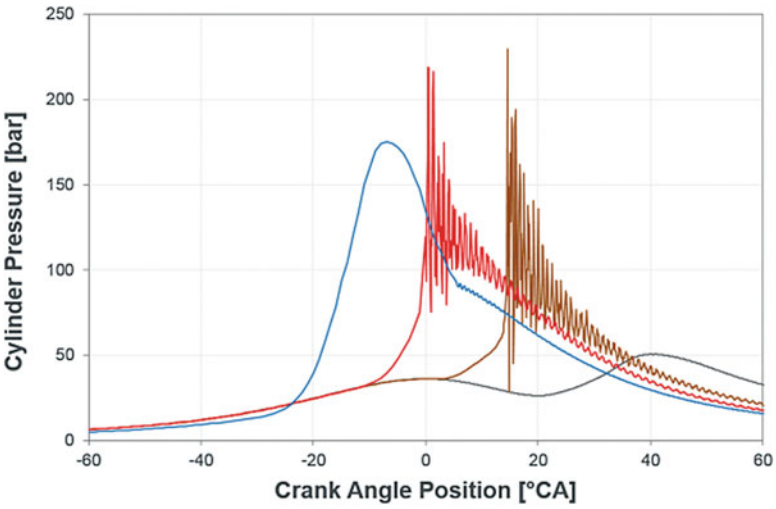

Fig. 9.18 Pressure profiles containing autoignition of different intensity/combustion phasing [45]

and mix with oxygen and autoignite, probably aided by some catalytic reactions, to form the initial ignition center. Lubricant, like diesel fuel, can be expected to be very prone to autoignition since it is made up large, straight chained hydrocarbons. There is also plausible experimental evidence that metallic lubricant additives, particularly calcium additives, promote preignition [46].

The abnormal combustion due to preignition at low engine speed is denoted as low-speed preignition (LSPI) in modern engines. The occurring pattern of LSPI is different from traditional preignition which is classified as a surface ignition. The causes of traditional one are unsuitable spark plug, heat spot of combustion chamber edge, or carbon deposit. In spite of them, LSPI occurs suddenly and continues for a while together with normal combustion. Then, it disappears and recovers to normal combustion [48].

Figure 9.19 summarizes mechanistic pathways for LSPI. The primary steps in LSPI are influenced by the extent of fuel adhesion on the liner wall and the properties of the lubricant oil that it interacts with on the liner wall. Although several pathways to LSPI are demonstrated, common to all is the involvement of lubricant oil-derived contents as preignition sources [48]. Figure 9.20 illustrates the well-known mechanism which assumes lubricant oil-containing droplets from piston crevice as a candidate of preignition source. Droplet of lubricant oil and fuel mixture, caused by adhesion of fuel spray on liner wall, will fly and preignite before spark ignition.

Studies have shown fuel/lubricant droplets to be a much more probable primary ignition source, and the effects of fuel and lubricant properties, as well as the interaction of fuel sprays and lubricating oil in the top crevice region, are investigated. Piston ring motion and turbulence variations have also been proposed as possible transport-related causes of the apparently stochastic nature of LSPI [49]. Preignition, which is also governed by stochastic processes, establishes a

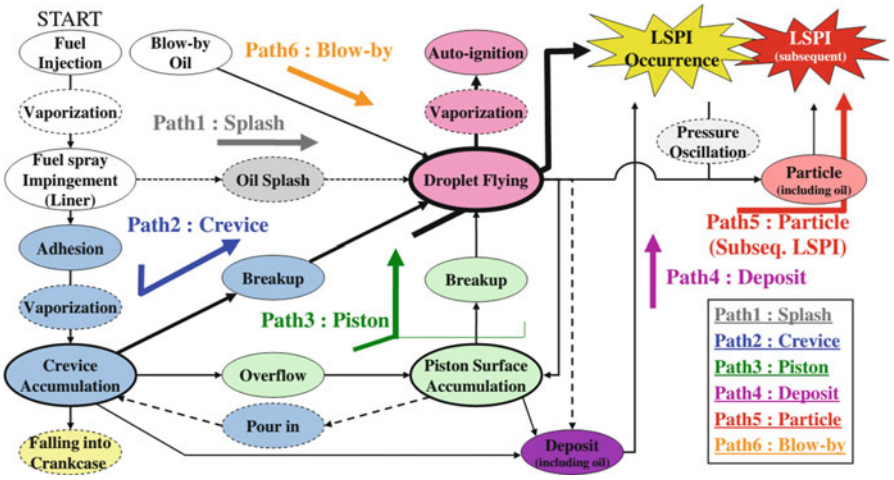

Fig. 9.19 Mechanistic pathways for low-speed preignition (LSPI) occurrence [47]

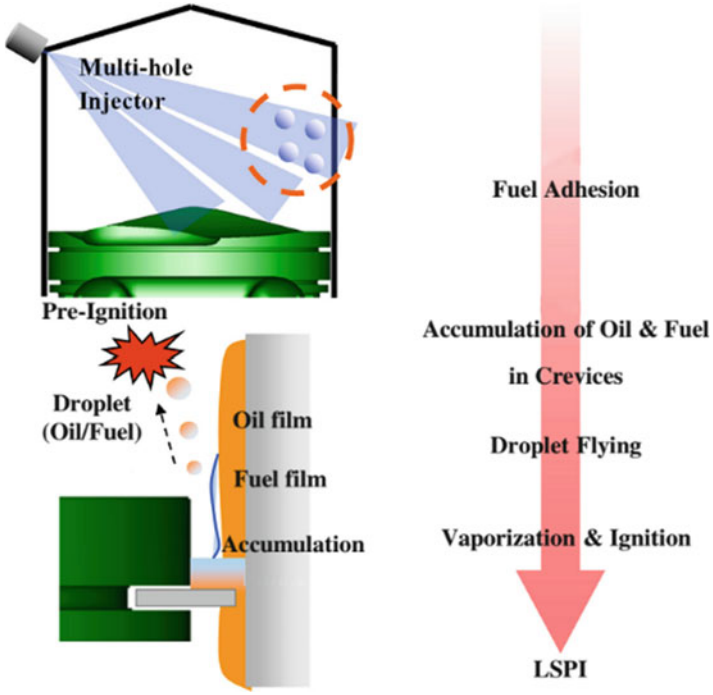

Fig. 9.20 Mechanism of piston crevice droplet triggered low-speed preignition [47]

flame before the spark fires and can cause knock onset to occur at high pressures and increase the chances of super-knock [46]. The preignition cycle occurs randomly maybe after thousands of cycles. Each individual LSPI cycle are typically characterized using three parameters: LSPI event start location, LSPI dwell duration, and LSPI intensity which is illustrated in Fig. 9.21a. LSPI dwell duration is denoted as the time required to achieve maximum pressure after preignition has started, and LSPI intensity quantifies the increase in maximum cylinder pressure relative to the maximum pressure of the median trace. Additionally, the total LSPI event number count and the cluster count of each fuel are also compared [49]. The LSPI dwell duration affects the intensity of super-knock. Figure 9.21b illustrates that longer LSPI cycles with a long dwell time exhibit negligible end-gas knock.

Figure 9.22 illustrates the distribution of preignition origins evaluated using high-speed camera. The figure shows the view through the endoscope into the combustion chamber, and each dot represents the origin of one optically detected preignition. The figure illustrates that the preignition origins are spread over a wide range in the plane of the cylinder head gasket. Detailed analyses presented no significant correlation between the engine operating conditions and the distributions of preignition origin [1]. Figure 9.22 also shows that there is no accumulation of preignition positions at any component of the engine cylinder. Preignition sometimes occurs in the form of intermittent sequences consisting of multiple cycles with preignition alternating with regular burning cycles [50].

Figure 9.23 presents the examples of preignition sites in different combustion cycles. The figure shows that in some cycles, several preignition locations occur in different positions approximately at the same time. Other cycles have movable preignition kernels, while preignitions outside of the viewing area of the combustion chamber can also be observed. It is found that the locations of autoignition can occur with enormous variability. In preignition condition, the flame propagation starts normally at the wrong location and additionally too early. These two effects of preignition flame provoke the fulminating knocking combustion [50]. Thus, the preignition should be avoided to improve the engine performance.

9.2.4 Characteristic Knock Frequencies

To analyze engine combustion during knocking, the determination of the characteristic frequency of pressure oscillation and the mode of oscillation is essential. During knocking combustion, intensive pressure waves and even shock waves are propagating and reflecting within the combustion chamber. The pressure waves in the cylinder may lead to resonance based on its natural frequency. Thus, cavity resonances in the combustion chamber further help describe the mechanism of knock or super-knock [43]. The engine knock frequencies are determined by the acoustic vibration modes specific to the combustion chamber. The high rate of heat is released during autoignition of charge in the combustion chamber. The energy release will in turn excite specific vibration modes. These modes cause pressure waves to traverse

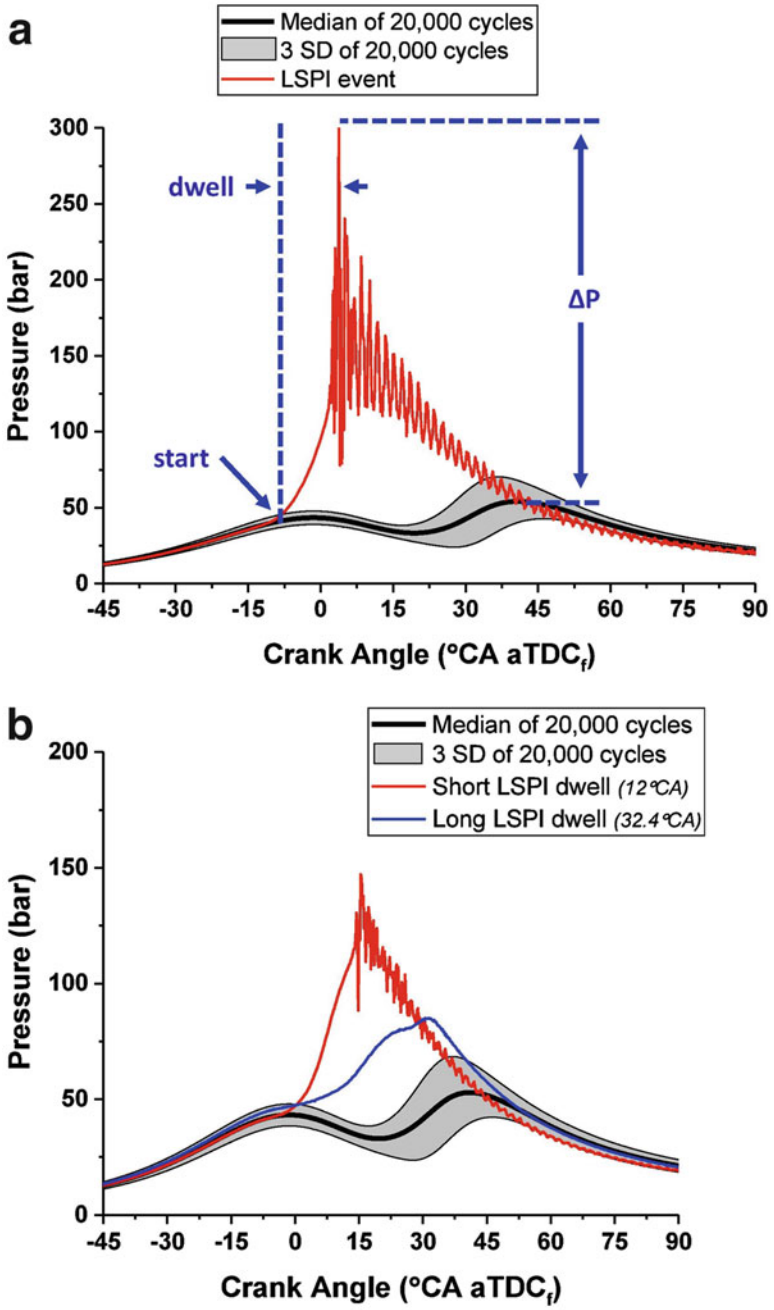

Fig. 9.21 (**a**) LSPI event characterization parameters and (**b**) effect of LSPI dwell times on knocking behavior [49]

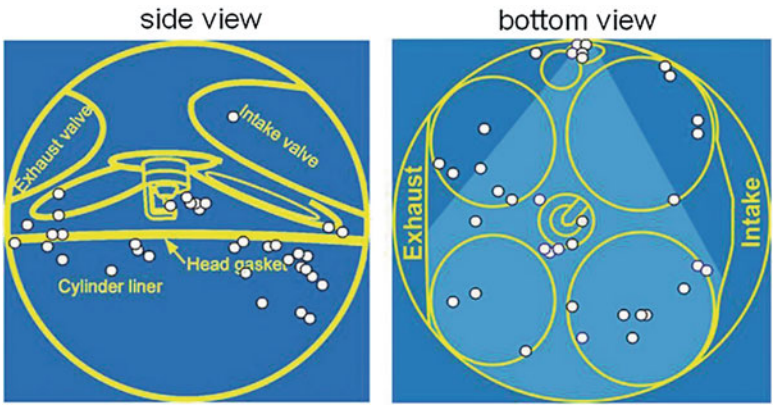

Fig. 9.22 Individual combustion cycles with several locations of preignition [50]

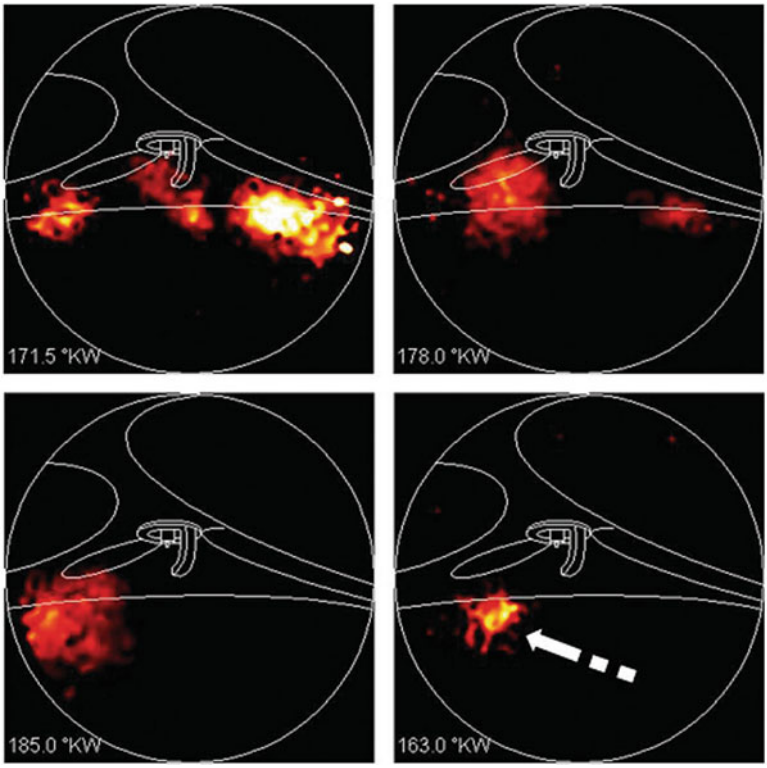

Fig. 9.23 Individual combustion cycles with different kinds of autoignition [50]

the combustion chamber at the local speed of sound, i.e., the acoustic velocity. The modes can be of both circumferential and radial nature, and the axial mode is typically negligible because the cylinder height at TDC is small compared with the engine bore diameter. Thus, the cavity resonance in the combustion chamber is dependent on shape size of the chamber and the local speed of sound [51].

Pressure resonance consists of high-frequency (few kHz) oscillations produced by pressure waves in the engine combustion chamber. The analytical solution of the wave equation can be used to determine the frequencies of different resonant modes. To estimate the resonance frequencies, Draper approach [52] can be used by a cylindrical combustion chamber assumption. Draper solved the wave equation with Bessel functions for a cylindrical geometry, and the resonance frequency is determined using Eq. (9.18). This equation relates the resonance frequency ($f_{i,j}$) with the cylinder diameter (D), the speed of sound (a), and a Bessel constant ($B_{i,j}$) related with radial modes. The axial modes (g) can be neglected because the frequencies associated with h (height of the combustion chamber) are too high.

$$f_{i,j} = a\sqrt{\frac{{B_{i,j}}^2}{(\pi D)^2} + \frac{g^2}{(2h)^2}} = \frac{aB_{i,j}}{\pi D} \tag{9.18}$$

The speed of sound can be determined by measuring the trapped mass m and the in-cylinder pressure P and estimating the instantaneous volume of the chamber V.

$$a = \sqrt{\gamma PV/m} = \sqrt{\gamma RT} \tag{9.19}$$

The specific heat ratio γ is a temperature-dependent variable, and it decreases as the temperature increases. Thus, local speed of sound depends on the crank angle position.

Figure 9.24 illustrates the variation of frequency content with a crank angle position in a HCCI engine. The evolution of the amplitude of the harmonics has been computed through a short-time Fourier transform (STFT) in the middle plot and through a Wigner distribution (WD) in the bottom plot. The frequency evolution derived from the cylindrical theory, by Eq. (9.18), is shown with a continuous black line, and three windows are highlighted with vertical lines [53].

A study used image-intensified high-speed video to determine the acoustic modes or pressure oscillations, in the HCCI combustion chamber by using an image analysis technique that extracts the different acoustic modes [54]. Figure 9.25 illustrates the amplitude of different frequencies depicting pressure oscillations or acoustic modes in the combustion chamber. Acoustic modes estimated from image analysis show good agreement with modes determined from measured cylinder pressure. In Fig. 9.25a, the nodes and antinodes of the four acoustic modes are apparent and illustrated schematically in Fig. 9.25b. This particular cycle is selected as an example as it is one of the few cycles where all four modes occurred [54]. Typically, the first circumferential mode (A1) is the dominant mode in HCCI combustion.

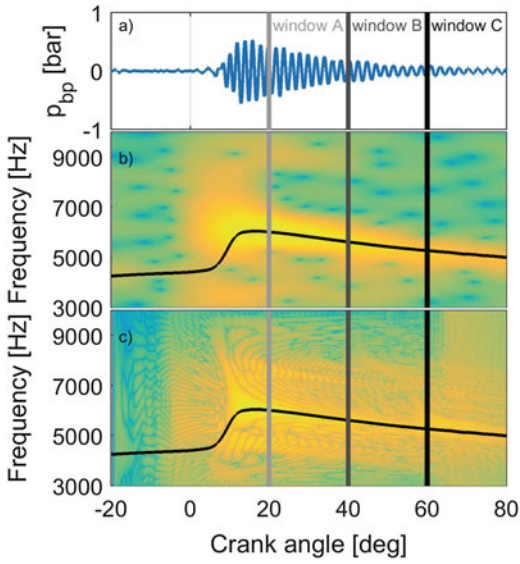

Fig. 9.24 Pressure oscillations using a band-pass filter between 3 and 10 kHz (top), STFT (center), and WD (bottom) of a cycle in HCCI combustion engine at 2000 rpm and low load [53]

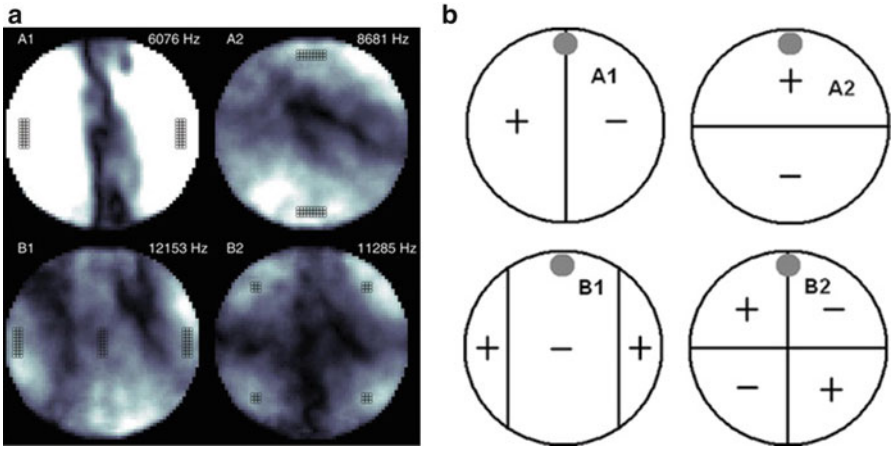

Fig. 9.25 (**a**) Spatially resolved amplitudes (a brighter color indicates higher amplitudes) of four different frequencies extracted from the high-speed video sequence showing the acoustic modes [54]. (**b**) Schematic of the four acoustic modes (lines represent the nodes) [54]

Another study on the HCCI engine concluded that the pressure waves manifested largest intensities for the first vibration mode, a mode suggesting radial propagation of the pressure waves in the combustion chamber [51]. The frequency for this mode was 4 kHz based on the pancake-shaped combustion chamber geometry. Altering the engine's combustion chamber geometry affects the properties of the oscillations. For the bowl-shaped combustion chamber geometry, the frequency for the first vibration mode was about 5 kHz. The directions of the pressure waves seem to be

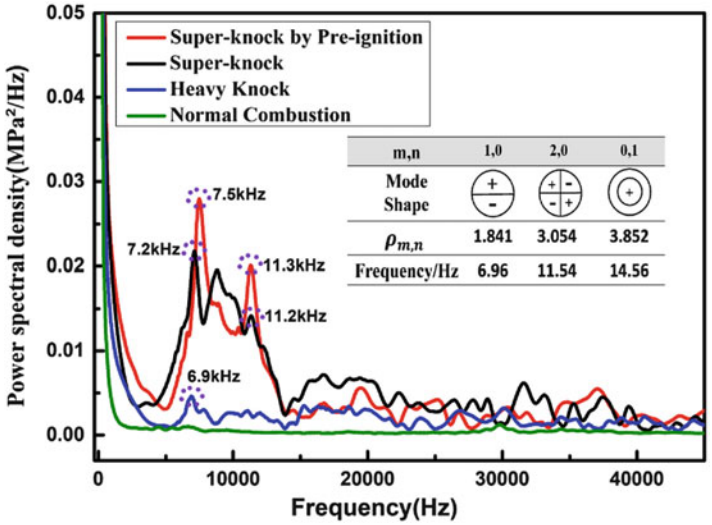

Fig. 9.26 Fast Fourier transform of in-cylinder pressure at different knock combustion modes in SI engine [43]

random. A consequence of this is that cyclic variations in the frequency domain are very prominent [51]. It was also found that the first two circumferential resonant frequencies that occur in the ranges of 2–4 kHz and 4–6 kHz accounted for more than 80% of the integrated power in the acoustic vibrational range for all HCCI, RCCI, and CDC cases. This suggests that in general, the audible ringing noise generated by compression ignition (CI) strategies on this engine platform primarily originates from circumferential pressure waves [55].

Figure 9.26 illustrates the fast Fourier transform (FFT) of cylinder pressure data for two typical super-knocks, the normal combustion and heavy-knock. The calculation of different resonance modes using characteristic frequencies reveals a correlation with experimentally measured frequency by using cylinder pressure data (Fig. 9.26). The characteristic frequencies of the first radial mode (1, 0) and the second radial mode (2, 0) have calculated resonant frequencies of 6.96 kHz and 11.55 kHz, respectively, which is consistent with the experimentally determined frequencies. Thus, the pressure wave generated during knocking resonated with the natural frequency of the engine combustion chamber to enhance the pressure wave energy, which leads to strong pressure oscillation [43]. However, the high energy in the high-frequency part during the super-knock conditions cannot be explained by acoustic theory. Therefore, it can be speculated that the pressure wave caused by super-knock may be a shock wave or detonation wave [43].

The combustion mode of the CI diesel engine is mostly the diffusion combustion. However, premixed combustion dominates the reactions in the preliminary stage of diesel combustion, and thus, the pressure oscillation is still an important part of the combustion process in diesel engine [56]. Modern diesel engines are typically using

the multiple injections in one cycle. The pressure oscillations (frequency content) are typically dependent on engine load, engine speed, and injection timings. In the diesel engine with pilot-main injection strategy, the pilot injection plays a significant role in every combustion stages. The amplitude of pressure oscillation in pilot injection combustion (PIC) is the maximum, and the proportion of oscillation energy in PIC is significantly high. Figure 9.27 shows the time-frequency distribution and heat release rate at different engine loads. The figure shows that there are significant differences between the time-frequency distribution of the pressure oscillation at full-load and half-load operating conditions. At full load, the oscillation energy is mainly distributed in 13–16 kHz, while that under half load is distributed in a lower frequency band of 4–10 kHz. The pressure oscillations start at the beginning of pilot injection combustion at both the engine loads.

Figure 9.28 shows the time-frequency distribution of the pressure oscillation with a main injection advanced angle (MIAA) of -10° CA and -5° CA, respectively. The oscillation components below 10 kHz attenuate with injection timing of -10° CA to -5° CA, while those at 12–18 kHz are enhanced. Additionally, the oscillation energy around 12 kHz in the post-combustion stage almost disappears. The main pressure oscillation energy distributing between 12 and 18 kHz from the early pilot injection combustion to main injection combustion also moves to a slightly higher frequency band with the advance of MIAA [56]. Study summarizes that the advance of the MIAA not only increases the amplitude of pressure oscillation in the time domain but also amplifies the signals at main oscillation frequency band (12–16 kHz), which is evident from cylinder pressure signal [56].

9.3 Cylinder Pressure-Based Knock Analysis

The detection of the abnormal combustion (knock) onset and the determination of knock intensity are crucial issues in engine and fuel development. Various methods have been proposed and used for the detection of knock onset and intensity such as methods based on (1) cylinder pressure analysis, (2) block vibration analysis, (3) gas ionization analysis, and (4) heat transfer analysis [57]. The cylinder pressure-based method allows direct measurements of primary knock effects and detailed investigations on the abnormal combustion process. This is the most widely used method in laboratory tests for engine and fuel development. However, the necessity of one sensor for each cylinder and the high cost of the pressure transducers limit the use of this detection method to laboratory research, while most of the techniques that are currently employed on mass-produced engines for knock detection and control are based on engine block vibration analysis. The high-frequency pressure oscillations inside the cylinder, caused by abrupt end-gas autoignition, are transmitted through the engine structure, thus causing vibrations that can be detected by means of an accelerometer installed on the engine block. The knock detection methods involve different signal processing methods and algorithms depending on the sensor used for analysis.

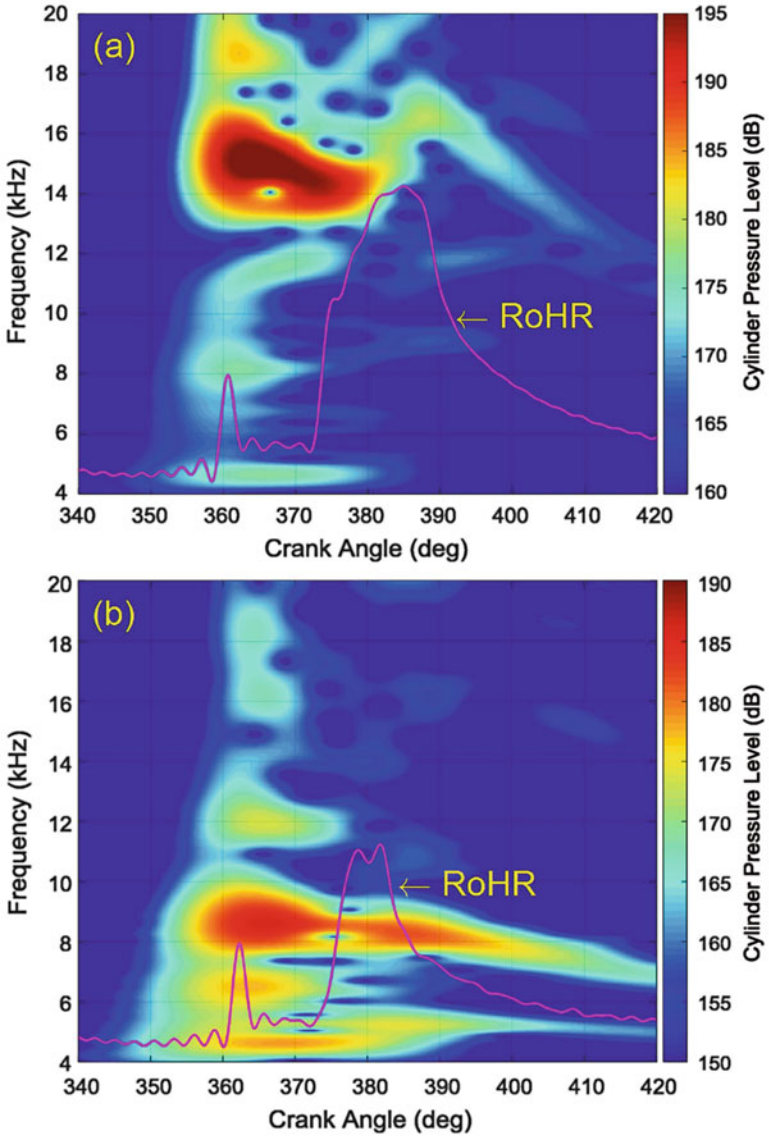

Fig. 9.27 Time-frequency distribution of the in-cylinder pressure for (**a**) full load and (**b**) half load at 1800 rpm [56]

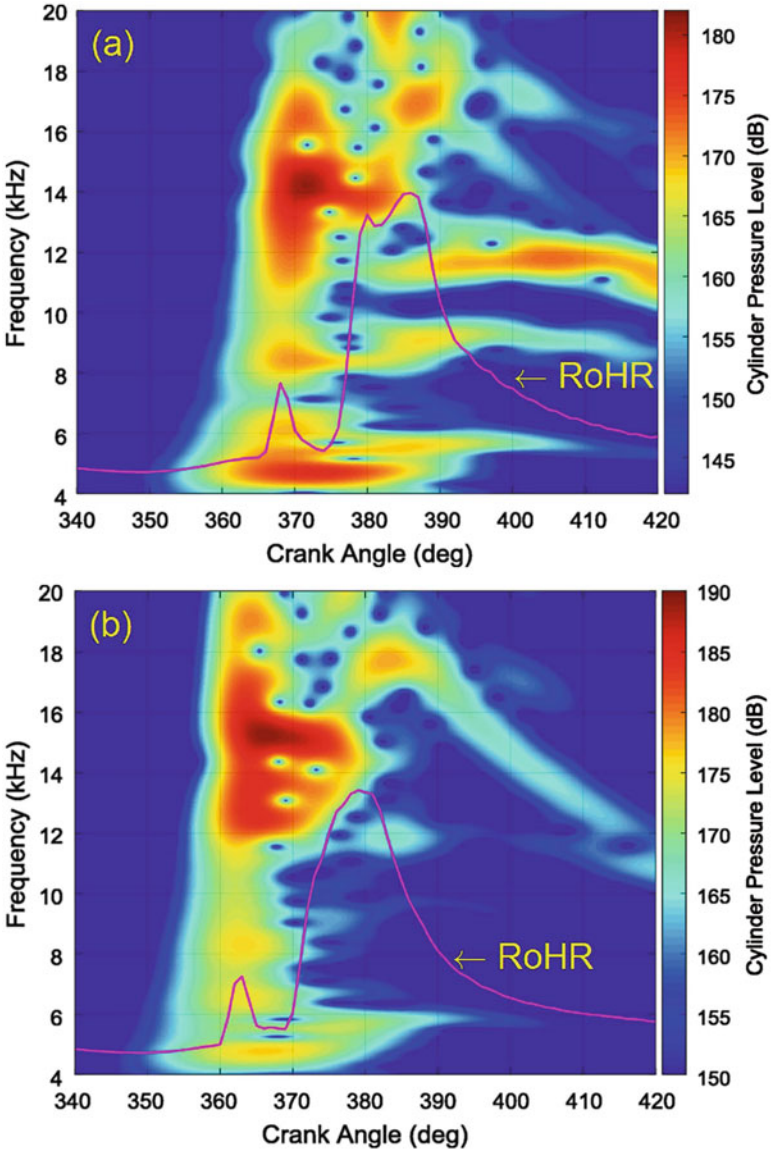

Fig. 9.28 Time-frequency distribution of the in-cylinder pressure for main injection advanced angle (**a**) −10° CA and (**b**) −5° CA at full load and 1400 rpm [56]

9.3.1 Signal Processing

Before calculating knock pressures and intensities from the measured cylinder pressure data, it is essential to ensure that the signals are free from unwanted effects such as transducer and it's installation cavity resonance, signal noise, and signal aliasing. Particularly, it is important to check when a relatively low sampling frequency is being used (mainly at low engine speed with crank angle based measurements). Non-flush mounting may lead to the problems with either cavity resonance or low sensitivity to the knock vibrations. Additionally, it is important to ensure that the transducer is actually producing signals when the engine is knocking and that these signals are at frequencies corresponding to the main acoustic vibration modes [58].

Sampling (or acquisition) frequency is an important parameter that needs to be considered while measuring cylinder pressure data for knocking combustion analysis. The acquisition frequency is required to ensure that the raw curve is sampled at a high enough rate that none of the high-frequency components are lost due to aliasing or under-sampling of the signal [5]. Generally, higher frequency that can be used is better, but the absolute minimum is set by the Nyquist criterion which suggests at least twice the highest frequency of significance needs to be used. Although digital filters and FFT algorithms may need even higher frequencies to function correctly. Since knock frequencies for the different modes are typically up to 20 kHz, which means an absolute minimum of 40 kHz sampling frequency requirement assuming that higher resonances and vibrations are not present. Typically, for crank angle-based cylinder pressure measurement, the resolution of the angle encoder is the most important factor. The calculated knock intensity is reduced when coarser crank angle resolution is employed, especially at low engine speeds, and a resolution of 0.2° or better resolution is suggested for routine knock measurement [58]. The disadvantage of high sampling rates is that a higher specification data acquisition system is required and a greater volume of data is acquired for processing and perhaps storage.

The effect of sample size also affects the knock intensity calculation and analysis. The variability of peak knock pressure data is very large, and a sample size of approximately 1000 cycles is recommended for the calculation of knock intensity [58]. Another important parameter which has a significant effect on the volume of data to be processed is the knock window. In addition to the filtering of the measured raw pressure data, the dataset is often windowed, which means that it is acquired only within a specific crank angle range on the pressure curve where knock typically occurs. The cylinder pressure data outside the window range will then be ignored, or acquired at a lower crank degree resolution, in order to optimize the available memory on the acquisition hardware [5]. A knock window crank angle range of TDC to 40° ATDC is recommended for general applications although most peak knock pressures should occur between 10° and 30°A TDC [58].

Pressure transducers should have a high natural frequency to prevent knock-induced transducer resonance, and typically a natural frequency above 100 kHz is recommended. The pressure transducer should ideally be flush mounted (Chap. 2) to avoid resonance in the connecting passage; long connecting passages must be

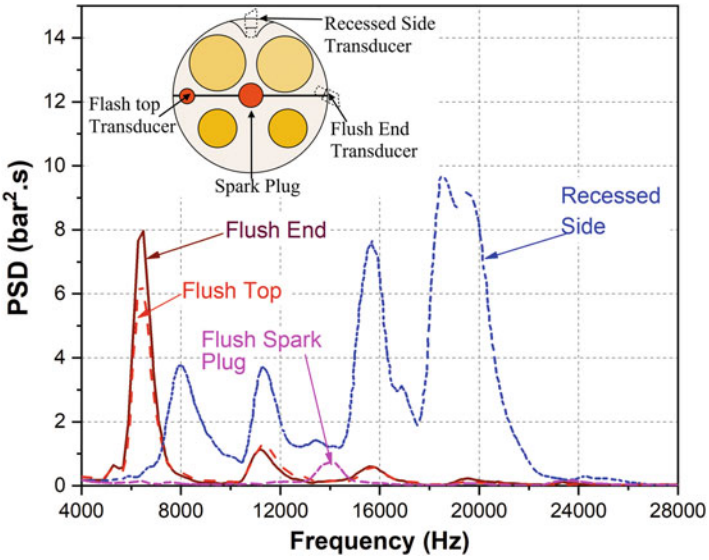

Fig. 9.29 Comparison of the power spectral densities from the four different transducers at the same engine operating conditions (adapted from [58])

avoided. Figure 9.29 illustrates the effect of flush and recessed mounting as well as the effect of sensor location on frequency measurement. The pressure transducer mounting position has a significant effect on the magnitude and characteristics of the knock signals obtained and, thus, the calculated knock pressures and intensities. Location of the transducer at the center of the combustion chamber has been shown to give low sensitivity to the main knock vibration modes [58]. To measure the maximum pressure oscillations, the position of the pressure transducer should be far from the center of the combustion chamber, however, not close to the quench zone.

9.3.2 Knock Indices

The knock-detection methods based on in-cylinder pressure analysis can be classified as methods based on (1) the evaluation of a single pressure value, (2) pressure derivatives, (3) frequency domain manipulations, and (4) heat release analysis [57]. Two main important parameters related to engine knock analysis is knock onset and its intensity, which can be evaluated using different methods and sensors. Figure 9.30 illustrates the different knock intensity (KI) metrics used for analysis in different engine combustion modes. The knock intensity calculation can be performed in the time domain or in the frequency domain. Further, the KI can be based on the pressure signal and its derivatives or on the heat release rate and its derivatives. Finally, knock intensity metrics can be based on a single value, (for example, the maximum value of a quantity) or an average or integrated value

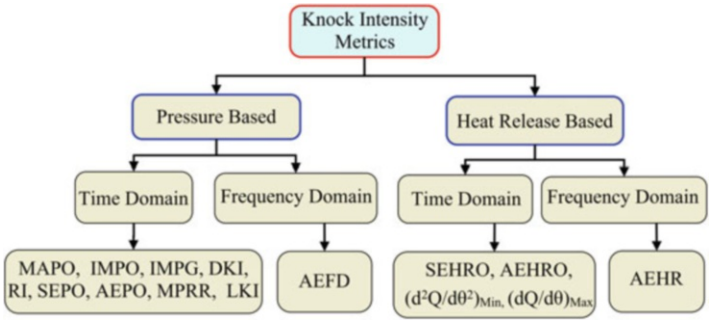

Fig. 9.30 Various knock intensity parameters for reciprocating engines

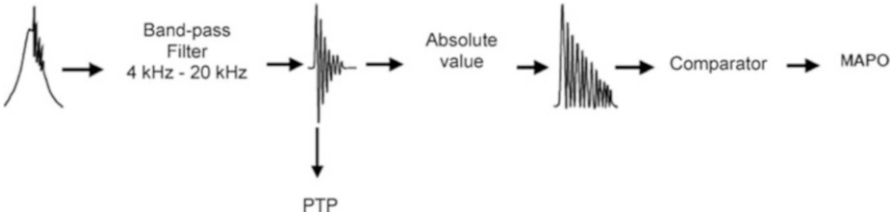

Fig. 9.31 Illustration of MAPO calculation method using in-cylinder pressure signal [60]

[30]. All time-domain knock metrics are typically based on a filtered pressure trace; either high- or band-pass filtering is performed to eliminate the low-frequency content of the signal associated with compression and the standard flame propagation heat release. Thus, filter characteristics such as the filter type and order, its roll-off characteristics, etc. (Chap. 5) affect the results of knock intensity calculations.

9.3.2.1 Pressure-Based Methods

During knocking combustion, the sharp pressure peak usually occurs, and thus, the simplest way to detect and characterize knock can be by the peak pressure itself [57, 59]. However, only high knock intensities can be reliably detected using this method, and the physical quantity measured is significantly affected by the engine parameters and operating conditions. A more effective knock index can be estimated by using the increase of pressure from the normal combustion conditions. The determination of the knock-related pressure peak from the normal pressure curve corresponds to the band-pass filtering of the pressure signal over the knock-characteristic frequency range. The most common time-domain pressure-based method to characterize KI is often known as the maximum amplitude of pressure oscillations (MAPO). The peak-to-peak (PTP) value of pressure oscillations is also used to quantify the KI. Figure 9.31 illustrates the calculation methods of PTP and MAPO.

The cylinder pressure signal is measured in a time window around TDC (from θi to $\theta i + W$) that is filtered by a band-pass filter 4–20 kHz to obtain the knocking pressure oscillations [60]. In another study, the high-frequency component was determined by first applying an optimized moving average process to smooth out most of the higher-frequency component and then subtracting the smoothed pressure curve from the original data to generate the high-frequency knocking pressure wave [58]. Two significant advantages of using the moving average smoothing routine instead of a high-pass digital filter are that it should be more tolerant to the coarser crank angle resolution (i.e., lower sampling rate) and that it captures all knock mode signals. The smoothing algorithm is also numerically very efficient.

The MAPO calculation can be mathematically represented by Eq. (9.20):

$$\text{MAPO} = \max\{P_{\text{filt}}\}|_{\theta i, \theta i+w} \tag{9.20}$$

Single value can be affected by noise, and it does not signify the duration of knock or further oscillation. Integral-based methods are used to represent the average value of pressure oscillation. This method involves summing up of the individual amplitudes of pressure oscillations to quantify the magnitude of knock and is typically referred as integral of the modulus of pressure oscillations (IMPO) [3]:

$$\text{IMPO} = \frac{1}{N}\sum_{1}^{N}\int_{\theta_i}^{\theta_{i+w}} |P_{\text{filt}}| \cdot d\theta \tag{9.21}$$

where N is the number of computed cycles.

Another pressure-based method of knock intensity is defined from the signal energy of pressure oscillations (SEPO), which is determined by integrating the square of P_{filt} over that crank angle window from knock onset, θ_0, to $\theta_0 + \Delta\theta$ [30]:

$$\text{SEPO} = \int_{\theta_0}^{\theta_0+\Delta\theta} \{P_{\text{filt}}\}^2 \cdot d\theta \tag{9.22}$$

where $\Delta\theta$ is typically 5–20 CAD.

A similar method is to average the signal's energy over $\Delta\theta$; this method is called average energy of pressure oscillations (AEPO) [30, 40]:

$$\text{AEPO} = \frac{1}{\Delta\theta}\int_{\theta_0}^{\theta_0+\Delta\theta} \{P_{\text{filt}}\}^2 \cdot d\theta = \frac{\text{SEPO}}{\Delta\theta} \tag{9.23}$$

A dimensionless knock indicator (DKI) is developed from existing knock indices (IMPO and MAPO) [61] which is calculated by Eq. (9.24):

$$\text{DKI} = \frac{\text{IMPO}}{\text{MAPO} \cdot W} \tag{9.24}$$

where W is the width of the computational window. The DKI is the ratio between two values that can be interpreted as two surfaces. The DKI value will decrease with the increase of KI independent of the engine geometrical characteristics and settings.

The pressure signal can be decomposed into a series of harmonic waves using a Fourier transform. The frequency range spans $0 \leq f \leq f_{\text{Nyq}}$, where f is frequency and f_{Nyq} is the Nyquist frequency given by $f_s/2$ with f_s as the sampling frequency of data acquisition. Since Fourier transform of a signal is a complex-valued function, the real-valued power spectrum needs to be used instead, which has units of kPa^2/Hz for pressure reported in kPa [30]. Naturally, the result comes as energy, and thus, the average energy of pressure computed in the frequency domain, over the range of frequencies defined by $f_1 < f < f_2$, is given by Eq. (9.25):

$$\text{AEFD}_{f_1-f_2} = \int_{f_1}^{f_2} \wp(f) \cdot df \tag{9.25}$$

where $\wp$ is the pressure power spectrum.

9.3.2.2 Pressure Derivative-Based Methods

The pressure rise rate (PRR) can be used for both knock onset detection and knock intensity measurements as it is greatly increased by end-gas autoignition. Even though the change in the pressure first derivative is well related to the amount of the cylinder charge that undergoes autoignition, the several knock-independent factors, which can affect the PRR, represent the greatest disadvantage of this method [57]. Maximum pressure rise rate (MPRR) is used to limit high load boundary or knock boundary in HCCI engines [62]:

$$\text{MPRR} = \left(\frac{dP}{d\theta}\right)_{\max} \tag{9.26}$$

Alternative knock indicators based on further pressure derivative have been proposed. For example, due to the abrupt curvature change which accompanies the sharp knock pressure peak, the minimum value position of the third derivative of cylinder pressure can be used as a knock indicator [57, 63].

Based on the understanding of the energy associated with pressure oscillation in HCCI engine, Eng [64] proposed another metric called ringing intensity (RI) by using maximum pressure ($P_{\max}$), maximum temperature ($T_{\max}$), and MPRR in the cylinder. The RI is given by Eq. (9.27):

$$\text{RI} = \frac{\sqrt{\gamma R T_{\max}}}{2\gamma P_{\max}} \left[\beta \left(\frac{dP}{dt}\right)_{\max}\right]^2 \tag{9.27}$$

This metric is commonly used for knock intensity evaluation in low-temperature combustion mode engines [62].

Integral of the modulus of pressure gradient (IMPG) is also defined similar to IMPO for KI calculation and represented by Eq. (9.28):

$$\mathrm{IMPG} = \frac{1}{N}\sum_{1}^{N}\int_{\theta_i}^{\theta_{i+w}}\left|\frac{P_{\mathrm{filt}}}{d\theta}\right|\cdot d\theta \tag{9.28}$$

9.3.2.3 Heat Release Analysis-Based Methods

The intense local heat release (due to end-gas autoignition) causes a substantial shift from the normal combustion heat release profile. Thus, heat release rate can also be used as knock indicators. The detailed calculation method of heat release is presented in Chap. 6. Analogous to the pressure-based metrics, knock can be defined as the maximum amplitude of heat release oscillations (MAHRO), signal energy of heat release oscillations (SEHRO), and average energy of heat release oscillations (AEHRO), which can be defined by Eqs. (9.29) to (9.31) [30, 40]:

$$\mathrm{MAHRO} = \max\left\{\left(\frac{dQ}{d\theta}\right)_{\mathrm{filt}}\right\} \tag{9.29}$$

$$\mathrm{SEHRO} = \int_{\theta_0}^{\theta_0+\Delta\theta}\left(\frac{dQ}{d\theta}\right)_{\mathrm{filt}}^{2}\cdot d\theta \tag{9.30}$$

$$\mathrm{AEHRO} = \frac{1}{\Delta\theta}\int_{\theta_0}^{\theta_0+\Delta\theta}\left(\frac{dQ}{d\theta}\right)_{\mathrm{filt}}^{2}\cdot d\theta = \frac{\mathrm{SEHRO}}{\Delta\theta} \tag{9.31}$$

Because of linearity, the filtered heat release can be acquired either by using the measured pressure and filtering the heat release or by filtering the pressure before calculating the heat release [30].

In the frequency domain, the average energy of the heat release (AEHR_{f1-f2}) can be defined by Eq. (9.32) similar to pressure-based metric:

$$\mathrm{AEHR}_{f_1-f_2} = \int_{f_1}^{f_2} dQ(f)\cdot df \tag{9.32}$$

A study concluded that methods based on a calculated heat release are redundant with other metrics [30]. It is also demonstrated that the superposition of multiple resonant waves can lead to interference and beating phenomena, which render the magnitude of the resulting time-domain signal not representative of the total energy

of the base signals. As such, single-value metrics, e.g., MAPO, can be biased. Integrated energy-based quantities provide the most bias-free estimates of the knock intensity. The integration can be performed either in the time or frequency domain [30].

9.4 Methods of Knock Detection and Characterization

Knocking combustion in the reciprocating engine cannot be precisely predicted due to its random nature. The random nature of engine knocking is created by the cyclic pressure fluctuations as well as some unobservable effects, such as residual mass variations or temperature hot spots [65]. Thus, an accurate prediction of engine knocking is almost unaffordable for real applications. Presently employed knock control algorithms are based on the combination of open-loop control actions with some stochastic rules, which allows adapting the engine operation on the basis of the knock detection events in the previous combustion cycles. The engine knock detection is essential for conventional controller performance because failure in knock detection can result in engine damage and a false knock detection of particular cycles can lead to a reduction in the engine efficiency. For commercial applications, ion sensors or accelerometers are used. However, knock detection methods based on cylinder pressure are the most precise. Most of the methods based on measured cylinder pressure quantify the pressure oscillations in the time domain or frequency domain for engine knocking analysis.

Engine knock prediction methods typically focus on the two important attributes, namely, (1) exact detection of the knock onset and (2) quantification of knock intensity. The identification of the knock location in the combustion is also an important attribute, which needs further analysis and possible by installing multiple pressure sensors [66] or using optical methods. Typically band-pass filtered pressure signal is used for knock intensity and knock onset detection. Knock onset is defined as the crank angle position at which a threshold value is exceeded or maximum amplitude of oscillation occurs. Knock intensity is defined as maximum amplitude (MAPO) or integral over a range or energy density over a range (Sect. 9.3.2). First or third derivative-based methods are also used for knock onset and intensity determination.

In the threshold exceeding based index, the value threshold needs to be sufficiently high to avoid pressure oscillations produced by combustion process [67] but still must be as small as possible to detect weak knocking cycles [68]. The detection of weak knocking cycles can significantly improve knock control algorithms [69]. On the other hand, normal SI combustion can be confused with end-gas autoignition if a low threshold is selected. Spark ignition combustion and knock both can excite in-cylinder pressure resonance (oscillations). Though, the normal spark ignition combustion is controlled by spark timing and has significant but bounded cyclic variations, while knocking has a random nature creating larger variations of resonance excitation [65]. Figure 9.32 illustrates the pressure oscillations in normal and knocking combustion cycles in a SI engine. In Fig. 9.32 the heat

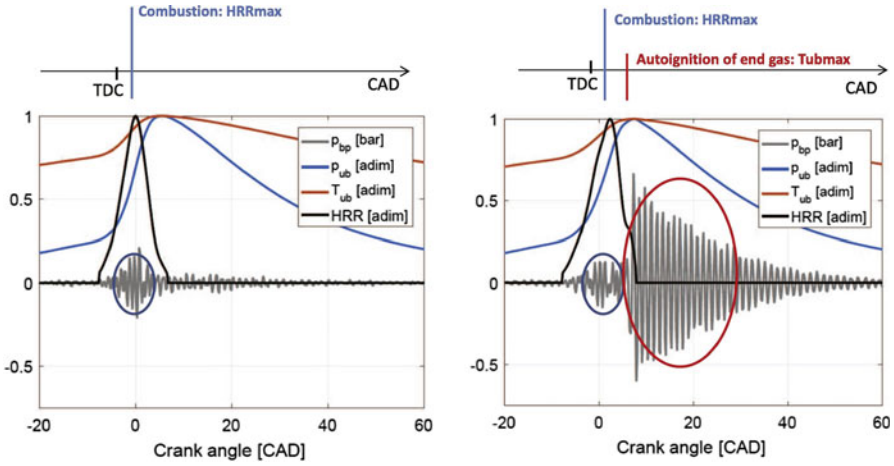

Fig. 9.32 In-cylinder pressure oscillations for normal cycle (left) and knocking cycle (right) at 1500 rpm in a SI engine [65]

release rate (HRR), the unburned temperature (T_{ub}), and the unburned gas pressure (p_{ub}) are presented as normalized value, while the band-pass filtered pressure (p_{bp}) data is presented in bar.

Figure 9.32 reveals that the excitation of the cylinder resonance due to combustion is similar in both normal and knocking combustion cycles. However, the oscillations due to autoignition of the end gas (charge) are positioned in the vicinity of the end of combustion (EOC). It is also found that oscillations due to autoignition differ significantly from cyclic basis [65]. The time domain does not provide the information regarding the resonant frequencies, which can be differentiated using short-time Fourier transform (STFT) or the wavelet transform. Figure 9.33 shows the short-time Fourier transform (STFT) spectrum of a normal cycle and a knocking cycle shown in Fig. 9.32. The figure depicts that the frequencies are only excited near the maximum HRR for the non-knocking cycle, while in the knocking cycle important resonance excitations generated near the end of combustion (around 10 CAD after TDC). After the frequencies are excited, only the resonant modes vibrate in the chamber, particularly the first radial mode (between 6 and 8 kHz) [65].

A knock event definition is proposed based on the comparison of the resonance oscillation at the maximum HRR and at the maximum unburned temperature (near EOC). It is assumed that the higher resonance at the EOC is result of knocking process (autoignition of end gas). Figure 9.34 illustrates the knock detection method based on the resonance at two locations. Two windows at different locations (one centered at maximum HRR and other centered at maximum unburned gas temperature) are used to separate combustion by autoignition. The resonance amplitude is calculated using fast Fourier transform (FFT). Two indices (I_C and I_A) are calculated by integrating the signal over the resonance frequencies. Knock event is detected only when the resonant content of the I_c is greater than I_A [65].

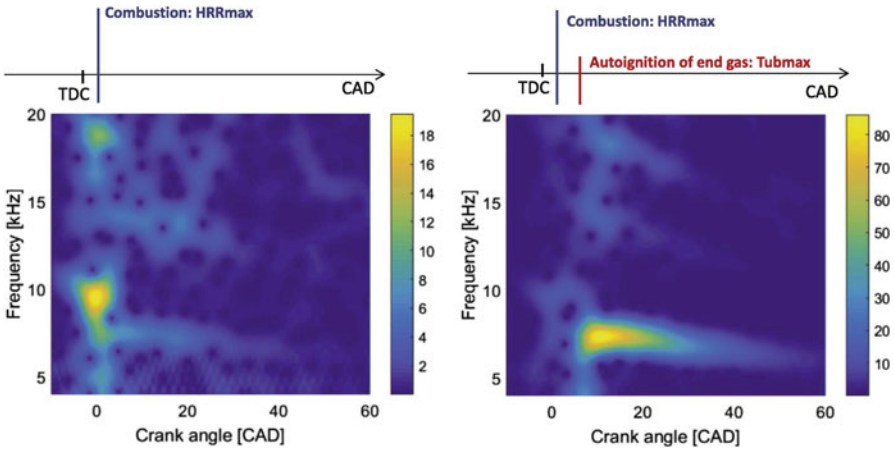

Fig. 9.33 Short-time Fourier transform (STFT) spectrum of a normal cycle (left) and a knocking cycle (right) [65]

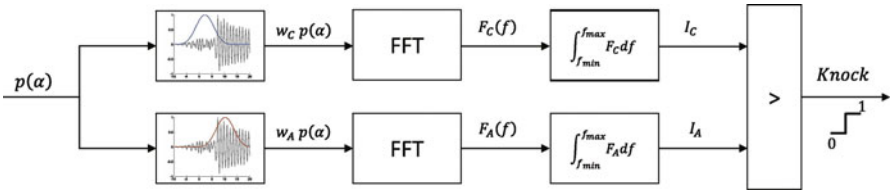

Fig. 9.34 Schematic diagram of knock determination procedure [65]

A knock indicator known as derivative at maximum pressure (DMP) is proposed for knocking analysis in dual-fuel engine [60]. The value of the pressure derivative is almost zero at peak pressure location for a non-knocking cycle. In the knocking condition, the value of this derivative increases due to pressure oscillations. Gradually, as the knocking intensifies, pressure oscillations become more important, and the value of this derivative becomes higher [60]. The DMP is calculated by Eq. (9.33).

$$\mathrm{DMP} = \left(\frac{dp}{d\theta}\right)_{\theta_{p\max}} \tag{9.33}$$

where θ_{pmax} is the crank angle corresponding to the maximum pressure of engine cycle. This parameter correlates very well with the commonly used MAPO knock indicator. Advantages of this method are an easy and fast calculation.

An engine combustion cycle can be characterized by a numeric value correlated to the knock event using MAPO. However, cycle-to-cycle variations exist in SI engine, and thus, statistical methods are used to characterize the knock intensity (KI) of an engine operating point [67]. A critical value of MAPO ($\mathrm{MAPO_{th}}$) is defined for

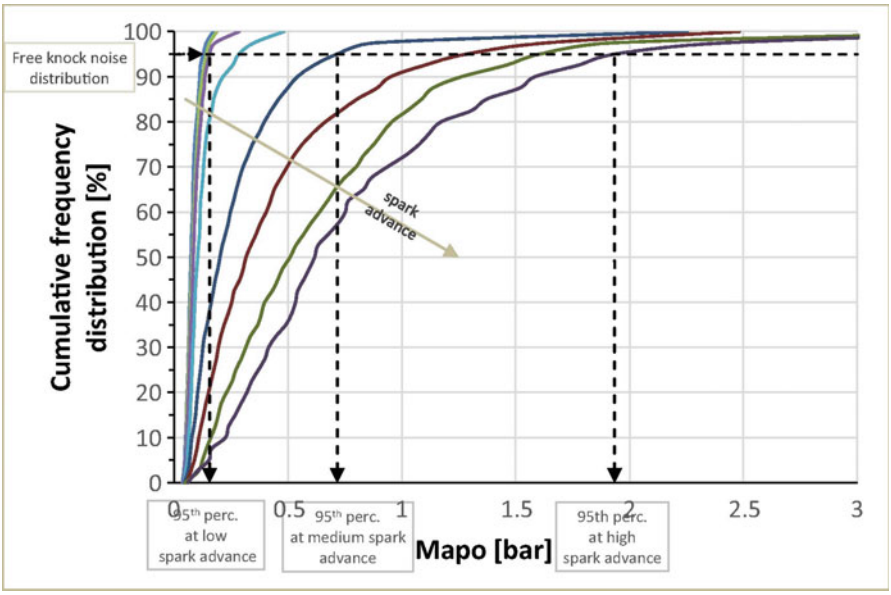

Fig. 9.35 Cumulative frequency distributions of MAPO values during knocking combustion [70]

the evaluation of knock intensity for a particular engine operating condition. For individual engine cycle, the knock intensity is usually calculated by Eq. (9.34) [70]:

$$I = \max\{(\text{MAPO} - \text{MAPO}_{\text{th}}), 0\} \tag{9.34}$$

where MAPO_{th} differentiates between knocking and non-knocking combustion cycles.

The MAPO distribution is very uneven because of cyclic variations at particular engine operating conditions. Figure 9.35 illustrates the cumulative frequency distribution plot of MAPO at different spark timings. The 95th percentile of MAPO distribution has been used to characterize the KI of each engine operating point. Figure 9.35 provides good discrimination between the different knock levels with varying spark timing. The 95th percentile can be used to characterize every engine operating point by means of a single numerical value [67]. Figure 9.36 illustrates the variation of the 95th percentile of MAPO distribution. The figure shows that for low spark advance timing (at particular test condition), the 95th percentile increases very slowly with the spark advance with almost constant value. This region is typically a non-knocking condition of engine operation. At higher spark advance timing, the 95th percentile increases rapidly with the spark advance timing indicating more and more heavy knock phenomena [70].

In the non-knocking region, the 95th percentile of MAPO distribution shows a constant value, which can be considered as the threshold to differentiate between

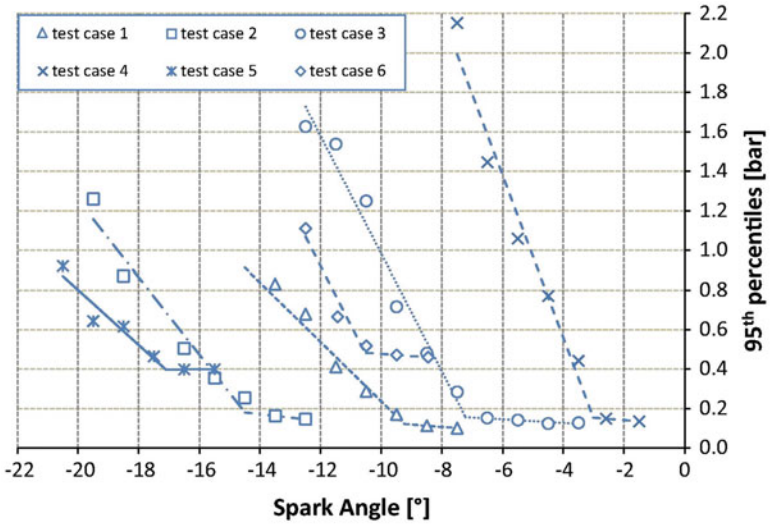

Fig. 9.36 The 95th percentile of MAPO distribution behavior [70]

non-knocking and knocking combustion [67, 70]. This threshold value depends on the engine operating conditions (Fig. 9.36) such as engine speed and load.

The KI of a particular engine cycle (j) can be calculated by Eq. (9.35), while the KI of an engine operating point can be calculated by Eq. (9.36) with N_{cyc} number of acquired cycles for knocking analysis [67, 70]:

$$I1_j = \frac{\max\{(\text{MAPO} - \text{MAPO}_{\text{th}}), 0\}}{\text{MAPO}_{\text{th}}} \tag{9.35}$$

$$KI1 = \frac{\sum_{j=1}^{N_{\text{cyc}}} I1_j}{N_{\text{cyc}}} \tag{9.36}$$

To overcome the dependency of the threshold value on engine operating conditions, a dynamic method has been proposed to determine the KI of a particular engine cycle [67]. For every cycle, a specific threshold is calculated by Eq. (9.37):

$$\text{MAPO}_{\text{th},j} = k \cdot \max\left\{ p_{\text{knock},j}(\theta)\Big|_{\text{SA}}^{\theta_{60\%}} \right\} \tag{9.37}$$

where SA is the spark angle, $\theta_{60\%}$ is the angle corresponding to the 60% of the mass burned fraction, and k is a constant value.

The KI of a particular engine cycle (j) can be calculated by Eq. (9.38), while the KI of an engine operating point can be calculated by Eq. (9.39) with N_{cyc} number of acquired cycles [70]:

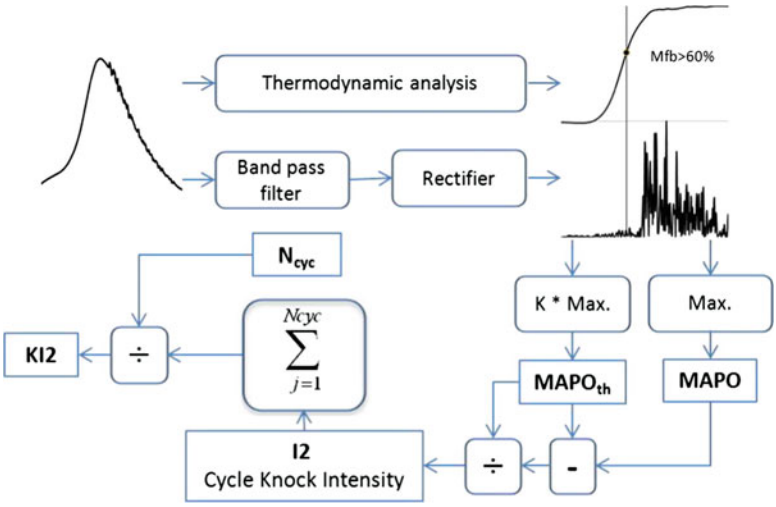

Fig. 9.37 Schematic diagram for KI2 calculation [70]

$$I2_j = \frac{\max\left\{\left(p_{\text{knock},j}(\theta)\Big|_{\theta_{60\%}}^{\theta_{99\%}} - \text{MAPO}_{\text{th}}\right),0\right\}}{\text{MAPO}_{\text{th}}} \tag{9.38}$$

$$KI2 = \frac{\sum_{j=1}^{N_{\text{cyc}}} I2_j}{N_{\text{cyc}}} \tag{9.39}$$

where $\theta_{99\%}$ is the angle corresponding to the end of the combustion.

Figure 9.37 schematically demonstrates the calculation of dynamic knock intensity in a spark ignition engine using cylinder pressure measurement. It can be noted that these knock indices (KI1 and KI2) are dimensionless numbers which allow comparing engine operating conditions characterized by a different value of speed or load.

A critical first step in the analysis of the knock intensity data is to investigate the extent to which the data behave as a cyclically independent random process. Knock intensities are fundamentally uncontrollable if it is random, and deterministic control theory no longer applies. By adopting a more stochastic approach, however, it is still possible to regulate some statistical property of the data. Most knock controllers, for example, regulate the knock event rate or empirical knock probability rather than the (random) knock intensity signal itself [71]. An initial analysis has provided strong evidence, both from autocorrelation functions and from the Pearson chi-squared test statistic, that knock intensities closely approximate a cyclically uncorrelated process. The process is then completely described by its marginal probability density function (PDF) whose mean and variance were observed to increase as the spark timing is advanced [71].

The knock intensity is strongly influenced by cycle-to-cycle variations for a fixed operating condition. It is demonstrated that a strong relationship exists between knock intensity index and the charge turbulent motion near the spark plug or the in-chamber temperature distribution. Physical knock models derived from the studies can be efficiently calibrated to determine the knock onset and the knock-limited spark advance (KLSA) or, more recently, to predict the trend of a MAPO percentile with respect to spark timing [72].

The observation that knock intensities closely approximate a cyclically independent random process means that the process is completely characterized by its probability density function (PDF) or equivalently by its cumulative distribution function (CDF). A study demonstrated that the log-normal distribution can be used to characterize the knock intensity distributions in SI engines for both the pressure and accelerometer and determine quantitative metrics of mean, standard deviation, knock percentiles, skewness, and peakedness [73].

Figure 9.38 shows the probability distributions of gasoline compression ignition (GCI) and SI combustion modes from non-knocking to knocking conditions using 200 consecutive engine combustion cycles. In SI engines, at retarded spark timing conditions, the distribution of MAPO is concentrated at relatively low knock intensities. For SI combustion, knock and non-knock operating conditions are obviously categorized by a particular spark timing (ignition timing of 22° CA bTDC), which has knock borderline value of 0.1 MPa (Fig. 9.38b). Additionally, the probability distribution of MAPO for the two combustion modes is quite different. In GCI mode, advancing injection timing from 20 to 30° CA bTDC only results in slightly higher MAPO mean. However, further advanced injection timing from 30 to 34° CA bTDC, significant increase in MAPO mean can be observed (Fig. 9.38a). With advanced injection timing, the distribution shifts toward higher intensities, broadening and becoming increasingly skewed. The upper tail of the distribution therefore increasingly protrudes into the very high-intensity region, causing the knock event rate to rise rapidly.

Figure 9.39 further illustrates the knocking characteristics of GCI and SI mode by presenting the cyclic variations of MAPO for knock-free, critical knock, and knock conditions. Three statistics terms, mean (μ), standard deviation (σ), and relative standard deviation (RSD) which is also coefficient of variation (CoV), are used to describe the MAPO distributions. Figure 9.39 a1 to a3 shows that advancing the injection timings leads to an increase in mean and standard deviation of MAPO. However, the RSD (coefficient of variation) remains almost unaffected from non-knocking to knocking operating conditions, which suggests that the increase of KI in GCI combustion mode doesn't change the MAPO distribution pattern fundamentally. Moreover, the results show that the in-cylinder pressure oscillations have negligible effects on combustion mode, and only burning rate, HRR, and the amplitude of pressure oscillations are changed as a result of rapid combustion [74]. Figure 9.39 b1 to b3 shows the MAPO variation for SI combustion mode. In this combustion mode, higher variations of MAPO distribution are observed, and significant change in RSD value is found from non-knocking to knocking operating

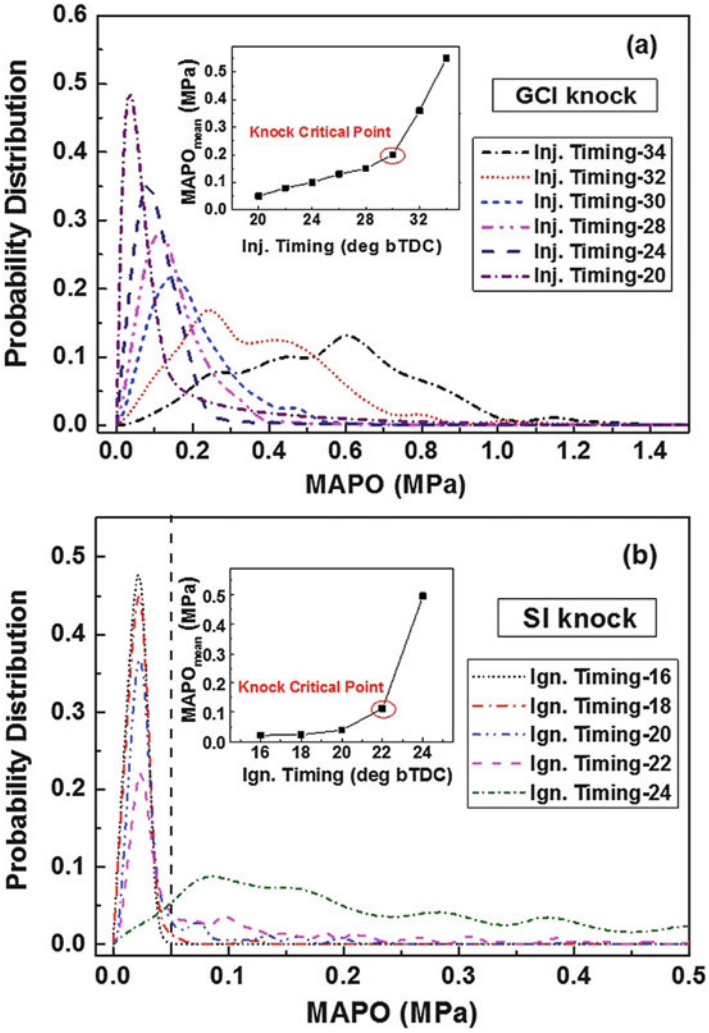

Fig. 9.38 Probability distributions of GCI and SI from knock-free to knock conditions [74]

conditions. The extremely high-pressure oscillation can be observed occasionally (Fig. 9.39b3). The reason for the distribution difference between the two combustion modes is supposed to be the nature of random end-gas autoignition under SI knocking conditions. To further illustrate the knocking differences in SI and low-temperature combustion modes, Fig. 9.40 shows the MAPO distribution for homogeneous charge compression ignition (HCCI), spark-assisted compression ignition (SACI), and SI combustion. The figure shows that the KI distributions of HCCI and SI are quite different. The average KI of SI knock is less than the HCCI knock, but randomly very high KI can be observed (Fig. 9.40). The RSD value of SI

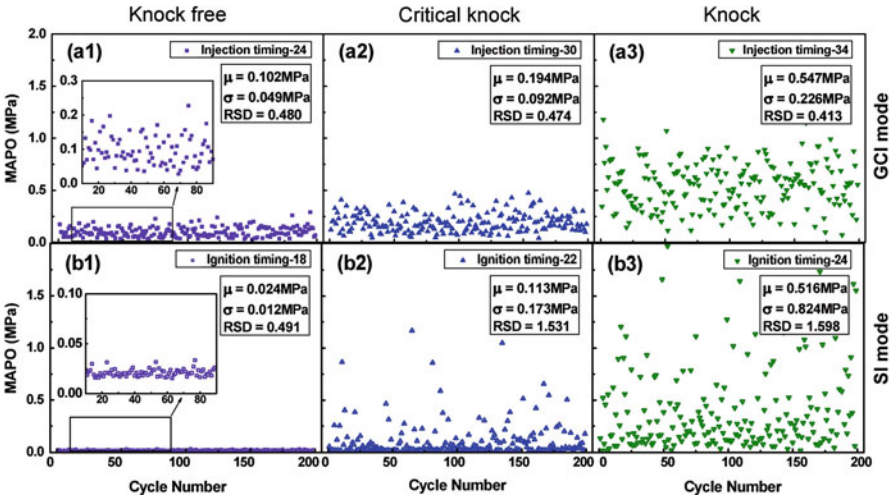

Fig. 9.39 Detailed MAPO variation of GCI (a1 to a3) and SI (b1 to b3) combustion from knock-free to knock conditions [74]

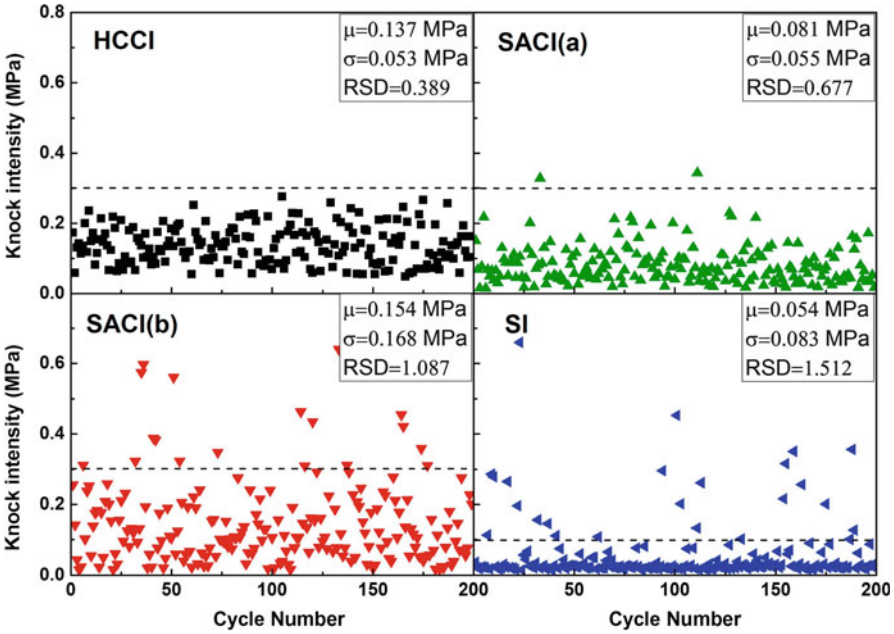

Fig. 9.40 Knock intensity distributions of HCCI, SACI, and SI combustion modes [75]

knock condition is 1.512, which is almost four times the value of HCCI (0.389) due to the differences in the process leading to knock phenomenon in HCCI and SI engine. The HCCI knock is generated by intensive multipoint autoignition and too

fast burning rate, while SI knock is due to the random autoignition of end gas, which greatly relies on flame propagation [75]. In the two SACI conditions, KI distribution combines the characteristics of both HCCI and SI knock conditions (Fig. 9.40).

The engine knock event is not uniquely defined by the time history of the end gas's thermochemical history in SI engine. In a study, it is demonstrated that three cycles are identical up to the point of knock onset combustion event, but the resulting KI differed by a factor of 8 [76]. The KI is not uniquely described by the unburned mass fraction at knock onset. However, the upper limit of KI, as defined as the 95th percentile of the cumulative distribution in a narrow window of unburned mass fraction, did correlate with KI. A methodology to predict the maximum possible KI based on the volumetric expansion rate of the end gas was developed, and the expansion rate was modeled based on blast wave theory, which is proportional to the energy of the initial explosion. The pressure rise was predicted to be linear with the energy available at knock onset [76]. Another study showed that the ratio of KI and gross indicated mean effective pressure (GIMEP) follows a log-normal distribution with mean μ and standard deviation σ, which is estimated using experimental data [10]. The value of μ decreases linearly with the ignition delay at the knock point, and σ is found to be a constant. The log-normal distribution can be used to determine the statistical distribution of KI in an engine simulation.

9.5 Knock Detection by Alternative Sensors

Presently, there are several methods for knock detection such as autoignition detection, ion current detection, in-cylinder combustion pressure detection, engine block vibration detection, and combustion noise detection. Figure 9.41 illustrates the different knock detection approaches based on the knocking process and its effects.

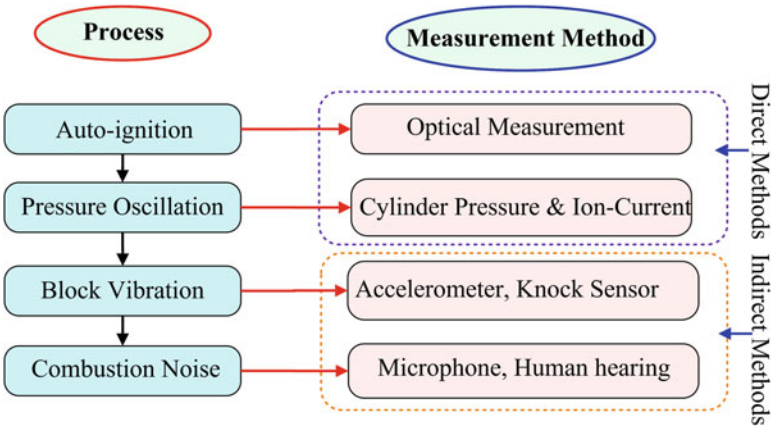

Fig. 9.41 Knock detection methods in reciprocating engines

In-cylinder combustion pressure detection is the most widely used approach in the laboratory for precise knock detection in each cylinder, because of its high signal-noise ratio, high sensitivity, but high cost.

Methods for knock detection can be classified into two broad categories, namely, direct and indirect methods [77]. Direct methods typically include the knock detection by directly measuring the knocking in the combustion chamber such as optical methods, ion current measurement, and cylinder pressure measurement. The in-cylinder pressure measurement can detect the typical high-frequency knock signature, related to the combustion chamber resonant frequencies. The typical drawback of cylinder pressure-based indices is that they are sensitive to local information provided by the pressure transducer. As knock occurs, huge pressure non-homogeneities take place inside the combustion chamber [59]. Thus, the measured pressure wave amplitude has only a local meaning, and cannot be considered as the maximum value of the whole combustion chamber pressure wave. Another intrusive (direct) knock sensor is based on ion current measurement. With years of development, ion current detection is more and more widely used due to its high detection precision, high signal-noise ratio, low cost, and rich combustion information content from each cylinder [78].

The indirect methods of knock detection include block vibration detection, engine noise detection, and exhaust temperature detection. Engine block vibration detection method (knock sensor) is broadly equipped in production vehicles. One engine normally mounts only one knock sensor. Thus, it is not so effective to distinguish each knocking cylinder or other vibrations caused by such as high-speed valves hitting valve seats, due to its fixed mounting point. The combustion noise detection is not frequently used, due to its low signal-noise ratio and low detecting precision. The exhaust gas temperature measurement can be utilized to identify knocking combustions because it reduces in knocking conditions as a consequence of increased wall heat fluxes inside the cylinder. This technique, moreover, is not affected by mechanical noise and can be applied for all types of engines [79]. Main drawbacks are related to the need of comparing the temperature level provided by the thermocouple to the one stored in a map, representative of a knock-free operation in the same engine speed, load, and air-fuel ratio operating conditions [77]. Table 9.1 shows the comparison of the different knock sensors on the basis of engine modification, cost, durability, and signal quality.

It can be summarized that all sensors respond to the resonant characteristics of knocking combustion but differ in robustness, cost, bandwidth, monitoring capability, and signal-to-noise ratio [80]. On the one hand, sensors like accelerometers are relatively cheap and robust sensor capable of detecting knock event but limited by the poor signal-to-noise ratio (SNR), particularly at high engine speeds and loads. On the other hand, cylinder pressure sensors provide good-quality signals adequate for detailed combustion analysis, but at the expense of cost and robustness. Ionization probes and production cylinder pressure sensors are now becoming viable as a compromise between these two extremes [80].

Table 9.1 Knock sensor comparison (Courtesy of Spelina, J. M, adapted from [80])

Sensor	Engine modification	Durability	Signal-to-noise ratio (SNR)	Cost	Remarks
Accelerometer	Nonintrusive	Good	Poor at high speed	Fairly cheap	Easy to mount and less accurate and not a fundamental measurement
Cylinder pressure sensor	Intrusive	Fair to poor	Good	Very expansive	Accurate and fundamental measurement. Difficult to mount
Ionization probe	Intrusive	Good	Poor at high speed	Fairly cheap	
Optical sensor	Intrusive	Poor	Good		Fundamental studies
Strain gauged cylinder head bolts	Nonintrusive	Fairly good	Vibrational interference	Fairly expansive	

Typically, the major factors considered for knock detection includes the cost of measurement, repeatability, and accuracy, time of measurement and analysis, and the required engine modifications for sensor installation. A brief description of these alternative sensors is provided in following subsections.

9.5.1 Optical Methods

Optical methods of knock detection are typically conducted on optical engines. Photographic observations of knocking combustion have been performed based on the progress of high-speed imaging techniques [8]. Photographic images of combustion chamber have been an important source of insight into the fundamentals of the knocking process because of the combustion process leading to the occurrence of knocking proceeds extremely fast. The optical measurement by the combustion light is a method for knocking measurement without being affected by mechanical noises. Widely used in the optical measurement is such a method that measures hydroxyl (OH) radical emission intensity by diffracting the combustion light and converting OH radical emission intensity to the voltage using a photomultiplier tube [81]. Emissions from chemical luminescence have been used to analyze the chemical reactions caused by autoignition of the end gas [8, 82]. A study used high-speed Schlieren photography and multi-optical fiber techniques to investigate the flame propagation and shockwaves on cycle-to-cycle resolved knocking combustion [82].

The methods for measurement of combustion light or image in the engine cylinder include such that a part of the cylinder liner or the piston is made of transparent glass, or an optical probe is installed in the spark plug or the combustion chamber. In either way, the measurable operating conditions are often limited from the mechanical strength of the light transmission route. There is a need of means for

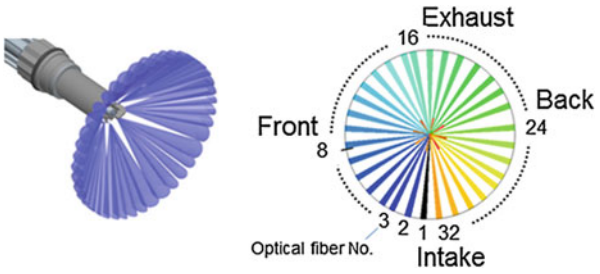

Fig. 9.42 Optical pressure wave measurement sensor and optical fiber configuration [85]

optical measurements under a wide variety of engine operating conditions including high-load conditions of commercial engines taking advantages of the outcomes from studies of optical measurement using experimental engines in order to develop more efficient engines. The high-durability optical probe has been developed and demonstrated as an instrument for optical measurement of combustion [83]. The optical probe has enabled measurement of knocking under high-speed and high-load conditions while minimizing restrictions to engine operating conditions. The optical probe is demonstrated for the detection of knocking, and based on the measurement, knocking damage index (KDI) is developed [81].

The localization of knock events in the combustion chamber of a SI engine is a key diagnostic activity to support its full-load development. A plug built-in-type optical sensor (AVL visio knock) is also used for knock detection [84]. Figure 9.42 illustrates the optical sensor-based knock measurement system. The sensor consists of 32 channels of optical fibers located in the radial direction of the spark plug and piston. Through these optical fibers, the sensor takes sample of the optical signals in the radial direction in the combustion chamber [85]. The signal intensity of optical sensor and the cylinder pressure have a linear relationship, which is used to get the local changes in the cylinder pressure during the knocking process. The knock onset direction is determined at this time by detecting the origin of the high-frequency vibration. Typically, a reference light source is used to calibrate each optical fiber channel to the same output characteristics.

9.5.2 Ion Current Sensor

The prevailing conditions in the engine cylinder during combustion lead to gas ionization. A current can be produced by applying a voltage (of the order of a hundred volts) between two electrodes because the ionized combustion gases are conductive. Generally, the voltage inside the cylinder is applied using the spark plug tips as electrodes. The principle of the ion current sensor is discussed in Sect. 2.3.1. As the ion density increases as the cylinder pressure increases, the ion current provides another measure of cylinder pressure signal. The problem with ion current measurement is that it represents the combustion intensity in a very small volume around the spark plug/ion probe and not the entire combustion chamber, and it also

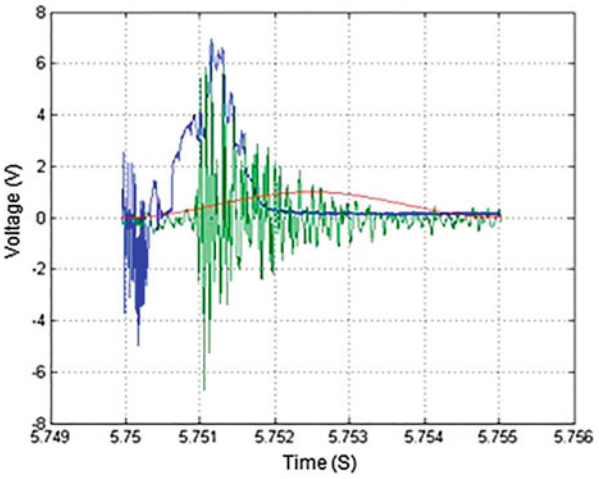

Fig. 9.43 Ion current signal (blue) along with pressure oscillation (green) in a heavy knock condition [87]

requires significant additional circuitry [80]. Thus, knock detection depends on the location of spark plug or ion current sensor.

Several studies used ion current sensor for the knock detection and characterization [78, 86–88]. Figure 9.43 illustrates the ion current signal during heavy knock conditions. The figures show that there is a high-frequency oscillation with larger amplitudes in the ion current signal during heavy knock conditions. Thus, it can be used for the knock detection and control. Ion current signal shows a good correlation with in-cylinder combustion process and the cylinder pressure signal. Ion current peak value can distinguish knock cycles from normal cycles fast and easily [78]. Both ion current band filter signal and integral value can distinguish different knock cycles from normal combustion cycles and show high linear correlation with the knock intensities during light knock and heavy knock. Ion current signal proves to be an effective method to discriminate different knock intensities [78, 86].

9.5.3 Engine Block Vibration

The engine knock can be sensed through accelerometers (piezo-ceramic sensors), mounted on the engine block, which evaluate the vibration transmitted from the knocking cylinder. Combustion noise is primarily transferred through the piston and connecting rod. This is dominant only below 1000 Hz [89]. A secondary combustion noise path which proves more useful for knock detection is through the cylinder block and cylinder head, which is utilized by the accelerometer. These knock detection methods can suffer from disturbance caused by other noise sources (valve closing, piston slap, etc.). Poor noise transmission from the knocking cylinder to the sensor can happen because of the sensor's location [86]. Additionally, the disturbances increase with engine speed. Due to the location issue, four-cylinder

engines need one or two sensors, but six and more cylinder engines need at least two sensors [90]. The main disadvantages of this method are (1) the dramatic deterioration in the signal-to-noise ratio (SNR) of the sensor response at higher engine speed due to the increase of other vibrations related to the operation of the valve-train system and of other rotating/moving parts and (2) the impossibility to recognize the knocking cylinder, which clearly excludes the individual control of spark timing [86].

Engine knock detection using vibration signals is normally more accurate than using noise signals. However, the vibration signal can have signals from other vibration sources or electrical noise. Thus, the vibration signal cannot be directly used for knock detection, and an effective signal processing method needs to be used [91]. A recent study proposed the knock detection method based on the wavelet denoising and empirical mode decomposition (EMD) methods using vibration signal [92]. The wavelet denoising is used to eliminate the high-frequency noise which is not produced by the engine knock. After the wavelet denoising, EMD can effectively identify the knock characteristics (including the light knock) from a vibration signal. This method can significantly improve computational time while maintaining reliable analysis.

9.5.4 Microphone

The combustion noise detection method using a microphone can be used to determine the engine knock by analyzing the noise frequency spectrum of the engine combustion. The knock intensity can be estimated by evaluating sound pressure level in a certain frequency band. This method of knock detection is low cost and does not require changing the engine structure. However, the combustion noise signal can easily interfered with other noises, and the detection accuracy is difficult to guarantee, and therefore this method is rarely used [92]. A study used microphones for combustion timing detection for feedback control of HCCI engines with reliable results at medium and higher engine loads [93].

9.6 Knock Mitigation Methods

In conventional SI engine, the knock occurs due to competition between the flame propagation speed and ignition delay of end gas. Thus, the basic principle for mitigation of knock is to ensure that the flame propagation time is less than ignition delay. Figure 9.44 summarizes the measures and technologies that can be utilized to reduce the knocking tendency of gasoline engine.

Apart from the influence of oil and fuel quality, the majority of measures leads to a lower working gas temperature during compression and combustion process

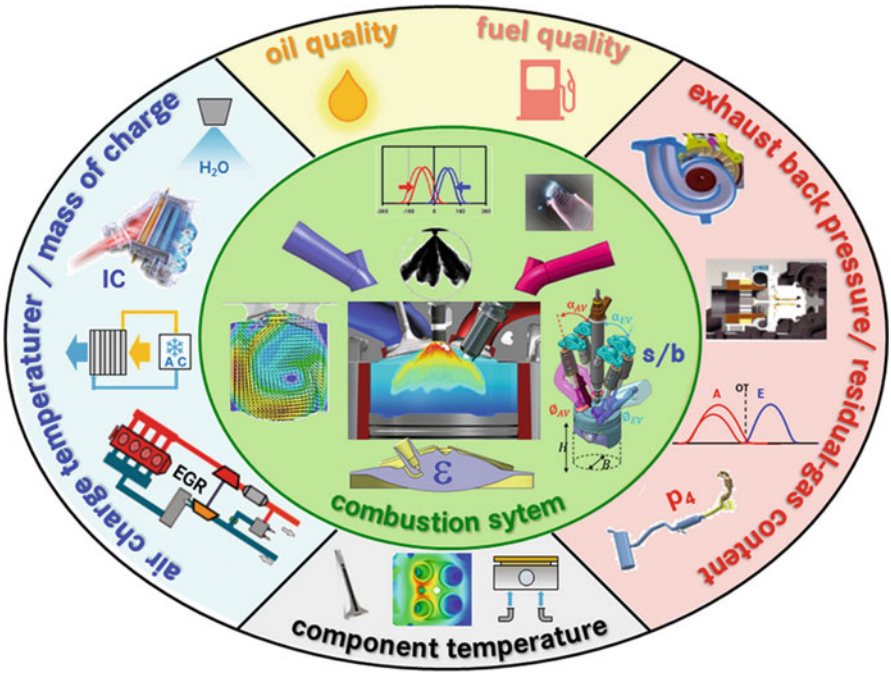

Fig. 9.44 Technologies for avoiding knocking combustion in gasoline engines [94]

[94]. Lowering the final compression temperature is considered as an effective measure for avoiding gasoline engine knock.

In conventional SI engine, the knock can be avoided by retarding spark timing; improving octane number and enriching fuel-air mixture, exhaust gas recirculation (EGR), and dual-fuel spark ignition with direct injection (DI) and port fuel injection (PFI); increasing turbulence; increasing cooling of the components and water injection; and lowering effective compression ratio [1].

Super-knock in a modern gasoline engine can be avoided by two methods: (1) by eliminating preignition and (2) by decoupling the shock wave and the heat release [1]. Figure 9.45 summarizes the measures that can be employed for avoiding the preignition in modern engines.

Water injection and cooled EGR are proposed practical solution for avoiding knocking combustion in a gasoline engine. Knocking is significantly influenced by the unburned zone temperature in the cylinder, and reduction in temperature leads to a reduction in knocking tendency. Table 9.2 depicts three possible technology approaches which are capable of decreasing combustion temperature and thus avoiding knocking combustion. Reduced knocking tendency allows the earlier combustion phasing operation, which improves the combustion efficiency and reduces the exhaust gas temperature. Additionally, lower combustion temperature results in reduced heat loss, lower NOx emission, and increased polytropic coefficient leading to a higher thermal efficiency [95]. In contrast to the Miller cycle, cooled EGR and water injection benefit from an increased mass within the

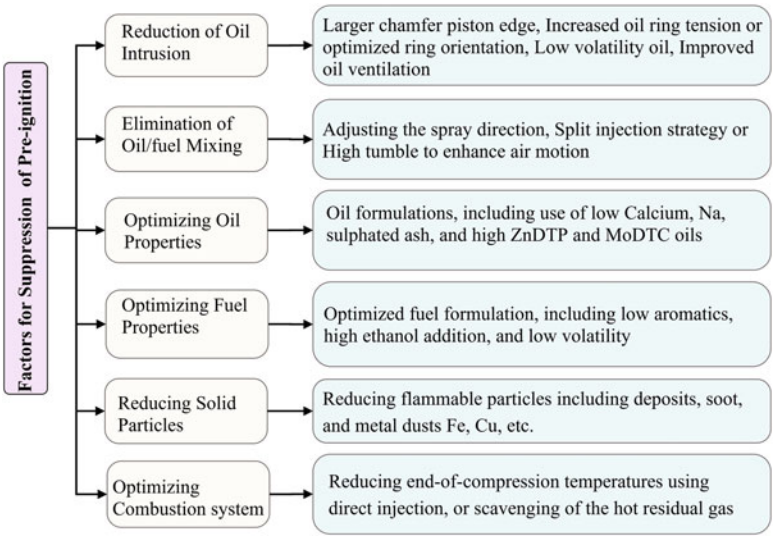

Fig. 9.45 Measures for avoiding preignition in modern gasoline engines (adapted from [1])

Table 9.2 Technology approaches for knock mitigation [95]

Water injection	Miller cycle	Cooled EGR
Increasing efficiency		
$MFB_{50\%} \downarrow$ Gas property ($\kappa \uparrow\downarrow$) Water heat losses $\downarrow$	$MFB_{50\%} \downarrow$ Gas property ($\kappa \uparrow$) Water heat losses $\downarrow$	$MFB_{50\%} \downarrow$ Gas property ($\kappa \uparrow\uparrow$) Water heat losses $\downarrow$
Reducing NO_X emission		
Evaporation + heat capacity	Miller effect	Total heat capacity
Reducing exhaust gas temperature		
$MFB_{50\%} \downarrow$ Evaporation + heat capacity	$MFB_{50\%} \downarrow$ Reducing effective compression	$MFB_{50\%} \downarrow$ Total heat capacity

combustion chamber leading to higher total heat capacity, even if the cooling effect in case of water injection occurs mainly by water evaporation. Thus, cooled EGR and water injection have a greater impact on the isentropic coefficient than just by lower temperature.

Cooled EGR is often used in reciprocating engines. In principle, different EGR system configurations are possible which are frequently known by their exhaust sampling point and the point where the gas is fed back to the intake air. Figure 9.46 schematically shows the two widely used EGR systems, namely, low-pressure EGR and high-pressure EGR. Among others, one key criterion for an EGR system is the pressure difference between sampling and feeding point as a measure for the maximum external EGR rate which is possible to use in real engine [95]. Considering this condition, the low-pressure EGR has an advantage in low engine speed region (Fig. 9.46), while high-pressure EGR can achieve higher EGR rates at high engine speeds, e.g., rated power.

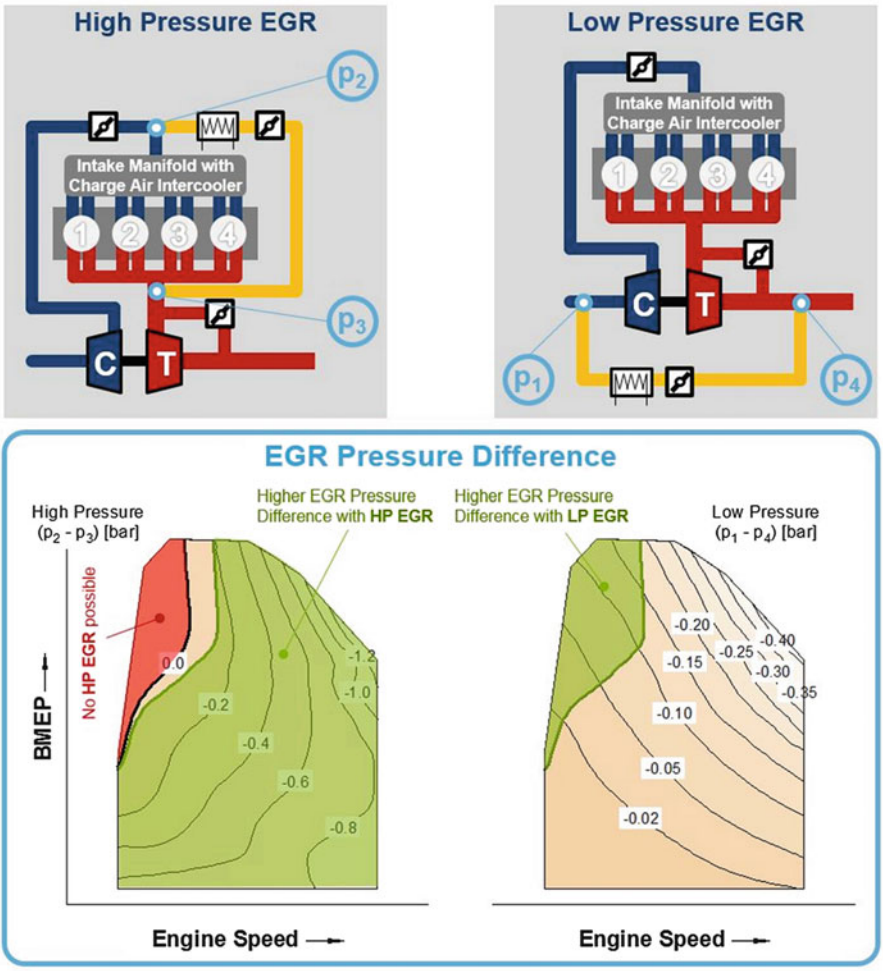

Fig. 9.46 Comparison of low- and high-pressure exhaust gas recirculation (EGR) in reciprocating engine [95]

9.7 Combustion Noise Determination

The estimation of combustion noise directly from the measured cylinder pressure data can be beneficial in the development of reciprocating engines especially in diesel engines and related fuel injection systems. Optimization of engine noise is becoming increasingly important in the development process and is often a calibration strategy target for diesel engines in addition to performance, economy, and emissions. The combustion noise measurement determined using cylinder pressure data helps to improve the understanding of the noise from combustion without expensive acoustic measuring equipment or the environment. Combustion noise plays a considerable role in the acoustic tuning of engines and vehicles.

Internal combustion engine radiated noise can be divided into mechanical noise, combustion noise, and noise resulting from the accessories. Among them, combustion noise contributes a large part of the overall engine noise.

The combustion process-related noise itself, i.e., the load-dependent noise, can be separated furthermore into direct and indirect combustion noise as well as flow noise [96]. The structure of an internal combustion engine is excited by the gas force and several additional forces. The acting forces can be divided into two categories according to their time characteristics. The first group of forces includes the cylinder pressure (gas force), and the resulting noise radiated by the structure is defined as direct combustion noise. The second group follows the rotary force curve that produces the indirect combustion noise, mainly resulting from the momentum load of the crankshaft and piston side force. The flow noise is typically produced by intake and exhaust system components, which is also ascribed to the (combustion) process noise, as it is a load-related noise, too [96]. The combustion noise is caused by load-dependent forces in the engine which cause the engine components to vibrate in their natural frequencies.

Typically, the combustion noise is known as the noise radiated from the surfaces of the engine structure as they vibrate and resonate in response to the fast pressure development in the combustion chamber during combustion. The high pressure developed in the cylinder deflects the engine structure, causing it to resonate in a number of vibration modes. The external surfaces of the engine that are in direct contact with the surrounding environment, and vibrations in the structure radiate energy as sound pressure [5]. Generally, the combustion noise can be directly related to the combustion event and the pressure rise rate in the cylinder. However, it is not possible to estimate the combustion noise directly from the pressure rise; experimental results have shown that the correlation is poor and cannot be relied upon for all combustion modes and engine operating conditions.

9.7.1 Combustion Noise Calculation and Metrics

In general, combustion noise is a result of the interaction between combustion and turbulence [97]. The contribution of both phenomena to the overall noise emissions may be completely different depending on the application [98]. In conventional diesel combustion (CDC) engines, the pressure instabilities generated during the premixed combustion phase mainly dominate the acoustic source, rendering the pressure oscillations induced by turbulence-combustion interaction [98, 99]. Therefore, a better fundamental understanding of noise is needed for evaluating the relationship between combustion and its corresponding acoustics. In addition to the pressure instability induced by combustion itself, the generated pressure waves resonate inside the cylinder, interacting with the cylinder walls, thus acting as an extra acoustic source. This complex phenomenon is generally known as combustion

chamber resonance. The combustion chamber resonance significantly affects the radiated engine noise due to the characteristic excitation frequency span that is in the highly sensitive human perception range [100, 101].

After the acoustic excitation, acoustic perturbations are transferred through the engine block into the vehicle and the environment. The NVH (noise, vibration, and harshness) analysis has shown the complexity of the propagation patterns of acoustic energy [102]. During combustion, a sudden pressure rise is produced which leads to the vibration of the engine block that in turn radiates aerial noise. The engine block vibration is produced both by pressure forces exerted directly by the gas and mechanical forces associated with piston slap, bearing clearances, elements deformation, and friction, which are powered by the pressure forces during combustion [103]. Additionally, pressure forces strongly depend on the combustion process, which is dependent on the combustion mode, fuel, as well as fuel injection parameters.

Based on the physical mechanism of noise generation, two possible methods can be used to estimate the combustion noise, i.e., (1) determining the transmission path and the emitter characteristics and (2) a direct correlation between the source and the radiated noise. Figure 9.47 schematically illustrates the physical mechanisms of engine noise radiation analysis approaches. The first method is complex and needs a high computational effort because of the time-variant and nonlinear features of the block response [103].

The sound pressure level (SPL) of noise is assumed to be the sum of the combustion noise level (CNL) and mechanical noise level (MNL). Combustion noise level is assumed to be the cylinder pressure level (CPL) attenuated through

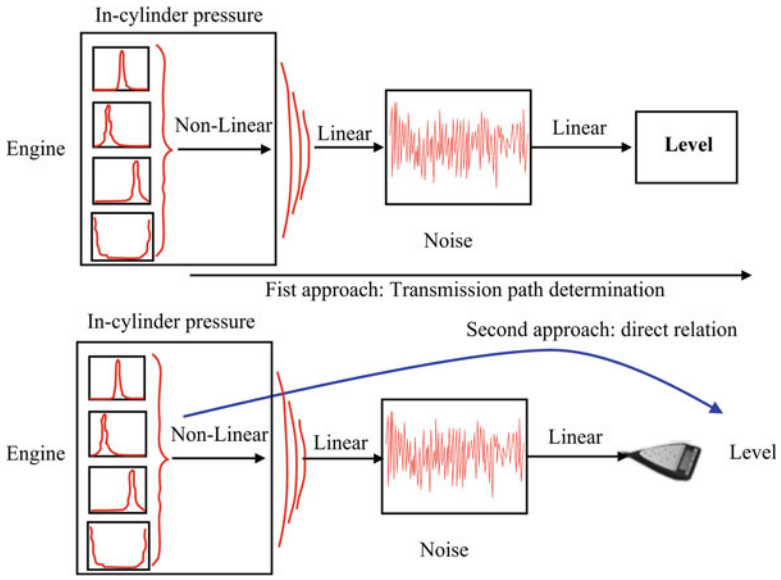

Fig. 9.47 Two approaches for determination of combustion noise level in diesel engines [103]

the engine structure in a linear relation, which is defined as structure attenuation (SA) [104]:

$$\mathrm{SPL} = \mathrm{CNL} + \mathrm{MNL} = \mathrm{CPL}/\mathrm{SA} + \mathrm{MNL} \tag{9.40}$$

The SA indicates a subtraction of CNL from CPL with a unit of dB. Thus, SA is considered as an index for evaluating the noise and vibration performance of the engine structure for the combustion excitation. Separating MNL from SPL is very difficult on running an engine with combustion [104]. The attenuation properties of most engine structures are very similar, and a standard, average structural response curve was proposed (often known as SA1) [5]. Engine structure attenuation was found to increase with improved design, and because the increased attenuation was almost consistent at all frequencies, a new attenuation curve was proposed called SA1-7 (SA1being the original curve and −7 representing an extra 7 dB attenuation) [105].

Typically, combustion noise calculation from measured cylinder pressure data includes the prefiltering of pressure data, application of a filter to represent the attenuation of a standard engine structure, and application of a filter that represents the human ear response [5]. A study proposed the combustion noise calculation method by considering the structural attenuation and human hearing system response [106]. The algorithm of combustion noise calculation is schematically illustrated in Fig. 9.48. First, the measured pressure data is converted into the frequency domain using Fourier transform, and then the filter is applied to account

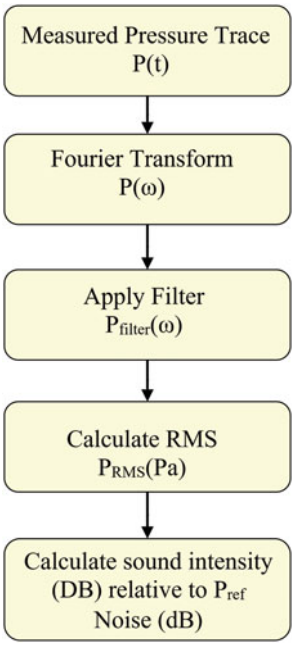

Fig. 9.48 Combustion noise level determination algorithm (adapted from [106])

for structural attenuation and human hearing system response. The root mean square (RMS) value of the filtered pressure (P_{RMS}) is calculated, and the final noise level is obtained by comparing P_{RMS} to a reference sound level (20 μPa) [106].

The structure attenuation (SA) function implemented in Fig. 9.48 is given in Eq. (9.41):

$$\mathrm{SA(dB)} = \begin{cases} \sum_{i=0}^{6} a_i f^i & 100 \leq f \leq 2300 \\ \sum_{i=0}^{6} b_i f^i & 2300 < f < 10000 \end{cases} \tag{9.41}$$

where f is the frequency in [Hz], SA is in units of dB, and the coefficients a_i, and b_i are constants. Outside of the frequency range given is fully attenuated. The equation for the A-weighting filter is given by Eqs. (9.42) and (9.43):

$$A(f) = 1 + 20 * \log_{10}(R_A(f)) \tag{9.41}$$

$$R_A(f) = \frac{12200^2 * f^4}{\left(f^2 + 20.6^2\right) * \sqrt{\left(f^2 + 107.7^2\right) * \left(f^2 + 737.9^2\right) * \left(f^2 + 12200^2\right)}} \tag{9.42}$$

The total transmission filter, $T(f)$, is given by Eq. (9.43), and combustion noise is calculated by Eq. (9.44):

$$T(f) = 10^{(\mathrm{SA}(f) + A(f))/20} \tag{9.43}$$

$$\mathrm{Noise\,(dB)} = 20 * \log_{10}\left(\frac{P_{\mathrm{RMS}}}{20\,\mu pa}\right) \tag{9.44}$$

Standard attenuation curves from another study are presented in Fig. 9.49. The algorithm presented in Fig. 9.48 is implemented using MATLAB code, and results showed excellent agreement with AVL noise meter. A more complete detail can be found in the original study [106].

Combustion noise can also be estimated by in-cylinder pressure decomposition proposed by the study [107]. Based on this method, three frequency bands in the pressure spectrum are identified where each linked to one of the three parts of the engine cycle: compression-expansion phase, combustion event, and resonance phenomenon. This process of cylinder pressure decomposition allows determining the most influential parameters in each frequency band. Using this information, studies [98, 100, 101] have found cause-effect relationships between the noise source and both the objective and subjective effects of noise.

Figure 9.50 illustrates the pressure decomposition approach (top plot). The excess pressure can be obtained by subtracting the compression (motored) pressure from the

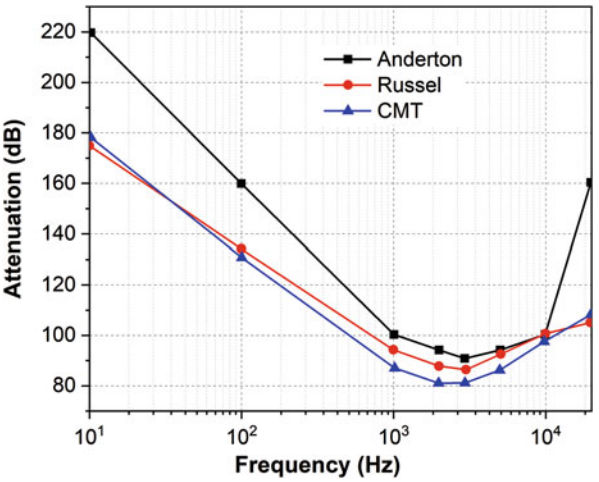

Fig. 9.49 Standard attenuation curves [103]

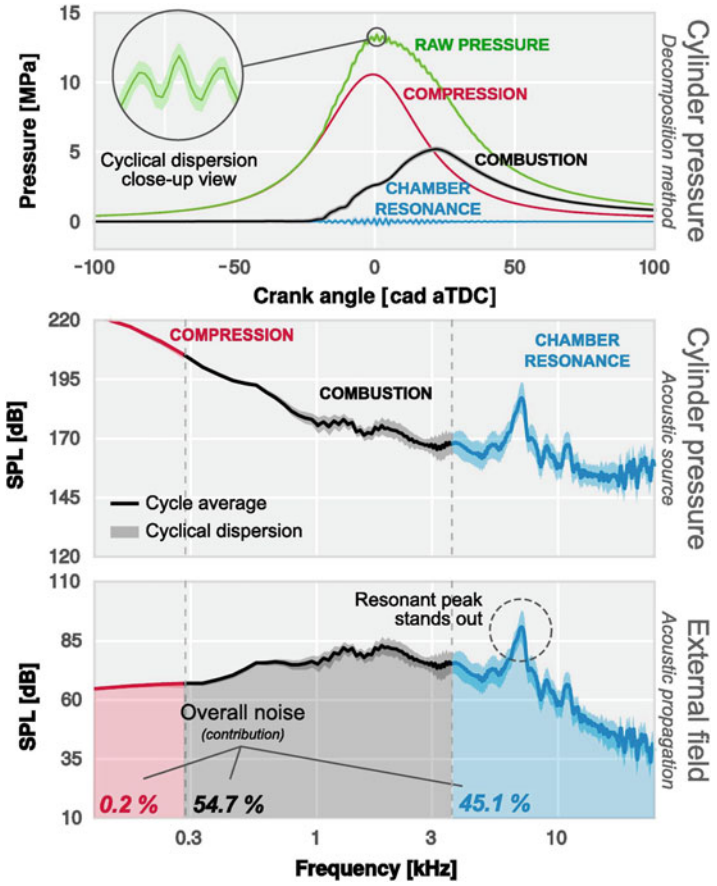

Fig. 9.50 Pressure decomposition technique illustration shown in-cylinder pressure along with each contribution in the time domain (top plot), frequency content (middle plot), and estimated radiated sound pressure levels (bottom plot) [108]

measured raw pressure data. The motored pressure can be obtained by switching off the fuel line and measuring the cylinder pressure. The subtraction of motored pressure from measured pressure during combustion provides the excess pressure due to combustion, which contains the pressure evolution due to fuel burning (combustion signal) as well as the resonant pressure fluctuations in the cylinder excited by pressure gradient during combustion [107]. Pressure fluctuation related to resonance can be determined by high-pass filtering of excess pressure and recomposing it in the time domain. The combustion pressure is obtained by subtracting the resonance signal from the excess pressure data (Fig. 9.50). The frequency content of each component is also shown in Fig. 9.50.

The relationship between the engine radiated noise or overall noise (ON) and three indicators are demonstrated [100]. Three indicators include the operation indicator that quantifies the effect of engine speed (I_n) and two combustion indicators (I_1 and I_2) indicating the in-cylinder pressure rise and the high-frequency gas oscillations inside the cylinder. The overall noise can be obtained by Eq. (9.45):

$$\mathrm{ON} = C_0 + C_n I_n + C_1 I_1 + C_2 I_2 \tag{9.45}$$

where C_i are coefficients which are dependent on the engine concept and size. The indicators can be calculated by Eqs. (9.46) to (9.49). The indicators I_i are considered as fundamental noise parameters and are linked to a specific bandwidth of frequency in response to the source [98, 100]:

$$I_n = \log\left[\frac{n}{n_{\mathrm{idle}}}\right] \tag{9.46}$$

The operation indicator (I_n) is a function of both the engine speed (n) and the idle engine speed (n_{idle}), and this parameter is associated with low frequencies. The combustion indicator (I_1) characterizes the sudden pressure rise due to combustion, and it is related to the medium bandwidth of frequencies [98]:

$$I_1 = \frac{n}{n_{\mathrm{idle}}}\left[\frac{(dp/dt)_{\mathrm{comb}}^{\mathrm{max}_1} + (dp/dt)_{\mathrm{comb}}^{\mathrm{max}_2}}{(dp/dt)_{\mathrm{comp}}^{\mathrm{max}}}\right] \tag{9.47}$$

where the two pressure derivative terms of Eq. (9.47) in the numerator are the two maximum peak values of the pressure rise rate (PRR) during combustion and the pressure derivative term in the denominator indicates the maximum peak value of the PRR of the pseudo-motored signal. The resonance indicator (I_2) indicates the contribution of the resonance phenomena inside the chamber and calculated by Eq. (9.48):

$$I_2 = \log\left[E_0 \frac{E_{\mathrm{res}}}{\mathrm{E}_{\mathrm{comp}}}\right] \tag{9.48}$$

$$E_{\text{res}} = \int_{\text{IVC}}^{\text{EVO}} p(t)_{\text{res}}^2 dt \tag{9.49}$$

where E_0 is a convenient scaling factor and E_{res} is the signal energy of the resonance pressure oscillations.

Another study [101] used the same two combustion indicators to correlate with the perceived sound quality of the combustion noise. The sound quality is quantified by a mark ranging from 0 to 10 which indicates the customer satisfaction degree and represented by Eq. (9.50):

$$\text{MARK} = 10 - C_3 I_1 - C_4 I_2 \tag{9.50}$$

where C_i are other coefficients dependent on the engine size and concept.

Combustion noise variables are also investigated by statistical analysis, and empirical correlation for combustion noise determination is proposed in terms of maximum heat release rate (HRR_{max}), combustion duration (CD), and combustion phasing, which affects the combustion process [109]:

$$\text{CNL}[\text{dB}] = -0.544\left(\text{CD}\left[^{\circ}\text{CA}\right]\right) + 0.0275\left(\text{HRR}_{\text{max}}\left[\text{J}/^{\circ}\text{CA}\right]\right) + 85.526 \tag{9.51}$$

where combustion duration (CA) is calculated as the duration between 10% and 90% mass burn positions.

9.7.2 Combustion Noise Characteristics

Combustion noise characteristics depend on the different engine operating parameters and combustion modes. Figure 9.51 illustrates the effect of fuel injection timing, oxygen concentration, and fuel (gasoline and diesel blend) on overall noise (calculated using Eq. 9.45) and noise Mark (calculated using Eq. 9.50) in a PCCI engine. The figure illustrates that overall noise (ON) is inversely proportional to the mark which indicates sound quality. Additionally, the noise is increased as the injection timing is retarded, and there is a great impact of the oxygen concentration in the intake on the noise issues (Fig. 9.51). Combustion noise is improved with reduced oxygen concentration for all the injection timings and fuels.

Reducing the maximum rate of pressure rise is known as an empirical method to reduce the combustion noise of premixed diesel engines. Reductions in combustion noise are necessary for high-load diesel engine operation, and multiple fuel injections can achieve this with the resulting reductions in the maximum rate of pressure rise [111]. Combustion noise produced in the second combustion could assist in reducing the combustion noise of the first fuel injection and termed this "noise cancelling spike combustion (NCS combustion)" [112]. The start timing of the second fuel injection changes the noise reduction frequency range: the noise

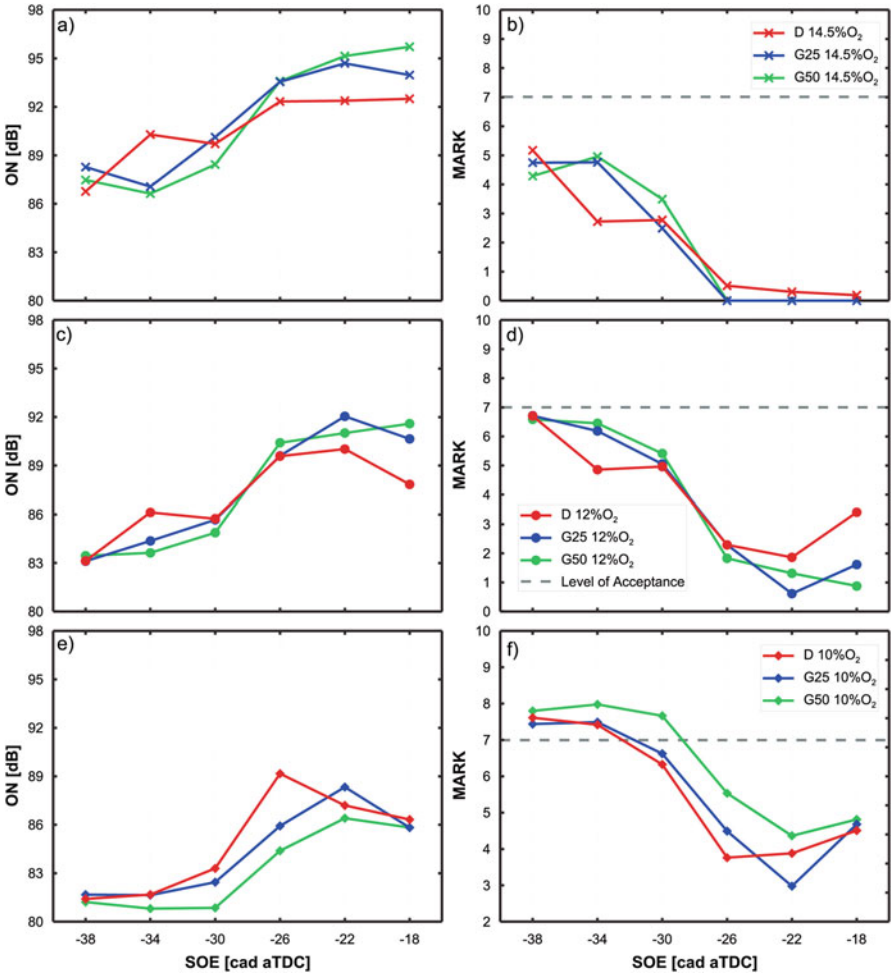

Fig. 9.51 Effect of injection timing, oxygen concentration, and fuel on engine noise: ON (left column) and Mark (right column) [110]

reduction frequency range moves less with the retarded timing of the second fuel injection. Thus, there is an optimum timing of the start of the second fuel injection achieving maximum reduction of the combustion noise generated by the first fuel injection [111]. The heating values in the first and second stage heat release do not change the noise reduction frequency range, but the intensity of the noise reduction effect changes. Another study showed that the multiple fuel injections near TDC are effective for combustion noise reduction maintaining a high degree of constant volume, because of the reduction in the maximum rates of heat release in each heat release and the noise reduction effect by the noise canceling spike (NCS) combustion [113]. The NCS processes become increasingly complex with more

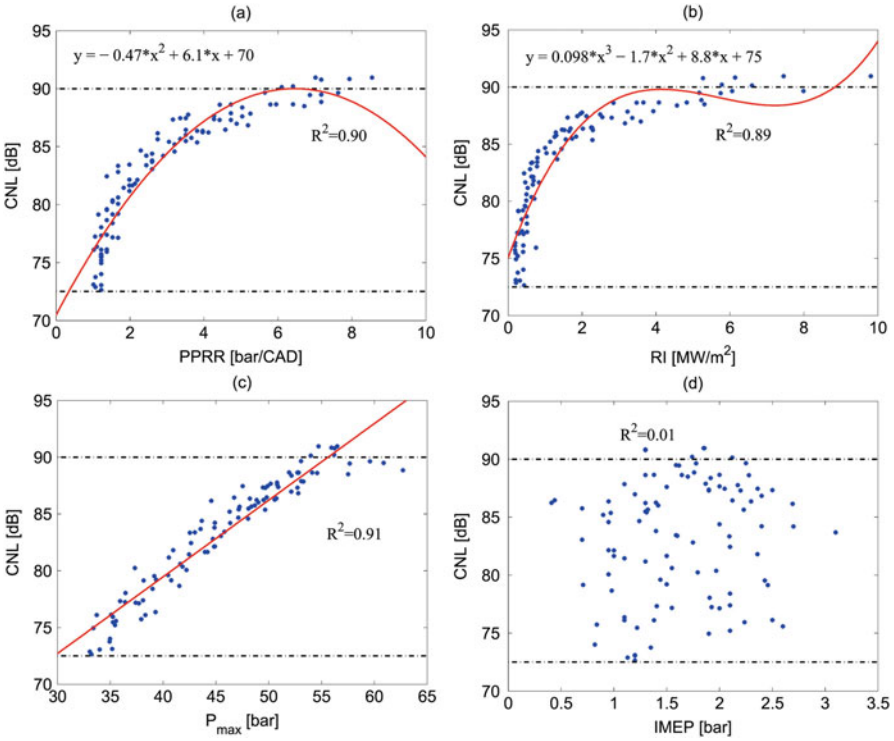

Fig. 9.52 Variation CNL with the PPRR, RI, P_{max}, and IMEP at steady-state HCCI combustion [114]

fuel injections, and the amplifying and canceling frequencies can be controlled by the length of time in crank angle between the peaks of the rates of pressure rise.

The combustion noise level (CNL) calculated using Eq. (9.44) is also used as a reliable indicator because it has been developed based on actual engine noise measurements. Figure 9.52 illustrates the variation of CNL with peak pressure rise rate (PPRR), ringing (RI), maximum cylinder pressure (P_{max}), and indicated mean effective pressure (IMEP) at steady-state conditions in HCCI engines. The solid red lines (Fig. 9.52) indicate the regression fit, and the two horizontal dashed lines represent the misfire and ringing limits. Figure 9.52a, breveals the quadratic and cubic polynomial regression curve to indicate the strong correlation ($R^2 = 0.9$) between CNL with PPRR and RI, respectively [114]. Additionally, the CNL becomes more than 90 dB for PPRR>8 bar/CAD (Fig. 9.52a), and HCCI operation at these high values should be avoided. The combustion community has long relied on the PPRR, as an indicator of engine noise. Citing discrepancies between observed sound levels and PPRR, the ringing intensity was introduced as an indicator of engine noise [64]. The higher PPRR engine operation leads to engine ringing and excessive heat transfer. Figure 9.52b shows almost constant RI with a large variation of CNL from 72 to 84 dB in steady-state data points. Figure 9.52c depicts a strong

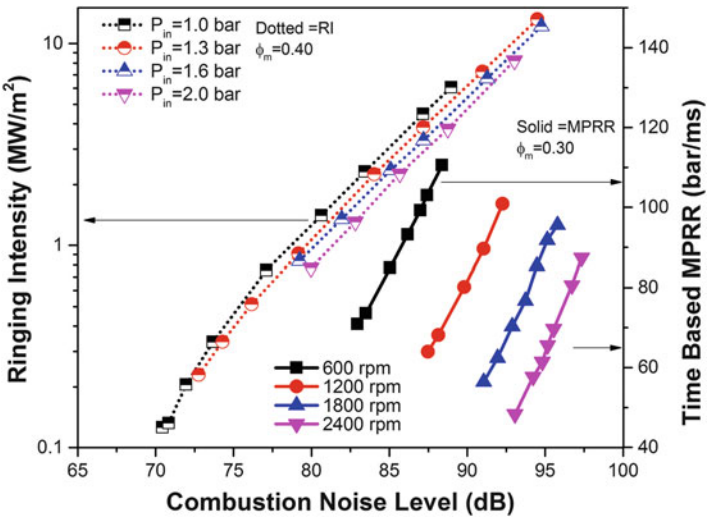

Fig. 9.53 CNL variation with RI and MPRR at different engine operating conditions in HCCI combustion (adapted from [115])

linear correlation between the CNL and P_{max} ($R^2 = 0.91$). No correlation is found between CNL and IMEP (Fig. 9.52d).

Figure 9.53 illustrates the relationship between RI and maximum pressure rise rate (MPRR) in time scale with CNL in the HCCI engine at different operating conditions. It can be noticed that the CNL increases linearly with log(RI) for CNL above 80 dB at particular intake pressure (P_{in}) condition. Additionally, the CNL increases by ~2.2 dB with an increase in P_{in} from 1.0 to 2.0 bar for any RI (~0.8 to 7 MW/m^2) as indicated by Fig. 9.53. The CNL significantly increases with an increase in engine speed (Fig. 9.53). It can also be noticed from the figure that the spacing between the data curves (CNL vs. MPRR) for various engine speeds is unequal, which suggests that slope of the increase in the CNL with engine speed decreases with higher engine speeds [115].

Ringing intensity is a metric that correlates with the sound produced by the resonating wave leading to knock. Thus, the RI appears to be a better criterion for the sake of avoiding unwanted knocking combustion regimes and the associated characteristic noise [115]. The RI is a better metric for controlling the detrimental effects of knocking such as irritating noise, loss of thermal efficiency, and engine damage. However, the CNL is valuable for estimating the overall loudness of an engine, particularly the noise induced by the normal combustion process. The RI and the CNL provide two distinctly different but complementary measurements. The CNL is not significantly affected by the high-frequency components related to the ringing/knock phenomenon [115]. Therefore, an appropriate metric needs to be selected for a particular application.

In the conventional diesel combustion (CDC), mid-frequency, broadband combustion noise dictated by MPRR and resonant noise characterized by higher

frequency peaks can contribute equally to overall noise (ON) levels. The resonant peaks are dominating the spectral signature of the noise in CDC mode [108]. While in advanced partially premixed combustion (PPC), the contribution of resonance levels to ON levels is much lower. Thus, in optimizing the noise radiated from CDC engines, the reduction of wave resonance is a crucial factor, but this factor is of little importance in PPC noise [108].

Discussion/Investigation Questions

1. Discuss the difference between normal and abnormal combustion in spark ignition engine. Describe the various factors responsible for abnormal combustion in SI engine.
2. Describe the term "knock" in a reciprocating engine. Discuss the possible reasons for engine knocking in SI engine, and explain the adverse effects of engine knocking over a long period.
3. Write the engine or operating variables affecting the temperature and density of the unburned charge toward the end of combustion in SI engine.
4. Discuss the factors responsible for cycle-to-cycle variations in the engine knocking. Describe the typical distribution of knock intensity on a cyclic basis.
5. A PFI gasoline SI engine is designed to operate at compression ratio 9 using gasoline with octane number (ON) 90 (typical gasoline). Discuss the expected problems that arise due to the increase in compression ratio to 12 (with modified engine) while running at the same fuel. Write the possible solution to the expected problems. Can ethanol or methanol be used on the modified engine at a compression ratio of 12?
6. Discuss the methods that can be used for the detection of knock onset in SI engine. Explain the merit and limitations of the methods.
7. Discuss the different modes of knock combustion in the engines. Write the different parameters affecting the transition of knock mode from deflagration to developing detonation.
8. Why measurement and characterization of knocking are important in internal combustion engines? Discuss the reason for knocking in SI, CI, and LTC (HCCI, RCCI, etc.) modes of engine operation. Draw a typical knocking cylinder pressure curve for all three modes of engine combustion.
9. What is engine super-knock? Discuss reasons for super-knock and method of characterization and mitigation of super-knock.
10. Three possible positions of the spark plug (black circle) in a spark ignition (SI) engine are shown Fig. P9.1. Identify the intake and exhaust valves in the configuration shown. Arrange three configurations (A, B, and C) in ascending order for octane number (ON) of fuel required to run the SI engine in each configuration, and justify your answer with suitable reasons.

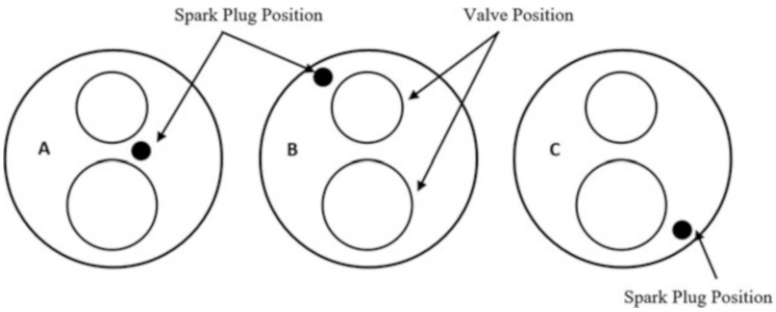

Fig. P9.1 Different spark plug installation configuration

11. Based on the two different designs of combustion chambers shown in Fig. P9.2, answer the following questions: **(a)** when combustion chamber design is changed from A to B, explain whether combustion rate will be faster, slower, or about the same rate. Justify your answer. **(b)** Which combustion chamber requires higher octane number fuel? If both engines are running on the same fuel, which engine can be operated at a higher compression ratio? Justify your answers.

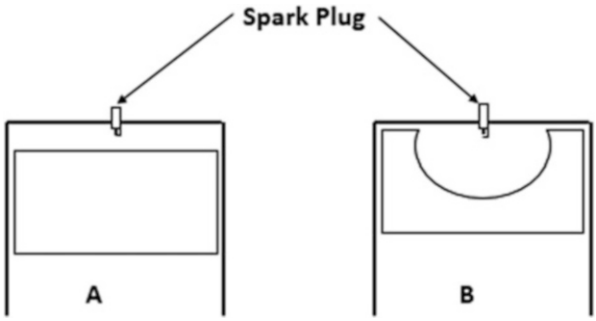

Fig. P9.2 Effect of piston bowl on combustion characteristics in SI engine

12. You are given the engine map (Fig. P9.3) for a conventional homogeneous charge SI engine. **(a)** Looking at the engine map, identify whether the engine is naturally aspirated or it is turbocharged/supercharged. Mark the regions in the map where engine is most (highest) and least susceptible to knocking combustion. Justify your answers for the highest and lowest susceptibility toward knocking. **(b)** Assume engine is operating in a region susceptible to knocking, suggest two ways (actions to be performed) to run the engine in the non-knocking combustion.

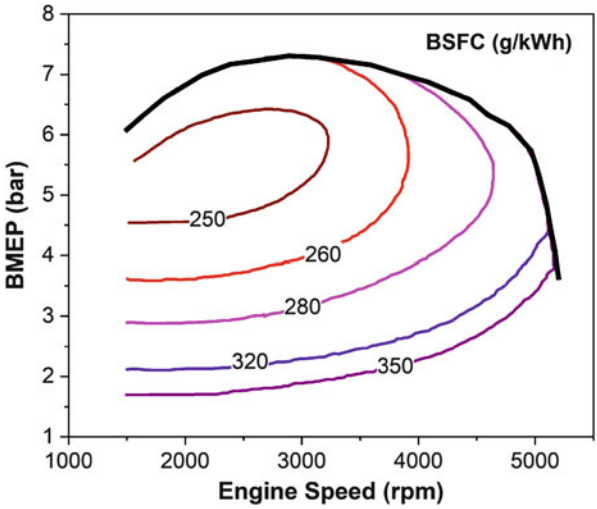

Fig. P9.3 Conventional SI engine map (adapted from [2])

13. Consider an SI engine in which the spark timing is maintained at the same crank angle and the air-fuel mixture is changed from stoichiometric to lean. What happens to the peak flame temperature as the air-fuel ratio is made lean from stoichiometric? Explain your answer. What would you expect to happen to the exhaust temperature for this situation? What about the tendency to knocking in such conditions?
14. Write the effect of engine operating variables on ignition, flame propagation, and knocking tendency by filling in the blanks in the Table P9.1 using the symbols provided. Discuss and justify your answers in terms of the governing phenomena or the factors responsible to it.

Table P9.1 Effect of ignition- and engine-related variables on flame propagation and knocking

	Effect		
Ignition system variables	Ignition	Flame propagation	Knocking tendency
Increased spark energy			
Hotter spark			
Increased electrode gap			
Sharp/thin electrodes of spark plug			
Engine variables			
Increased compression ratio			
Increased mixture swirl/turbulence			
Increased residual gas/EGR			
Close to stoichiometric mixture operation			

Helps ↑; hinders ↓; no effect –

15. Spark ignition engines' efficiency is mainly limited by three major factors, namely, knocking, fuel enrichment, and throttling. Figure P9.4 depicts the full-load curve of SI engine. Schematically identify zones corresponding to knocking, fuel enrichment, and throttling on engine operating map. You can draw few contour lines in the identified zones.

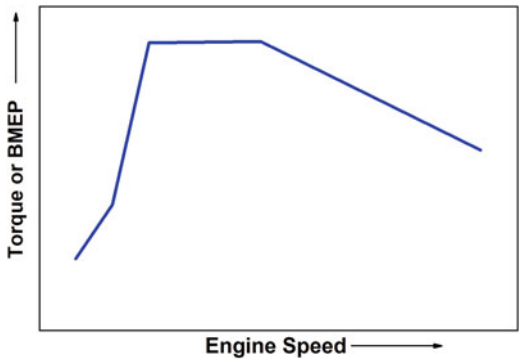

Fig. P9.4 Full-load torque curve of a SI engine

16. Knocking in SI engines is affected by several engine and operating parameters. Fill the following Table P9.2 showing the effect of increasing engine and operating variables on knock. Discuss these whether the engine parameters can be controlled by the engine operator or ECU to mitigate the knocking conditions.

Table P9.2 Effect of engine parameters on knock in conventional SI engine

Increase in engine parameter	Change in the state of end gases	Effect on knock (↓↑↔)
1. Compression ratio		
2. Spark timing advance		
3. Cylinder diameter		
4. Inlet air temperature		
5. Coolant temperature		
6. Engine speed		
7. Engine load		
8. Fuel octane number		
9. Humidity		
10. Altitude		

17. Discuss the differences in knocking in CI and SI engines. Write the typical characteristics of the parameters given in table to reduce the knocking tendency in SI and CI engines. Fill the Table P9.3 with qualitative values such as low/high and long/short.

Table P9.3 Characteristics tending to reduce engine knocking conditions

Characteristics	SI engines	CI engines
Ignition delay		
Intake temperature and pressure		
Compression ratio		
Autoignition temperature of fuel		
Cylinder wall temperature		
Engine speed		

18. Describe the difference between a conventional knock and super-knock. Discuss the sources of super-knock and mode of combustion of super-knock in SI engine.
19. Discuss the sources of preignition in SI engine. Write the possible methods to avoid the preignition in reciprocating SI engine. Explain whether preignition always leads to knocking, and discuss the severity of preignition.
20. Write the effect of knocking (over a long period of time) on engine performance and its state. Discuss the different methods of knock detection in combustion engines. How you can differentiate the pressure oscillations during a weak knock and pressure oscillation due to the non-flush mounting of the sensor (pipe oscillations).
21. Discuss the phenomena of acoustic wave generation during knocking conditions, and also write the equation to determine the frequency of acoustic mode oscillation. Explain why the axial mode of oscillations is typically not observed in reciprocating engines.
22. Calculate the characteristic frequency of oscillation modes: First circumferential (1,0), second circumferential (2,0), third circumferential (3,0), and first radial (0,1) with corresponding Bessel constants 1.841, 3.054, 4.201, and 3.832, respectively. Compute the frequency corresponding to temperatures 2000 K, 2500 K, and 3000 K. Discuss the effect of the equivalence ratio of the charge on the frequency of oscillations.
23. Discuss the different knock indices based on in-cylinder pressure and heat release used for characterization of knock in internal combustion engines.
24. Discuss how wavelets can be used for characterization of engine knocking under different engine operating conditions.
25. Assume a gasoline SI engine having bore 60 mm and displacement volume of 400 cc working on the stoichiometric mixture with spark timing 15° before TDC. The spark plug is located at the center of the engine head. Assuming constant turbulent flame speed of 8.56 m/s, determine whether or not engine knocking will occur in the combustion chamber. Unburned gas temperature and pressure can be assumed to be constant throughout combustion with value 1650 K and 5 bar, respectively. An empirical relation for autoignition delay of a stoichiometric gasoline-air mixture is given as

$$\tau_{\text{ignition delay}}[\text{ms}] = 0.08 \cdot \frac{1}{P^{1.5}[\text{MPa}]} \exp\left(\frac{3800}{T[K]}\right)$$

Clearly state your assumptions if any.

26. Discuss how the setting of knock threshold limits the efficiency of the engine. Describe the methods used for setting the knock threshold and how it can be optimized.
27. Fill the Table P9.4 by discussing the effect of particle and operating condition on preignition in SI engine. Write the effect on increasing the value of variable on preignition (increase or decrease) along with the mechanism responsible for preignition.

Table P9.4 Effect on preignition in SI engine

Variable	Effect on preignition	Responsible mechanism
Particle size		
Particle temperature		
Boost pressure		
Air-fuel ratio		
EGR/residuals		

28. Discuss the different sensing methodologies of engine knock in modern SI engine. Describe the merits and demerits of the method. Write the typical factors you will consider for selecting the knock detection methods.
29. Discuss the method for combustion noise level assessment in engines by means of in-cylinder pressure components? Explain various indices used for combustion noise determination base on cylinder pressure data.

References

1. Wang, Z., Liu, H., & Reitz, R. D. (2017). Knocking combustion in spark-ignition engines. *Progress in Energy and Combustion Science, 61*, 78–112.
2. Heywood, J. B. (1988). *Internal combustion engine fundamentals*. New York: McGraw-Hill Education.
3. Zhen, X., Wang, Y., Xu, S., Zhu, Y., Tao, C., Xu, T., & Song, M. (2012). The engine knock analysis—An overview. *Applied Energy, 92*, 628–636.
4. Wang, Z., Liu, H., Song, T., Qi, Y., He, X., Shuai, S., & Wang, J. (2015). Relationship between super-knock and pre-ignition. *International Journal of Engine Research, 16*(2), 166–180.
5. Rogers, D. R. (2010). *Engine combustion: Pressure measurement and analysis*. Warrendale: Society of Automotive Engineers.
6. Mahendar, S. K., Erlandsson, A., & Adlercreutz, L. (2018). *Challenges for spark ignition engines in heavy duty application: A review* (No. 2018-01-0907). SAE Technical Paper.
7. Mittal, V., Revier, B. M., & Heywood, J. B. (2007). *Phenomena that determine knock onset in spark-ignition engines* (No. 2007-01-0007). SAE Technical Paper.
8. Kawahara, N., Tomita, E., & Sakata, Y. (2007). Auto-ignited kernels during knocking combustion in a spark-ignition engine. *Proceedings of the Combustion Institute, 31*(2), 2999–3006.
9. Merola, S. S., & Vaglieco, B. M. (2007). Knock investigation by flame and radical species detection in spark ignition engine for different fuels. *Energy Conversion and Management, 48* (11), 2897–2910.

10. McKenzie, J., & Cheng, W. K. (2016). *The anatomy of knock* (No. 2016-01-0704). SAE Technical Paper.
11. Westbrook, C. K. (2000). Chemical kinetics of hydrocarbon ignition in practical combustion systems. *Proceedings of the Combustion Institute, 28*(2), 1563–1577.
12. Kalghatgi, G. (2018). Knock onset, knock intensity, superknock and preignition in spark ignition engines. *International Journal of Engine Research, 19*(1), 7–20.
13. Chen, L., Li, T., Yin, T., & Zheng, B. (2014). A predictive model for knock onset in spark-ignition engines with cooled EGR. *Energy Conversion and Management, 87*, 946–955.
14. Douaud, A. M., & Eyzat, P. (1978). *Four-octane-number method for predicting the anti-knock behavior of fuels and engines* (No. 780080). SAE Technical Paper.
15. Syed, I. Z., Mukherjee, A., & Naber, J. (2011). *Numerical simulation of autoignition of gasoline-ethanol/air mixtures under different conditions of pressure, temperature, dilution, and equivalence ratio* (No. 2011-01-0341). SAE Technical Paper.
16. Livengood, J. C., & Wu, P. C. (1955). Correlation of autoignition phenomena in internal combustion engines and rapid compression machines. In *Symposium (International) on Combustion* (Vol. 5, No. 1, pp. 347–356). Elsevier.
17. Kim, K. S., & Ghandhi, J. (2012). *Preliminary results from a simplified approach to modeling the distribution of engine knock* (No. 2012-32-0004). SAE Technical Paper.
18. Mittal, V., Heywood, J. B., & Green, W. H. (2010). The underlying physics and chemistry behind fuel sensitivity. *SAE International Journal of Fuels and Lubricants, 3*(1), 256–265.
19. Kalghatgi, G., Head, R., Chang, J., Viollet, Y., Babiker, H., & Amer, A. (2014). An alternative method based on toluene/n-heptane surrogate fuels for rating the anti-knock quality of practical gasolines. *SAE International Journal of Fuels and Lubricants, 7*(3), 663–672.
20. Boot, M. D., Tian, M., Hensen, E. J., & Sarathy, S. M. (2017). Impact of fuel molecular structure on auto-ignition behavior–Design rules for future high performance gasolines. *Progress in Energy and Combustion Science, 60*, 1–25.
21. Kalghatgi, G. T. (2001). *Fuel anti-knock quality-Part I. Engine studies* (No. 2001-01-3584). SAE Technical Paper.
22. Amer, A., Babiker, H., Chang, J., Kalghatgi, G., Adomeit, P., Brassat, A., & Günther, M. (2012). Fuel effects on knock in a highly boosted direct injection spark ignition engine. *SAE International Journal of Fuels and Lubricants, 5*(3), 1048–1065.
23. Kalghatgi, G., Risberg, P., & Ångstrom, H. E. (2003). *A method of defining ignition quality of fuels in HCCI engines* (No. 2003-01-1816). SAE Technical Paper.
24. Kalghatgi, G. T., & Head, R. A. (2004). *The available and required autoignition quality of gasoline-like fuels in HCCI engines at high temperatures* (No. 2004-01-1969). SAE Technical Paper.
25. Kalghatgi, G. T. (2005). *Auto-ignition quality of practical fuels and implications for fuel requirements of future SI and HCCI engines* (No. 2005-01-0239). SAE Technical Paper.
26. Kalghatgi, G., Babiker, H., & Badra, J. (2015). A simple method to predict knock using toluene, n-heptane and iso-octane blends (TPRF) as gasoline surrogates. *SAE International Journal of Engines, 8*(2), 505–519.
27. Shahlari, A. J., & Ghandhi, J. (2017). *Pressure-based knock measurement issues* (No. 2017-01-0668). SAE Technical Paper.
28. Xiaofeng, G., Stone, R., Hudson, C., & Bradbury, I. (1993). *The detection and quantification of knock in spark ignition engines* (No. 932759). SAE Technical Paper.
29. Burgdorf, K., & Denbratt, I. (1997). *Comparison of cylinder pressure based knock detection methods* (No. 972932). SAE Technical Paper.
30. Shahlari, A. J., & Ghandhi, J. B. (2012). *A comparison of engine knock metrics* (No. 2012-32-0007). SAE Technical Paper.
31. Bradley, D., Morley, C., Gu, X. J., & Emerson, D. R. (2002). *Amplified pressure waves during autoignition: Relevance to CAI engines* (No. 2002-01-2868). SAE Technical Paper.
32. Gu, X. J., Emerson, D. R., & Bradley, D. (2003). Modes of reaction front propagation from hot spots. *Combustion and Flame, 133*(1-2), 63–74.

33. König, G., Maly, R. R., Bradley, D., Lau, A. K. C., & Sheppard, C. G. W. (1990). Role of exothermic centres on knock initiation and knock damage. *SAE Transactions, 99*, 840–861.
34. Wang, Z., Qi, Y., He, X., Wang, J., Shuai, S., & Law, C. K. (2015). Analysis of pre-ignition to super-knock: Hotspot-induced deflagration to detonation. *Fuel, 144*, 222–227.
35. Zeldovich, Y. B. (1980). Regime classification of an exothermic reaction with nonuniform initial conditions. *Combustion and Flame, 39*(2), 211–214.
36. Qi, Y., Wang, Z., Wang, J., & He, X. (2015). Effects of thermodynamic conditions on the end gas combustion mode associated with engine knock. *Combustion and Flame, 162*(11), 4119–4128.
37. Bradley, D., & Kalghatgi, G. T. (2009). Influence of autoignition delay time characteristics of different fuels on pressure waves and knock in reciprocating engines. *Combustion and Flame, 156*(12), 2307–2318.
38. Kalghatgi, G. T., & Bradley, D. (2012). Pre-ignition and 'super-knock' in turbo-charged spark-ignition engines. *International Journal of Engine Research, 13*(4), 399–414.
39. Hurle, I. R., Price, R. B., Sugden, T. M., & Thomas, A. (1968). Sound emission from open turbulent premixed flames. *Proceedings of the Royal Society of London A, 303*(1475), 409–427.
40. Kim, K. S. (2015). *Study of engine knock using a Monte Carlo method* (Doctoral dissertation). The University of Wisconsin-Madison.
41. Bates, L., Bradley, D., Paczko, G., & Peters, N. (2016). Engine hot spots: Modes of auto-ignition and reaction propagation. *Combustion and Flame, 166*, 80–85.
42. Pasternak, M., Netzer, C., Mauss, F., Fischer, M., Sens, M., & Riess, M. (2017, December). Simulation of the effects of spark timing and external EGR on gasoline combustion under knock-limited operation at high speed and load. In *International Conference on Knocking in Gasoline Engines* (pp. 121–142). Cham: Springer.
43. Zhou, L., Kang, R., Wei, H., Feng, D., Hua, J., Pan, J., & Chen, R. (2018). Experimental analysis of super-knock occurrence based on a spark ignition engine with high compression ratio. *Energy, 165B*, 68–75.
44. Dahnz, C., Han, K. M., Spicher, U., Magar, M., Schießl, R., & Maas, U. (2010). Investigations on pre-ignition in highly supercharged SI engines. *SAE International Journal of Engines, 3*(1), 214–224.
45. Döhler, A., & Schaffner, P. (2017, December). Optical diagnostic tools for detection and evaluation of glow ignitions. In *International Conference on Knocking in Gasoline Engines* (pp. 55–70). Cham: Springer.
46. Kalghatgi, G., Algunaibet, I., & Morganti, K. (2017). On knock intensity and superknock in SI engines. *SAE International Journal of Engines, 10*(2017-01-0689), 1051–1063.
47. Kassai, M., Shiraishi, T., & Noda, T. (2017, December). Fundamental mechanism analysis on the underlying processes of LSPI using experimental and modeling approaches. In *International Conference on Knocking in Gasoline Engines* (pp. 89–111). Cham: Springer.
48. Morikawa, K., Moriyoshi, Y., Kuboyama, T., Imai, Y., Yamada, T., & Hatamura, K. (2015). *Investigation and improvement of LSPI phenomena and study of combustion strategy in highly boosted SI combustion in low speed range* (No. 2015-01-0756). SAE Technical Paper.
49. Jatana, G. S., Splitter, D. A., Kaul, B., & Szybist, J. P. (2018). Fuel property effects on low-speed pre-ignition. *Fuel, 230*, 474–482.
50. Spicher, U. (2017, December). Detection and analysis methods for irregular combustion in SI engines. In *International Conference on Knocking in Gasoline Engines* (pp. 225–242). Cham: Springer.
51. Vressner, A., Lundin, A., Christensen, M., Tunestål, P., & Johansson, B. (2003). Pressure oscillations during rapid HCCI combustion. *SAE Transactions*, 2469–2478.
52. Draper, C. S. (1935). *The physical effects of detonation in a closed cylindrical chamber*. Technical report, National Advisory Committee for Aeronautics.
53. Guardiola, C., Pla, B., Bares, P., & Barbier, A. (2018). An analysis of the in-cylinder pressure resonance excitation in internal combustion engines. *Applied Energy, 228*, 1272–1279.

54. Dahl, D., Andersson, M., & Denbratt, I. (2011). The origin of pressure waves in high load HCCI combustion: A high-speed video analysis. *Combustion Science and Technology, 183* (11), 1266–1281.
55. Wissink, M., Wang, Z., Splitter, D., Shahlari, A., & Reitz, R. D. (2013). *Investigation of pressure oscillation modes and audible noise in RCCI, HCCI, and CDC* (No. 2013-01-1652). SAE Technical Paper.
56. Zhang, Q., Hao, Z., Zheng, X., & Yang, W. (2017). Characteristics and effect factors of pressure oscillation in multi-injection DI diesel engine at high-load conditions. *Applied Energy, 195*, 52–66.
57. Millo, F., & Ferraro, C. V. (1998). *Knock in SI engines: a comparison between different techniques for detection and control* (No. 982477). SAE Technical Paper.
58. Brunt, M. F., Pond, C. R., & Biundo, J. (1998). *Gasoline engine knock analysis using cylinder pressure data* (No. 980896). SAE Technical paper.
59. Puzinauskas, P. V. (1992). *Examination of methods used to characterize engine knock* (No. 920808). SAE Technical Paper.
60. Lounici, M. S., Benbellil, M. A., Loubar, K., Niculescu, D. C., & Tazerout, M. (2017). Knock characterization and development of a new knock indicator for dual-fuel engines. *Energy, 141*, 2351–2361.
61. Brecq, G., Bellettre, J., & Tazerout, M. (2003). A new indicator for knock detection in gas SI engines. *International Journal of Thermal Sciences, 42*(5), 523–532.
62. Maurya, R. K. (2018). *Characteristics and control of low temperature combustion engines: Employing gasoline, ethanol and methanol*. Cham: Springer.
63. Checkel, M. D., & Dale, J. D. (1989). *Pressure trace knock measurement in a current si production engine* (No. 890243). SAE Technical Paper.
64. Eng, J. A. (2002). *Characterization of pressure waves in HCCI combustion* (No. 2002-01-2859). SAE Technical Paper.
65. Bares, P., Selmanaj, D., Guardiola, C., & Onder, C. (2018). A new knock event definition for knock detection and control optimization. *Applied Thermal Engineering, 131*, 80–88.
66. Hettinger, A., & Kulzer, A. (2009). A new method to detect knocking zones. *SAE International Journal of Engines, 2*(1), 645–665.
67. Galloni, E. (2012). Dynamic knock detection and quantification in a spark ignition engine by means of a pressure based method. *Energy Conversion and Management, 64*, 256–262.
68. Nilsson, Y., Frisk, E., & Nielsen, L. (2009). Weak knock characterization and detection for knock control. *Proceedings of the Institution of Mechanical Engineers, Part D: Journal of Automobile Engineering, 223*(1), 107–129.
69. Peyton Jones, J. C., Spelina, J. M., & Frey, J. (2014). Optimizing knock thresholds for improved knock control. *International Journal of Engine Research, 15*(1), 123–132.
70. Galloni, E. (2016). Knock-limited spark angle setting by means of statistical or dynamic pressure based methods. *Energy Conversion and Management, 116*, 11–17.
71. Shayestehmanesh, S., Jones, J. C. P., & Frey, J. (2018). *Stochastic characteristics of knock and IMEP* (No. 2018-01-1155). SAE Technical Paper.
72. Cavina, N., Brusa, A., Rojo, N., & Corti, E. (2018). *Statistical analysis of knock intensity probability distribution and development of 0-D predictive knock model for a SI TC engine* (No. 2018-01-0858). SAE Technical Paper.
73. Naber, J., Blough, J. R., Frankowski, D., Goble, M., & Szpytman, J. E. (2006). *Analysis of combustion knock metrics in spark-ignition engines* (No. 2006-01-0400). SAE Technical Paper.
74. Wei, H., Hua, J., Pan, M., Feng, D., Zhou, L., & Pan, J. (2018). Experimental investigation on knocking combustion characteristics of gasoline compression ignition engine. *Energy, 143*, 624–633.
75. Zhou, L., Hua, J., Wei, H., Dong, K., Feng, D., & Shu, G. (2018). Knock characteristics and combustion regime diagrams of multiple combustion modes based on experimental investigations. *Applied Energy, 229*, 31–41.

76. Ghandhi, J., & Kim, K. S. (2017). *A statistical description of knock intensity and its prediction* (No. 2017-01-0659). SAE Technical Paper.
77. Siano, D., & Bozza, F. (2013). *Knock detection in a turbocharged SI engine based on ARMA technique and chemical kinetics* (No. 2013-01-2510). SAE Technical Paper.
78. Tong, S., Yang, Z., He, X., Deng, J., Wu, Z., & Li, L. (2017). *Knock and pre-ignition detection using ion current signal on a boosted gasoline engine* (No. 2017-01-0792). SAE Technical Paper.
79. Abu-Qudais, M. (1996). Exhaust gas temperature for knock detection and control in spark ignition engine. *Energy Conversion and Management, 37*(9), 1383–1392.
80. Spelina, J. M. (2016). *Knock characterization, simulation, and control* (PhD Thesis). Villanova University.
81. Kowada, M., Azumagakito, I., Nagai, T., Iwai, N., & Hiraoka, R. (2015). *Study of knocking damage indexing based on optical measurement* (No. 2015-01-0762). SAE Technical Paper.
82. Spicher, U., Kroger, H., & Ganser, J. (1991). *Detection of knocking of combustion using simultaneously high speed Schlieren cinematography and multi-optical fibre technique*. SAE Technical Paper 912312.
83. Nagai, T., Hiraoka, R., Iwai, N., Kowada, M., & Azumagakito, I. (2015). *Development of highly durable optical probe for combustion measurement* (No. 2015-01-0759). SAE Technical Paper.
84. Philipp, H., Hirsch, A., Baumgartner, M., Fernitz, G., Beidl, C., Piock, W., & Winklhofer, E. (2001). *Localization of knock events in direct injection gasoline engines* (No. 2001-01-1199). SAE Technical Paper.
85. Matsura, K., Sato, Y., Yoshida, K., & Sono, H. (2017). Proposal of knock mitigation method through enhancement of local heat transfer. In *International Conference on Knocking in Gasoline Engines* (pp. 3–16). Cham: Springer.
86. Giglio, V., Police, G., Rispoli, N., di Gaeta, A., Cecere, M., & Della Ragione, L. (2009). *Experimental investigation on the use of ion current on SI engines for knock detection* (No. 2009-01-2745). SAE Technical Paper.
87. Laganá, A. A., Lima, L. L., Justo, J. F., Arruda, B. A., & Santos, M. M. (2018). Identification of combustion and detonation in spark ignition engines using ion current signal. *Fuel, 227*, 469–477.
88. Daniels, C. F., Zhu, G. G., & Winkelman, J. (2003). *Inaudible knock and partial-burn detection using in-cylinder ionization signal* (No. 2003-01-3149). SAE Technical Paper.
89. Patro, T. N. (1997). *Combustion induced powertrain NVH-a time-frequency analysis* (No. 971874). SAE Technical Paper.
90. Kiencke, U., & Nielsen, L. (2005). *Automotive control systems: For engine, driveline, and vehicle*. Berlin: Springer Science & Business Media.
91. Liu, C., Gao, Q., Jin, Y. A., & Yang, W. (2010). Application of wavelet packet transform in the knock detection of gasoline engines. In *2010 International Conference on Image Analysis and Signal Processing (IASP)* (pp. 686–690). IEEE.
92. Bi, F., Ma, T., & Wang, X. (2019). Development of a novel knock characteristic detection method for gasoline engines based on wavelet-denoising and EMD decomposition. *Mechanical Systems and Signal Processing, 117*, 517–536.
93. Souder, J. S., Mack, J. H., Hedrick, J. K., & Dibble, R. W. (2004, January). Microphones and knock sensors for feedback control of HCCI engines. In *ASME 2004 Internal Combustion Engine Division Fall Technical Conference* (pp. 77–84). New York: American Society of Mechanical Engineers.
94. Hunger, M., Böcking, T., Walther, U., Günther, M., Freisinger, N., & Karl, G. (2017). Potential of direct water injection to reduce knocking and increase the efficiency of gasoline engines. In *International Conference on Knocking in Gasoline Engines* (pp. 338–359). Cham: Springer.
95. Fischer, M., Günther, M., Berger, C., Troeger, R., Pasternak, M., & Mauss, F. (2017). Suppressing knocking by using CleanEGR–better fuel economy and lower raw emissions

simultaneously. In *International Conference on Knocking in Gasoline Engines* (pp. 363–384). Cham: Springer.
96. Alt, N. W., Nehl, J., Heuer, S., & Schlitzer, M. W. (2003). *Prediction of combustion process induced vehicle interior noise* (No. 2003-01-1435). SAE Technical Paper.
97. Schwarz, A., & Janicka, J. (Eds.). (2009). *Combustion noise*. Berlin: Springer Science & Business Media.
98. Broatch, A., Novella, R., Gomez-Soriano, J., Pal, P., & Som, S. (2018). *Numerical methodology for optimization of compression-ignited engines considering combustion noise control*. SAE Technical Paper 2018-01-0193.
99. Flemming, F., Sadiki, A., & Janicka, J. (2007). Investigation of combustion noise using a LES/CAA hybrid approach. *Proceedings of the Combustion Institute, 31*(2), 3189–3196.
100. Torregrosa, A. J., Broatch, A., Martín, J., & Monelletta, L. (2007). Combustion noise level assessment in direct injection diesel engines by means of in-cylinder pressure components. *Measurement Science and Technology, 18*(7), 2131.
101. Payri, F., Broatch, A., Margot, X., & Monelletta, L. (2009). Sound quality assessment of diesel combustion noise using in-cylinder pressure components. *Measurement Science and Technology, 20*(1), 015107.
102. Stanković, L., & Böhme, J. F. (1999). Time–frequency analysis of multiple resonances in combustion engine signals. *Signal Processing, 79*(1), 15–28.
103. Payri, F., Torregrosa, A. J., Broatch, A., & Monelletta, L. (2009). Assessment of diesel combustion noise overall level in transient operation. *International Journal of Automotive Technology, 10*(6), 761.
104. Ozawa, H., & Nakada, T. (1999). Pseudo cylinder pressure excitation for analyzing the noise characteristics of the engine structure. *JSAE Review, 20*(1), 67–72.
105. Russell, M. F., Palmer, D. C., & Young, C. D. (1984). Measuring diesel noise at source with a view to its control. *IMechE, C142*(84), 97–105.
106. Shahlari, A. J., Hocking, C., Kurtz, E., & Ghandhi, J. (2013). Comparison of compression ignition engine noise metrics in low-temperature combustion regimes. *SAE International Journal of Engines, 6*(1), 541–552.
107. Payri, F., Broatch, A., Tormos, B., & Marant, V. (2005). New methodology for in-cylinder pressure analysis in direct injection diesel engines—Application to combustion noise. *Measurement Science and Technology, 16*(2), 540.
108. Broatch, A., Novella, R., García-Tíscar, J., & Gomez-Soriano, J. (2019). On the shift of acoustic characteristics of compression-ignited engines when operating with gasoline partially premixed combustion. *Applied Thermal Engineering, 146*, 223–231.
109. Shibata, G., Shibaike, Y., Ushijima, H., & Ogawa, H. (2013). *Identification of factors influencing premixed diesel engine noise and mechanism of noise reduction by EGR and supercharging* (No. 2013-01-0313). SAE Technical Paper.
110. Torregrosa, A. J., Broatch, A., Novella, R., Gomez-Soriano, J., & Mónico, L. F. (2017). Impact of gasoline and diesel blends on combustion noise and pollutant emissions in premixed charge compression ignition engines. *Energy, 137*, 58–68.
111. Shibata, G., Nakayama, D., Okamoto, Y., & Ogawa, H. (2016). Diesel engine combustion noise reduction by the control of timings and heating values in two stage high temperature heat releases. *SAE International Journal of Engines, 9*(2), 868–882.
112. Fuyuto, T., Taki, M., Ueda, R., Hattori, Y., Kuzuyama, H., & Umehara, T. (2014). Noise and emissions reduction by second injection in diesel PCCI combustion with split injection. *SAE International Journal of Engines, 7*(4), 1900–1910.
113. Shibata, G., Ogawa, H., Okamoto, Y., Amanuma, Y., & Kobashi, Y. (2017). Combustion noise reduction with high thermal efficiency by the control of multiple fuel injections in premixed diesel engines. *SAE International Journal of Engines, 10*(3), 1128–1142.
114. Bahri, B., Shahbakhti, M., & Aziz, A. A. (2017). Real-time modeling of ringing in HCCI engines using artificial neural networks. *Energy, 125*, 509–518.
115. Dernotte, J., Dec, J. E., & Ji, C. (2014). Investigation of the sources of combustion noise in HCCI engines. *SAE International Journal of Engines, 7*(2014-01-1272), 730–761.